

From Modular Origami Robots to Polygon-based Modular Systems: a New Paradigm in Reconfigurable Robotics

Présentée le 30 mars 2020

à la Faculté des sciences et techniques de l'ingénieur
Laboratoire de robotique reconfigurable
Programme doctoral en robotique, contrôle et systèmes intelligents

pour l'obtention du grade de Docteur ès Sciences

par

Christoph Heinrich BELKE

Acceptée sur proposition du jury

Prof. P. Dillenbourg, président du jury
Prof. J. Paik, directrice de thèse
Prof. K. Støy, rapporteur
Prof. J. Dai, rapporteur
Prof. A. Ijspeert, rapporteur

Abstract

A useful robot is one that fulfils its intended function. In a factory setting, where robots have been used successfully for decades, this function is often singular and clearly defined. Similarly, the surroundings of the robot are mostly known, sterile, and unobstructed. Taking robotic systems out of these conditions and into the real world comes with numerous challenges that are non-existent in factory cages. We want personal robots to cope with the uncertain and dynamic environments we inhabit, while at the same time managing and solving diverse tasks. Reconfigurable robots aim to achieve this by changing shape and function to address a variety of applications, environments, and users.

While reconfigurable robots carry a lot of promise, finding a balance between the system's adaptability, the extent to which it can alter shape and function, and the added complexity is difficult. Research efforts have largely focused on proof-of-concept studies with limited reconfigurability and application range, avoiding the increasingly overwhelming mechanical, computational, and electronic complexities. This thesis introduces a new paradigm to the world of reconfigurable robotics with an inherent adaptability through simplification of the underlying structure. Approximating physical structures through polygon abstractions, similar to computer graphics, such systems can assume a wide range of structural or functional three-dimensional shapes. Based on this paradigm, it also presents a new robotic platform combining the concepts behind both modular and origami robotics, as well as reconfigurable mechanisms and polygon meshing.

In order to take advantage of this new paradigm, a diverse set of problems must be investigated, spanning multiple robotic disciplines. With an increasing degree of reconfigurability, both within a module and the overall system, the growing physical and mechatronic requirements need to be analysed and addressed accordingly. New reconfiguration algorithms and control strategies need to be developed to cope with the large, and constantly changing, number of degrees of freedom. These must then be synchronised and scaled appropriately, leveraging modularity at multiple levels, to accomplish diverse sets of tasks and functions.

Addressing the challenges associated with this new robotic paradigm and proving its viability provides the context for this thesis. In a first phase it outlines the initial conception, studying scalability and applicability through the combination of modularity and origami robots with a first prototype and its use in multiple scenarios. It continues with the development and analysis of several building blocks of modular origami robots, both mechanical and algorithmic, analysing mechanisms for the coupling between modules and the reconfiguration process. In the second phase the proposed paradigm is elaborated into its full form, integrating and examining reconfigurable mechanisms and polygon meshing. The resulting morphological and functional flexibility is validated through the development

Abstract

and testing of a highly sophisticated modular robotic system. Individual modules can alter their own triangular shape, drive towards and attach to each other, and transform into functional three-dimensional configurations. The conceptual and physical systems developed and studied in this thesis answer some of the challenges posed by this new paradigm and underline the potential of reconfigurability in robotics.

Keywords: reconfigurable robots, modular robots, origami robots, polygon meshing, reconfiguration algorithms, mechanical design, control.

Résumé

Un robot utile est celui qui remplit sa fonction. Dans un environnement industriel où des robots ont été utilisés avec succès depuis des décennies, cette fonction est souvent unique et clairement définie. De même, l'environnement des robots est généralement connu et sans obstacle. Sortir les systèmes robotiques de ces conditions et les placer en situations réelles crée de nombreux défis qui n'existent pas en industrie. Notre objectif est de permettre aux robots personnels de faire face aux environnements incertains et dynamiques dans lesquels nous vivons, et en même temps gérer et résoudre des tâches diverses. Pour ce faire, les robots reconfigurables changent de forme et de fonction pour prendre en charge une variété d'applications, d'environnements et d'utilisateurs.

Bien que les robots reconfigurables soient prometteurs, il est difficile de trouver un équilibre entre l'adaptabilité du système, dans quelle mesure il peut changer de forme et de fonction, et la complexité ajoutée. Les efforts de recherche se sont largement concentrés sur des études de vérification de principe avec une reconfigurabilité et un domaine d'application limités, évitant ainsi les complexités mécaniques, informatiques et électroniques de plus en plus écrasantes. Cette thèse introduit un nouveau paradigme dans le domaine de la robotique reconfigurable avec une adaptabilité inhérente par la simplification de la structure sous-jacente. En se rapprochant des formes physiques avec des abstractions de polygones à la manière de l'infographie, ces systèmes peuvent prendre une large gamme de formes structurelles ou fonctionnelles en trois dimensions. Basée sur ce paradigme, cette thèse présente également une nouvelle plateforme robotique combinant les concepts de la robotique modulaire et origami, ainsi que des mécanismes reconfigurables et du maillage de polygones.

Afin de tirer parti de ce nouveau paradigme, il faut étudier un ensemble de problèmes divers, couvrant de multiples disciplines robotiques. En améliorant la reconfigurabilité, à la fois d'un module et de l'ensemble du système, les exigences physiques et mécatroniques augmentent et doivent être analysées et traitées. Il faut développer de nouveaux algorithmes de reconfiguration et des stratégies de contrôle pour faire face au grand nombre de degrés de liberté qui changent continuellement. Ceux-ci doivent ensuite être synchronisés, en exploitant la modularité à plusieurs niveaux, pour accomplir diverses tâches et fonctions.

Le but de cette thèse est d'aborder les défis associés à ce nouveau paradigme robotique et de prouver sa viabilité. Dans un premier temps, elle présente la conception initiale et étudie son évolutivité et son applicabilité, en combinant robotique modulaire et origami dans un premier prototype et son utilisation dans plusieurs scénarios. Cette étude se poursuit avec le développement et l'analyse, à la fois mécanique et algorithmique, de plusieurs composantes élémentaires de robots d'origami modulaires, en analysant les mécanismes de couplage entre les modules et le processus de reconfiguration. Dans

Résumé

un second temps, le paradigme proposé est élaboré dans sa forme complète, intégrant et examinant les mécanismes reconfigurables et le maillage des polygones. La flexibilité morphologique et fonctionnelle résultante est validée par le développement et les tests d'un système robotique modulaire sophistiqué. Les modules individuels peuvent modifier leur forme triangulaire, se rapprocher, se combiner et se transformer en configurations fonctionnelles en trois dimensions. Les systèmes conceptuels et physiques développés et étudiés dans cette thèse résolvent certains problèmes posés par ce nouveau paradigme et mettent en avant le potentiel de reconfigurabilité en robotique.

Mots-clés : robots reconfigurables, robots modulaires, robots origami, maillage de polygones, algorithmes de reconfiguration, conception mécanique, contrôle.

Acknowledgements

I would like to express my sincere gratitude to my supervisor, Prof. Jamie Paik. Her continuous support from the onset paved the way for this project, allowing me to pursue, develop, and implement my ideas for such unconventional systems. I am grateful to my thesis committee, Prof. Dillenbourg, Prof. Støy, Prof. Dai, and Prof. Ijspeert, for providing valuable insights and further shaping this work. I would also like to thank my collaborators, Zhenishbek, Jian-Lin, Meibao, Alex, and Kevin, along with the rest of our lab for sharing my enthusiasm and providing such a supportive and kind atmosphere.

I am deeply grateful to my parents, sister, and closest friends who have accompanied me through the years. They have shaped me into the person I am today and I would not be here without them. Thank you for all your care, support, and advice. Thank you for giving me a home in so many places and bringing joy to my life.

Most of all, I am forever grateful to my love, Alma. She has supported me in every way possible from considering a PhD to putting down the final few words. Her positivity, curiosity, and kindness fulfil me and her intellect inspires me. She has been my biggest supporter and best friend. Thank you and your family for everything!

Lausanne, 21.12.2019

C.H.B.

Contents

Abstract	i
Résumé	iii
Acknowledgements	v
Part I Introducing a Paradigm	1
1 Background: Setting the scientific scene	3
1.1 Reconfigurability in robotics	4
1.2 Modular robots and systems	4
1.3 Origami and robots thereof	5
1.4 A new robotic paradigm	6
2 Outline: What to expect	9
2.1 Problem statement	9
2.2 Structure and contributions	10
2.3 Application scenarios	13
Part II A Conceptual Study	15
3 Combining origami and modularity in robotics	17
3.1 Conceptual analysis	18
3.1.1 Scalability	19
3.1.2 Features and requirements	19
3.2 System overview	21
3.2.1 Structure and mechanisms	21
3.2.2 Electronics and control	22
3.2.3 Performance	23
3.3 Case studies	23
3.3.1 Modular reconfigurable surface	24
3.3.2 Mobility demonstration	25
3.3.3 Closed-loop manipulation	26
3.4 Discussion	30
	vii

4	Automatic coupling mechanisms for modular systems	33
4.1	Coupling features	33
4.2	System overview	35
4.2.1	Functional features	35
4.2.2	Electronics and control	37
4.3	Mechanical overload protection	38
4.3.1	Modelling	38
4.3.2	Testing	40
4.4	Coupling demonstration	42
4.5	Discussion	45
5	Reconfiguration algorithms based on origami principles	47
5.1	Planning strategies	49
5.1.1	Automatic modelling	50
5.1.2	Heuristic algorithm	53
5.2	Simulation and results	56
5.2.1	Optimal layout	57
5.2.2	Optimal folding sequence	59
5.3	Discussion	59
Part III	Towards a Universal Robot	61
6	Augmenting robotic reconfigurability through polygons	63
6.1	Morphological flexibility	63
6.1.1	Modular and origami robots	63
6.1.2	Polygon meshing	64
6.2	A new robotic paradigm	65
6.2.1	Characteristic features	65
6.2.2	Associated challenges	67
6.3	Discussion	68
7	A polygon-based modular robotic platform	69
7.1	Design considerations	69
7.2	System overview	70
7.2.1	Mechanical advances	71
7.2.2	Electronics and control	75
7.2.3	An adaptable platform	79
7.3	Functional testing	79
7.3.1	Adaptable morphology	80
7.3.2	Mobility	81
7.4	Proposed experiments	82
7.4.1	Functional adaptation	82
7.4.2	Morphological flexibility	83
7.4.3	Extensions and optimisation	84
7.5	Discussion	85

Part IV Towards a Robot Universe	89
8 Conclusion and outlook	91
8.1 Summary and contributions	92
8.2 Discussion	93
8.3 A reconfigurable future	94
 Appendix A Energy metric derivations	 97
List of Figures	101
List of Tables	103
Bibliography	105
Curriculum Vitae	115

Introducing a Paradigm **Part I**

1 Background: Setting the scientific scene

Robots. To the casual observer, a science-fiction dream of fully autonomous machines may come to mind – cute, terrifying, or otherwise. An engineer may think of a highly sophisticated system fulfilling repetitive tasks with high precision. To a researcher, the thought of a clumsy prototype successful in one out of ten trials is certainly inevitable. These are some of the many and often vastly different views that shape society's overall perception of robotics. For decades, due to the minute number of actual functioning systems, an idea is all that we had when it came to robots. Recent years, however, have seen a surge in the rate of adoption of a much bigger variety of robotic systems.

While robots and automated machinery found their first adopters amongst experts in industry, where tasks and operating conditions are clearly defined, progress outside of the industrial setting has been slow – for good reason. Taking robotics out of the factory and into the real world, whether it be our homes, public spaces, workplaces, or even space, requires addressing numerous challenges that are non-existent in factory cages. These challenges stem from the uncertain and dynamic environments we inhabit and demand our robots to cope with, natural, urban, and domestic. Various research areas are solely aimed at finding solutions to deal with these complexities by developing computer vision and localisation algorithms, control methods, physical sensors, actuators, and materials. Significant progress in these fields has allowed research efforts to focus on developing fully integrated systems that are capable of dealing with and adapting to the world around them, essential to realising the full potential of robotics [1].

In addition to coping with our dynamic surroundings, a robotic system needs to fulfil certain tasks or functions. In a factory setting robots tend to carry out a single or a small set of pre-programmed jobs with specific instructions. In the real world, however, the required task or function can vary as much as the environment itself. Rather than building a separate robot for each and every circumstance that may be encountered, researchers are developing robots that can change their shape and function depending on both the task and the environment at hand – *enter reconfigurability*. Similar to numerous appearances in popular film productions, various approaches to reconfigurable robots are being studied and implemented including modular systems and shape-shifting structures.

Sections 1.2 and 1.3 in this chapter contain material adapted from the following publication:

[2] C. H. Belke and J. Paik, "Mori: A Modular Origami Robot," *IEEE/ASME Transactions on Mechatronics*, vol. 22, pp.2153-2164, oct 2017, DOI: 10.1109/10.1109/TMECH.2017.2697310

This thesis introduces a new paradigm to the field, fusing multiple disciplines and concepts within the realm of reconfigurability, such as modularity and origami, to address the challenges associated with the development of physically adaptable robots. This chapter continues with a more general analysis of reconfigurability with respect to robots, followed by two sections detailing the background and state-of-the-art in both modular and origami robotics. As some of the technical terms used, such as modular and reconfigurable, can be interpreted and classified in various ways, the following sections each begin with a brief description of our understanding of each term.

1.1 Reconfigurability in robotics

Rather than defining a set configuration in advance, in the design or assembly process, reconfigurability implies a functional or structural transformation that a robot can undergo repeatedly during its functional life. Due to the abstract nature of the idea, it has not been qualified as a field of its own but instead spans across a multitude of disciplines. Although certain types of reconfiguration can be achieved solely through non-physical control architectures [3–7], this chapter focuses on physical reconfiguration and highlights several examples spread across the scientific community.

As the functions of robotic systems vary greatly, so do the types of reconfigurations. The reconfiguration process tends to either widen the spectrum of a single function [8–10], combine multiple functions [11, 12], or serve as the function itself [13]. Whether automated, such that the robot carries out the transformation itself [14], or extrinsic through manual adjustment or external stimuli [15], reconfigurability adds both versatility and complexity to the system. Considerable effort has been placed on studying reconfiguration processes in theory, in terms of kinematic analyses [16–18] and transformation algorithms [19, 20], while practical robotic systems, albeit abundant, continue to focus primarily on initial, proof-of-concept implementations with limited applicability. This is largely due to the soaring complexities and requirements encountered when up-scaling such efforts [21]. Critical factors, such as force or torque requirements, sensing capacities, power supply and distribution, alignment issues, and computational loads, quickly become overwhelming as the number of entities or degrees-of-freedom (DoFs) in a reconfigurable system increase. While this study also begins with proof-of-concept studies of the new paradigm, the second phase details the development of a system designed to be scalable to an extent where practical applications can be studied.

1.2 Modular robots and systems

Reconfigurable modular robots are self-contained robotic units that, in combination with each other, form robotic systems with the ability to change shape, configuration, and function. While some robotic systems employ a degree of modularity in the form of modular attachments, linkages, or control architectures, this section focuses on systems where the entities of the modular architecture are self-contained robots. These are classified by how modules are connected to one another, as well as by the type of modules within the system. Systems can be considered mobile, chain-type, or lattice-type [21] and individual modules can be homogeneous or heterogeneous [22]. These classifications are by no means exclusive [23] and many robots show overlapping features. Mobile-type reconfigurable robots, being the first such type presented in literature [24], are characterised by individual modules being highly mobile [25]. They are often closely related to the study of self-assembly and swarm robotics [26], where a large number of independent mobile robots can fulfil tasks independently or work together through simple attachments such as grippers [27].

Chain-type reconfigurable robots have a characteristic serial architecture amongst modules with a common possibility of tree-type configurations [28, 29]. Being the first to practically show the potential of reconfigurability, these robots are versatile in terms of locomotion patterns but computationally more demanding [21]. They typically have one or two degrees of internal actuation including bending and twisting. Resulting possibilities in gait patterns include side-winding, rolling, transforming, and walking amongst others [30–34]. Lattice-type reconfigurable robots, on the other hand, can be connected in a regular pattern either in 2D such as hexagons [35] or in 3D such as cubes [36]. This allows for a higher degree of reconfigurability and simpler alignment but complicates locomotion. More recent reconfigurable robots tend to combine these classifications into hybrid-type systems [37, 38].

Modules in reconfigurable robotic systems can be homogeneous [39], with all units being the same, or heterogeneous, with differing modules that can embody different functions [40]. Homogeneous systems are simpler overall and allow for modules to be replaced easily, while heterogeneous systems can have specialised modules with allocated functionalities, making individual modules simpler. Furthermore, systems can make use of passive modules to, for example, provide structural elements [41].

Another addition to the capabilities of reconfigurable modular robots that has been studied since their inception is the ability to self-reconfigure [42]. Rather than manually attaching and detaching individual modules, systems can achieve various morphologies autonomously. This requires an automated attachment mechanism, of which various types have been demonstrated, including hook systems [43], magnets [44], self-soldering [45] and hot melt adhesives [46]. The versatility of reconfigurable modular robots is yet to find its limits as researchers are producing various applications including furniture [47], space exploration [48], education [49], adaptive tools [46], and search and rescue [50].

1.3 Origami and robots thereof

From appearances in nature [51], computational geometry [52, 53], to potential applications in engineering [54–56], the art of paper folding, origami, provides insight and inspiration in various fields. Recently, it has proven a useful tool in the field of robotics and has been implemented in several ways, utilising the transformation of light-weight two-dimensional (2D) structures into three-dimensional (3D) shapes to change morphologies and address diverse tasks. The folding pattern can be used to achieve specific behaviours of the structure, while embedded actuators and sensors can provide the tools for versatile robots that can perform in diverse environments [57]. The low thickness and weight of origami robots make them easy to store, transport, and deploy as needed.

Self-actuating robotic sheets with a pre-defined crease pattern and embedded actuators can fold into a number of morphologies [58], closely embodying a true robotic conception of origami. Other approaches have focused on utilising origami characteristics in the form of passive parts to guide actuation [59–61], vary actuation [62] and to provide the means for external actuation [63]. Origami has been realised structurally to create complete robots from pre-cut foldable sheets [64] as well as in combining structure with actuation to create novel robotic concepts [65–67].

Smart materials have played a significant role in the development of self-folding robots [68–71] by reducing complexity of the mechanical assembly. Aside from traditional actuators in pre-assembled origami robots, fully integrated self-folding origami robots have been predominantly created using heat-activated shape memory materials [72–75]. These allow for a much lower thickness of the overall system compared to traditional actuators. Furthermore, 2D layer fabrication techniques can provide origami robots with distributed actuation and sensing to accommodate feedback and control systems [76–78].

1.4 A new robotic paradigm

This thesis introduces a new paradigm to the world of reconfigurable robotics, taking advantage of the concepts behind modular and origami robots, reconfigurable mechanisms, and polygon meshing. It presents a framework for shape-shifting, quasi-two-dimensional polygon modules that combine and transform into three-dimensional structures. The resulting paradigm represents an approach towards a universal robotic system capable of assuming a wide range of structural or functional shapes. The use of origami principles results in quasi-2D and light-weight structures, a self-contained modular architecture allows assemblies to reconfigure, and polygon meshing provides a global structural framework. While such a universal robotic system is unlikely to outperform any uni-functional robot at a particular task, its true benefit lies in the ability to carry out an abundance of tasks.

Although the ability to reconfigure into a multitude of functional assemblies can be advantageous in a wide range of situations, it is particularly so when transporting or storing a number of robots each executing a single function is not feasible, or when the exact applications or requirements are unknown in advance. In space applications, for instance, the high costs and difficulty of transportation, along with the limited spatial availability, demand space stations to be equipped with highly functional systems. Figure 1.1 presents a conceptual vision of how the new paradigm can be implemented in the form of a universal assistive system on-board a space station, addressing a variety of tasks. Robotic arms of various configurations work both independently and alongside astronauts, mobile structures transport and monitor throughout the station, while larger collections form interactive displays, spatial dividers, and nets.

In addition to transportation and storage, the unknown environments encountered when exploring extraterrestrial objects are difficult to account for in the design process. Figure 1.2 shows a conceptual vision of the paradigm in the form of a universal extraterrestrial exploration system, with mobile, structural, and functional elements based on the same framework. Quadrupedal, snake-like, rolling,

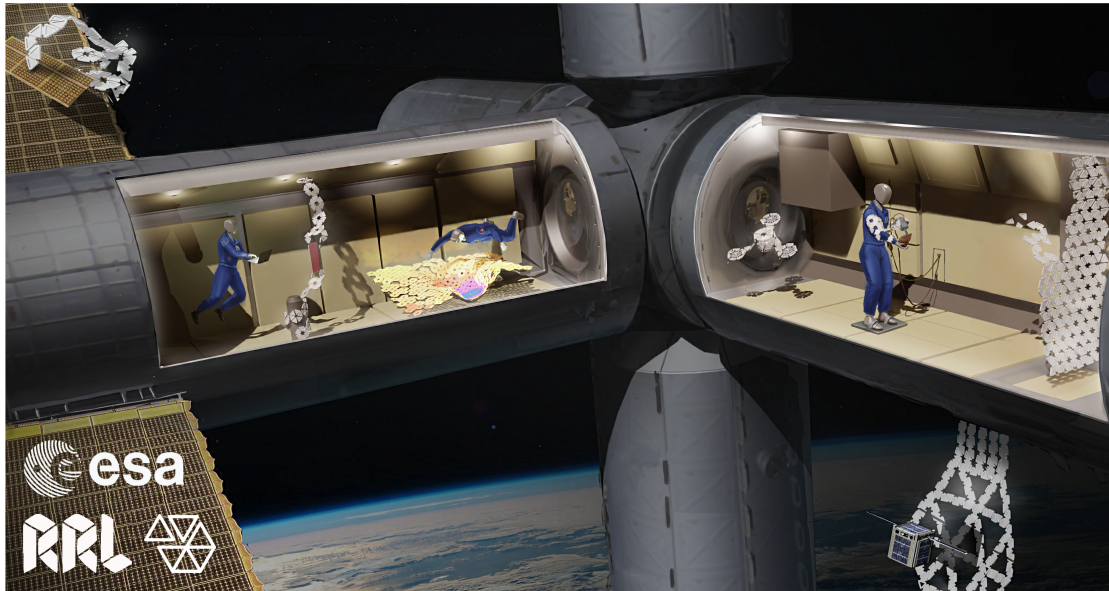


Figure 1.1 – Conceptual vision of the new paradigm in form of a universal assistive system for space. A modular robotic structure based on polygons configures itself into a variety of robotic arms, mobile systems, structural objects, and interactive 3D displays.



Figure 1.2 – Conceptual vision of the new paradigm in form of a universal extraterrestrial exploration system. A modular robotic structure based on polygons configures itself into a variety of mobile and structural assemblies such as domes, quadrupeds, snakes, and drones.

and flying configurations address the varying complexities of the terrain, while another set of modules forms temporary structures of varying shape and size, serving as housing and protection for scientific, communication, and maintenance equipment.

2 Outline: What to expect

Following the general introduction and background to the robotic paradigm above, this chapter provides a blueprint for the thesis. It begins with a description of the general challenges in the field, followed by a detailed structural outline along with the contributions contained within each chapter as well as the thesis as a whole. The chapter concludes with a few inspirational thoughts on the outlook of the paradigm in the form of application-oriented scenarios.

2.1 Problem statement

Reconfigurable robotics aims to create multi-functional systems that can adapt themselves to address different applications, environments, and users through physical transformations. While traditional robots oftentimes fulfil their function through some form of physical change, such as a robotic arm extending or contracting to reach different positions, their underlying kinematic structure remains unchanged during operation. By making the overall morphology of a robot adaptable, in addition to its operational features, numerous challenges are introduced that must be integrated with its augmented functionality.

With an increasing degree of reconfigurability, both within an individual entity and the overall system, the growing physical and mechatronic requirements need to be analysed and addressed accordingly. *What design approaches, reconfigurable mechanisms, and geometric structures enable morphological transformations of such systems to address different functions?*

Reconfigurable structures inherently consist of high numbers of joints, linkages, actuators, and constraints that must be synchronised and adapted appropriately to ensure the system's functionality. *What are the reconfiguration algorithms and control approaches that can cope with the large, and constantly changing, number of degrees of freedom?*

An increasing degree of morphological adaptability results in a larger set of possible functions the system can fulfil. At the same time, however, it adds a growing amount of complexity to each reconfigurable robot and the overall system. *How can this added complexity be balanced with the range and performance of the resulting functionality?*

As the desired adaptability depends on the intended set of functions and environments for the robotic system, the balance between complexity and functionality should be matched accordingly. Adjusting it in either direction based on expected and unexpected circumstances, both in the design process or

during operation, requires studying and developing the constituent technological building blocks with an inherent adaptability in mind. This forms part of a framework for a range of robotic systems with varying degrees of reconfigurability and applicability.

2.2 Structure and contributions

This thesis aims to advance the promising prospect of reconfigurable robotics by addressing some of the above challenges through the scientific and technological development of a new paradigm and a universal robotic framework. Following an introduction to the scientific endeavour in this first part, Part II covers various studies addressing the complexities arising from morphological flexibility. Part III provides a detailed account of the proposed paradigm and presents a robotic platform embodying our approach towards a universal robot. Part IV summarises the thesis and provides an outlook for the new paradigm and our robotic developments in the context of reconfigurable robotics. The various chapters in each of the subsequent parts are described in more detail below, including a summary of the contributions contained within.

Part II A Conceptual Study

In this part, we present three studies of different building blocks of reconfigurable robots that address the underlying challenges of introducing morphological flexibility. We develop and analyse scalability, design and control approaches, and reconfiguration algorithms for such systems as well as their impact on applicability.

Chapter 3: Combining origami and modularity in robotics

The fields of origami and modular robotics individually address different aspects of reconfigurability. In this chapter we propose and study the combination of origami and modularity in robotics and present a robotic platform addressing applicability, control methods, and scalability. The concept merges the advantages of both robot types into a mobile, quasi-two-dimensional, lattice-type reconfigurable modular origami robot, Mori. A detailed description and analysis of the concept is validated by the presentation of a first prototype that incorporates the key functionalities of the system. The modular robot prototype is mobile, can be connected to other modules of its kind, and fold up to create task-specific three-dimensional reconfigurable structures. We present three implementations using the prototype in different configurations in the form of individual modules, modular reconfigurable surfaces, and its application to closed-loop object manipulation. The experiments verify the capabilities and advantages of the system with respect to modularity, origami-folding, mobility, and versatility. The contributions of this chapter can be summarised as follows.

- Introduction, study, and analysis of a new reconfigurable modular robot that is specifically designed to enhance flexibility and applicability.
- Experimental results of two open-loop, application-oriented implementations that highlight the system's characteristics in terms of modularity, origami-like folding, and mobility.
- Modelling and validation of a floating three-DoF platform using Mori along with a demonstration of closed-loop object manipulation.

Chapter 4: Automatic coupling mechanisms for modular systems

Continuing to focus on the complexities of morphological flexibility, in this chapter we study one of the fundamental building blocks of modular systems, the coupling between individual entities. We analyse the overall requirements of automatic coupling mechanisms and address the challenges resulting from the high number of linkages and kinematic conditions in such systems. A novel safety feature for modular couplings is introduced that disengages two entities at a predefined torque threshold. A detailed analytical model of this overload protection mechanism is validated by testing two materials and fabrication methods. We further apply this mechanisms and the identified requirements to the coupling of a modular origami robot. A functional prototype of the genderless coupling is demonstrated by two modular robots driving towards one another, automatically connecting and disconnecting, detecting the connection, communicating in the process, and sensing the angle between them. The coupling as well as the embedded technologies and mechanisms present essential steps towards enabling fully self-reconfigurable robots combining modular and origami features, while advancing the process of introducing modularity into a wide range of robotic systems. The contributions of this chapter can be summarised as follows.

- Analysis of the requirements and functional challenges of the coupling mechanism in modular robotic systems, along with the design of an automated, self-centring, and genderless coupling.
- Introduction, modelling, and experimental validation of a novel mechanical overload protection mechanism for use in modular robotic systems.
- Demonstration and validation of a functional prototype of the automatic coupling mechanism with mechanical overload protection, incorporating connection detection, synchronisation, and angular sensing.

Chapter 5: Reconfiguration algorithms based on origami principles

Completing the initial conceptual study of the complexities in reconfigurable systems, this chapter addresses the challenges of planning and executing the reconfiguration process of modular robots. Utilising the principles behind origami structures folding from 2D configurations into 3D shapes, we develop and analyse different reconfiguration algorithms, minimising energy consumption and connectivity changes. The algorithmic framework includes and compares two approaches, an automatic modelling algorithm as well as a heuristic algorithm. It consists of an energy-optimal reconfiguration planner that generates an initial 2D assembly pattern and an actuation sequence for the modules. We further demonstrate the effectiveness of our method by applying the algorithms to modular origami robots in simulation. Our results show that the heuristic algorithm yields reconfiguration schemes with good performance compared with the automatic modelling algorithm, simultaneously saving a considerable amount of computational time and effort. The contributions of this chapter can be summarised as follows.

- Development, study, and evaluation of reconfiguration algorithms for modular robots based on the principles of origami folding.
- An automatic modelling algorithm generating the kinematic model, dynamic derivation and energy consumption of modular assemblies, represented by the hierarchical structure of a rooted tree.
- A heuristic algorithm for energy-optimal folding of modular robots, consisting of a 2D-layout and a folding sequence planner.
- Demonstration and assessment of the proposed algorithms using several 3D configurations of a modular origami robot.

Part III Towards a Universal Robot

Following the initial conceptual study of the complexities of morphological flexibility in robotic systems, in this part we present our efforts towards a universal robot, first conceptually and then practically. Our approach addresses existing limitations of reconfigurable robots in terms of morphological flexibility by changing the underlying architecture and provides a framework for balancing complexity and functionality.

Chapter 6: Augmenting robotic reconfigurability through polygons

In this chapter we elaborate the new robotic paradigm into its full form, merging the initial concept of a modular origami robot with polygon meshing and reconfigurable mechanisms. We analyse the limitations of existing reconfigurable system, focusing on morphological transformations, and present a framework for a new class of reconfigurable robots with an inherent morphological flexibility. By approximating physical structures through polygon abstractions, similar to computer graphics, such systems can assume a wide range of structural or functional 3D shapes in the form of physical polygon meshes. We provide a detailed analysis of the key characteristics and features of the framework, intended to serve as building blocks that can be adapted, extended, and reduced to suit any given requirements. We finally outline the challenges that need to be addressed in order to take full advantage of the proposed paradigm. The contributions of this chapter can be summarised as follows.

- Introduction of a new robotic paradigm merging modular and origami robots, reconfigurable mechanisms, and polygon meshing to endow morphological and functional flexibility.
- Analysis and evaluation of the characteristic features and underlying challenges associated with this proposed paradigm.

Chapter 7: A polygon-based modular robotic platform

Following the conceptual introduction and analysis of the proposed paradigm, in this chapter we detail the development of a robotic platform taking advantage of its core features. We present a highly sophisticated modular robotic system addressing various challenges posed by the paradigm, and in reconfigurable robotics in general. The platform consists of self-contained triangular robotic modules that can change their own shape, drive towards and attach to each other, and transform into functional 3D configurations. The inherent morphological flexibility is validated by incorporating and testing new mechanisms as well as mechatronic, communication, and control architectures. The system serves as a platform designed to study various key characteristics of the paradigm and to be extended and adapted towards a variety of functional requirements. The contributions of this chapter can be summarised as follows.

- Development of a novel self-reconfigurable robotic module for the physical representation of polygon meshes, where individual modules alter their triangular shape to modify the overall geometric assembly.
- Functional testing of the platform's building blocks including reconfiguration mechanisms and mobility, verifying control methods and models.
- Experimental design to validate the key characteristics of the platform in terms of functional adaptation, morphological flexibility, and optimisation.

Part IV Towards a Robot Universe

The last part summarises the contributions and developments towards reconfigurable robotic systems contained in this thesis and provides an outlook for the future of such robots.

Chapter 8: Conclusion and outlook

In this final chapter of the thesis we review the scientific and technological advancements of the overall thesis. We summarise the challenges that are addressed and contributions that are contained within each chapter. The chapter concludes with a general outlook for the paradigm, the short-term future endeavours based on the robotic platform presented in Chapter 7, and a long-term vision of its potential and applicability. The main contributions of this thesis can be summarised as follows.

- Geometric and functional analysis of the challenges and potential of incorporating reconfigurability in robotic systems, addressing morphological and functional flexibility, complexity, and scalability.
- Study and development of key building blocks of reconfigurable modular systems, including reconfiguration mechanisms and algorithms through prototypes and simulation.
- Introduction and analysis of a novel reconfigurable robotic platform with an inherent morphological flexibility, merging the concepts of modular and origami robotics with polygon meshing.

2.3 Application scenarios

The paradigm introduced in this thesis reflects our approach towards a universal robotic system. Similar to computer graphics, where a collection of variable polygons can represent virtually any 3D object, we envision systems of polygon-shaped modular robots that can assemble into a wide range of structural or functional shapes.

To illustrate the value and versatility of the concept, the following scenarios hint at the potential realm of applications that can be addressed through our paradigm. While some of these scenarios may require different scales, features, and technologies, they are all implementations of the same framework. No existing robot architecture can be applied to such a wide spectrum of applications, while some of the implementations are not at all possible with current systems or concepts. Figure 2.1 depicts some of the structural and functional shapes described.

Scenario A In a domestic setting, a compact stack of robotic modules is stored in a cupboard. Individual modules drive out of the stack, connect to one another, and assemble into a four-legged configuration. The robot trots into the bathroom, transforms into a long chain in order to reach the medicine cabinet, and picks up the user's daily ration by representing a robotic arm. It then makes its way to the user's workplace, turning into a variety of structures as needed to traverse the urban environment, such as rolling wheels and legged configurations of different size and shape.

Scenario B A design engineer is working on a new set of products in virtual reality. As they conceive the idea, a physical representation consisting of flat robotic modules assembles itself on the table next to them. Changes to the various parts of the design are automatically reflected by the robot. The designer can then directly view and interact with the physical model to refine the products.

Scenario C On a foreign planet, an abundance of robotic modules arrives in a spaceship. A first set of modules assembles into temporary structures of varying size and shape, serving as housing and

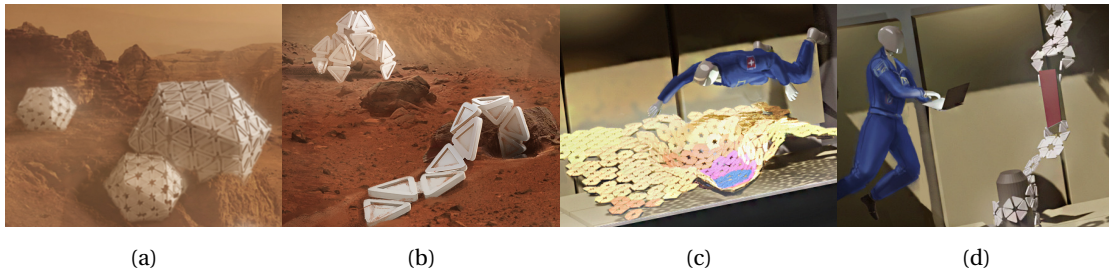


Figure 2.1 – Examples of structural and functional shapes utilising the new robotic paradigm. (a) shows temporary housing and storage structures of varying shape and size, (b) shows examples of mobile assemblies including a quadruped and a snake robot, (c) shows an interactive 3D surface display, and (d) features multiple robotic arms of different configurations.

protection for scientific, communication, and maintenance equipment. A second set of modules begins exploring the planet, transforming into various mobile structures such as quadrupeds, snakes, balls, and drones as necessary. Meanwhile, an astronaut monitors and directs the operation by interacting with a shape-shifting assembly of robotic modules displaying the planet's surface in 3D. This scenario is also illustrated in Figures 1.1 and 1.2.

The development of such truly reconfigurable systems, yielding versatile tools that can address a myriad of functions while coping with our dynamic society and environment, is as much an engineering challenge as it is a scientific endeavour. While this thesis focuses on the scientific progress towards a universal robotic system, it also aims to highlight the value of thorough engineering in science.

A Conceptual Study Part II

3 Combining origami and modularity in robotics

Reconfigurable modular robots are a promising solution to systems that can address a multitude of applications and augment human-robot interaction. Assembling a collection of self-contained modules into different configurations allows a single robotic system to adapt to different circumstances and achieve a diverse set of functions. As there is no theoretical limit to the number of units comprising a modular robotic system, recent research efforts are focusing on extending their potential. This has been facilitated by advancements in the building blocks of reconfigurable modular robots, including actuator and sensor development, computing capacities, materials, and fabrication methods. Similarly, the development of robotic origami, taking inspiration from the art of paper folding, has also been permitted by these advancements. It utilises the transformation of light-weight two-dimensional (2D) structures into three-dimensional (3D) shapes to change morphology and address different tasks. The folding pattern can be used to achieve specific behaviours of the structure, while embedded actuators and sensors can provide the tools for versatile robots that can perform in all sorts of environments. The low thickness and weight of origami robots make them easy to store, transport, and expand into functional robots when needed. The flexibility arising from a large number of degrees-of-freedom (DoF) allows robotic origami to easily mould to and interact with an object's surface such as the human body.

Although both modular and origami robots are inherently reconfigurable, the underlying architecture of existing systems limits their scalability and applicability. Modular robots are predominantly bulky collections of kinematic linkages that realise 3D structures by approximation using volumetric blocks, considerably limiting the morphological flexibility of assembled structures, with few examples countering the trend although with reduced functionality. Functional implementations have therefore mainly consisted of chains and branches that replicate kinematic structures of conventional robots. Conversely, robotic origami frequently features complex kinematic structures, taking advantage of constraints and linkages to achieve specific behaviours. However, similar to a sheet of paper, it is constrained to the dimensions of the folding structure. Once the overall dimensions, folds, and cut-outs of an origami sheet are defined, it cannot be separated and re-joined elsewhere to allow for different morphologies without damaging the structure. This implies that such robots are only configurable to morphologies that have been accounted for in the design process, greatly limiting their

The material presented in this chapter has been adapted from the following publication:

[2] **C. H. Belke** and J. Paik, "Mori: A Modular Origami Robot," *IEEE/ASME Transactions on Mechatronics*, vol. 22, pp.2153-2164, oct 2017, DOI: 10.1109/10.1109/TMECH.2017.2697310

adaptability to dynamically changing tasks. Furthermore, the materials and actuators comprising the kinematic elements of origami robots are principally ‘soft’. Although beneficial for interacting with the environment and avoiding singularities, this greatly reduces controllability and scalability.

In this chapter we address the individual limitations of such reconfigurable systems by studying the combination of origami and modularity in robotics. We analyse the requirements and scalability of this approach and present a new reconfigurable robotic system that takes inspiration from both concepts: *Mori, a modular origami robot*. A modular origami robot merges the features inherent to origami robots, namely low thickness, simplicity, and reconfigurability through folding, with the versatility achieved by modularity. The proposed concept consists of quasi-2D robotic modules that, when combined with one another, can fold up on each other to create versatile 3D configurations and fulfil tasks accordingly. We further present a first prototype, which has been implemented in multiple configurations, where each module is an equilateral triangle of thickness 6 mm, side length 80 mm, and a weight of 26 g. We finally validated the applicability of the novel concept and the accompanying prototype through three distinct, application-oriented implementations.

3.1 Conceptual analysis

A modular origami robot can fold like origami but is also entirely modular and reconfigurable. The proposed system consists of self-contained robotic modules that, when connected, can fold up on one another. When multiple modules are connected, the resulting system behaves like origami, transforming from 2D elements into various 3D configurations. While ‘modular origami’ has been explored as a way of achieving more complex folded paper-structures by joining smaller folded elements [79], our concept does not rely on this principle as individual modules are quasi-2D rather than pre-folded 3D elements. We propose an origami robot that is modular, a *modular origami robot*.

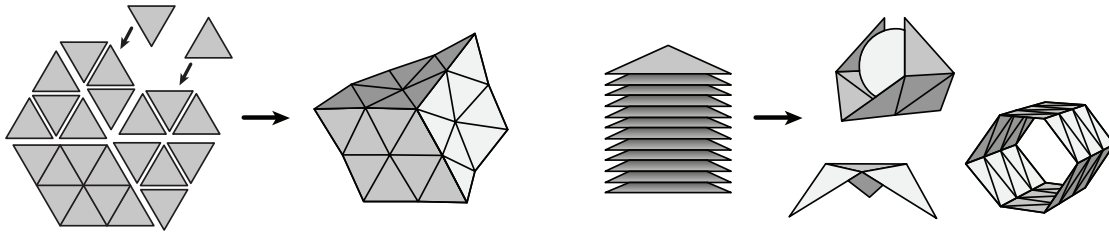


Figure 3.1 – Conceptual illustration of a modular origami robot. Left: single entities in the shape of equilateral triangles come together to form a modular reconfigurable surface. Such a surface can take the shape of an underlying object or serve as a stand-alone surface that can change its shape. Right: a stack of individual modules can be turned into a desired, task-specific shape such as a gripper, a platform, or a tube. The geometric concept illustrated in this figure is used in the development of the robot presented herein.

For a modular system to be fully reconfigurable, all modules need to be of an identical form that allows for a repeatable pattern, a lattice. While there are several 2D shapes that allow for this, including equilateral triangles, squares, and hexagons, we propose the use of equilateral triangles. This reduces the complexity of individual modules and results in a high degree of reconfigurability, as highlighted in Figure 3.1.

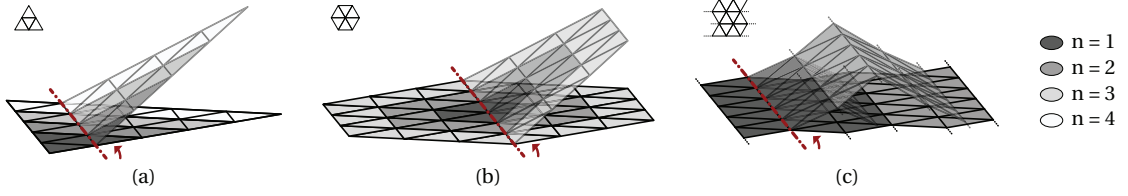


Figure 3.2 – Structural elements for analysing scalability with respect to torque requirements using the proposed geometry of modular origami robots (the folding axis is indicated by a red line): **(a)** an equilateral triangle actuated at the longest internal vertex where $n = 1$ contains four modules; **(b)** a hexagon actuated at the central vertex where $n = 1$ contains six modules; **(c)** a sheet of undefined size made up of modular robotic elements, where the fold is actuated by a single vertex and $n = 1$ lifts a single adjacent vertex.

3.1.1 Scalability

Complex assemblies and structures cannot be generalised in terms of physical requirements as these greatly depend on a variety of case-specific factors such as geometry, assembly sequence, and other reconfiguration strategies; therefore, they are often subject to optimisation. It is, however, possible to generalise the scalability of modular robotic systems on the basis of simple scenarios that are likely to pertain in a variety of cases. Figure 3.2 highlights three such scalable structures of a modular origami robot. Considering the geometries of these structures we can formulate the scaling of torque requirements, i.e. given the unscaled torque requirements we can determine the torque requirements for any scaling factor. Considering the proposed geometry of our modular robotic concept, for a scaling factor, n , the maximum torque per joint, τ^{max} , for the three example structures in Figure 3.2 is given by

$$\tau_{n=i}^{max} = \tau_{n=1}^{max} * n^2, \quad i \in \mathbb{Z}^+ \quad (3.1)$$

The maximum torque requirements of scaled elements can be reduced dramatically by optimising folding sequence and actuation pattern. Folding of elements in Figures 3.2a and 3.2b for $n > 1$ can be optimised by folding external vertices first, while folds along larger sheets such as in Figure 3.2c can be further optimised by actuating multiple vertices at once.

3.1.2 Features and requirements

Taking advantage of *origami robots*, on the one hand, requires a lightweight, reconfigurable, and low-profile architecture to allow for the transformation between quasi-2D to 3D configurations. Making a system fully *modular*, on the other hand, demands a coupling mechanism that allows any side of one module to be connected to any side of another, i.e. it must be genderless. Furthermore, while modular robotic systems rely on the combination and interaction of modules to fulfil tasks, the more self-contained each module is, the higher the versatility of the whole system. This may include attributes such as single module mobility, on-board sensing, and on-board control. Consequently, the overall requirements of a system combining modular and origami robotics can be summarised as follows. A modular origami robot needs

- to be reconfigurable at each interface with genderless mechanisms for attachment and actuation,
- to have an actuation system at each interface that allows folding over the coupling axis,
- each module to have a regular polygonal shape with a quasi-2D structure to maximise folding possibilities and range,
- to be mobile and largely self-contained.

While some of these core requirements apply to other modular reconfigurable systems, their combination constitutes the unique characteristics of a modular origami robot. Figure 3.3a provides an illustration of the requirements by a module in the shape of an equilateral triangle. Identical, genderless coupling and actuation mechanisms protrude at each edge, allowing any side of one module to be connected to another, as implemented in Section 3.2. The coupling mechanism serves as a hinge, restricting connected modules radially and axially but not in rotation. The actuation mechanism can fold and unfold connected modules and is also used for a single module to move independently when disconnected. The triangular body of the proposed modular origami robot houses all other necessary components including electronics, sensors, control components, and actuators.

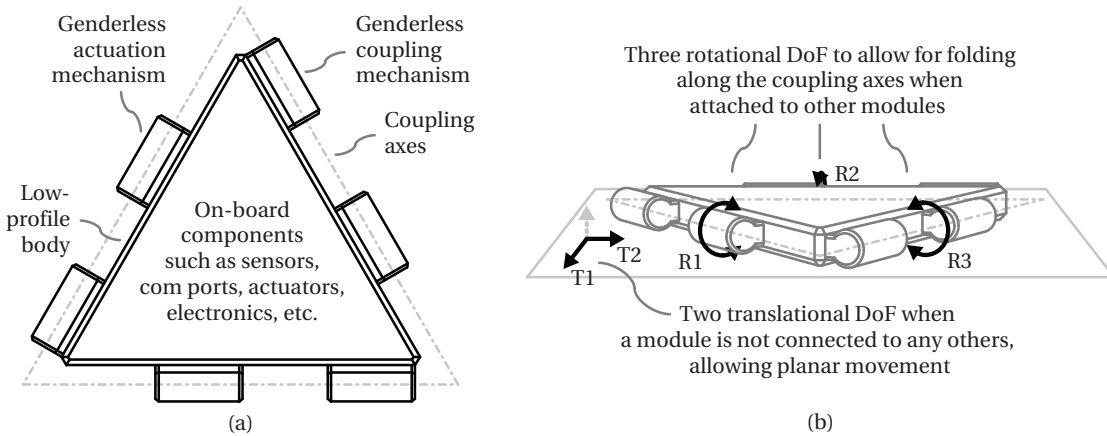


Figure 3.3 – Schematic illustration highlighting the core requirements of a modular origami robot: (a) a robotic module in the shape of an equilateral triangle with genderless mechanisms at each coupling axis and various on-board components; **(b)** each module has three rotational DoF, R, when connected to other modules and two translational DoF, T, when not connected to other modules, allowing for planar motion.

Given that the design includes a genderless and standardised coupling mechanism, additional features, components, and attachments can easily be implemented and used in tandem. This may be in the form of task-specific tools, modules with varying geometry or external support structures. The use of passive modules, simple connections between active modules where no actuation is needed, is also possible as demonstrated in Section 3.3.1. These passive modules can then be used to carry additional components, such as power supplies, or serve as structural support. Furthermore, the top and bottom faces of a module can be used to mount extra components, tools or additional modules directly to a module without affecting the geometric structure of a reconfigurable surface, as shown in Section 3.3.3. This greatly extends the potential of the modular origami concept as multiple structures, which may not be possible to combine into a single surface, can easily be joined together.

As highlighted in Figure 3.3b, the proposed concept has three rotational DoF as well as two translational DoF stemming from a single actuation system. When two modules are connected, the actuators provide rotation about the coupling axis in order to fold the two modules. However, when a module is not connected, the same actuators can drive across flat surfaces and make the robot mobile, as demonstrated in Section 3.3.2. These two modes of actuation from a single system greatly extend the robot's capabilities while maintaining mechanical simplicity.

3.2 System overview

Following the conceptual analysis of a modular origami robot this section describes our functional prototype, Mori, shown in Figure 3.4a. Its design parameters were carefully selected to address the challenges and limitations of reconfigurable robots, featuring low thickness, simplicity, and actuation at each interface of an equilateral triangle in order to achieve origami-like reconfigurability, modularity, and mobility.

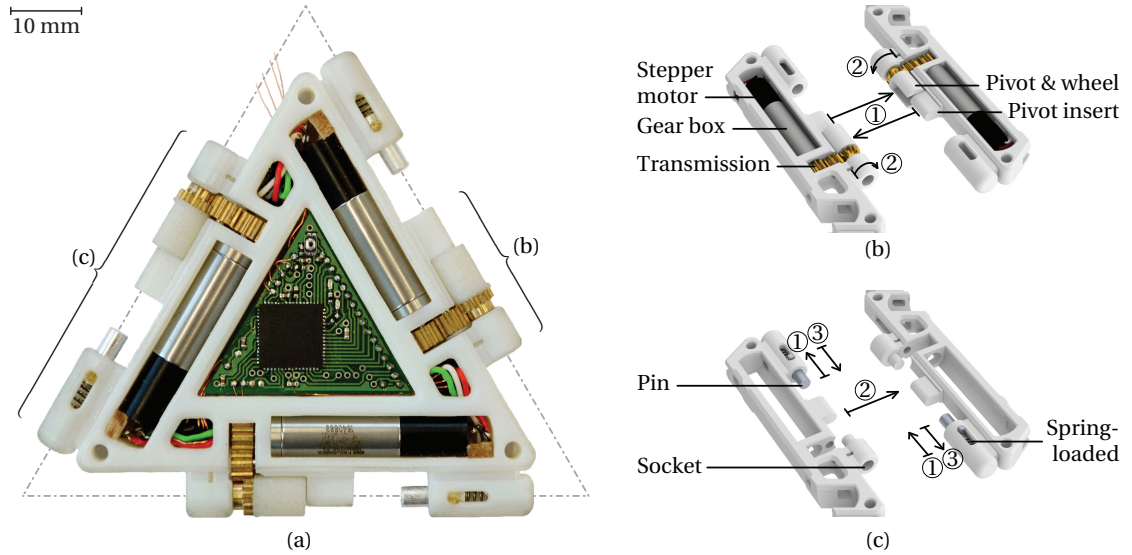


Figure 3.4 – The first functional prototype of Mori, a modular origami robot: (a) Full module with dotted lines indicating the coupling axes for attachment and folding. Two genderless mechanisms allow any side of one module to be connected to another (their sequences are shown in arrows and are numbered): (b) the drive mechanism serves both translational motion of an individual module as well as folding of two attached modules; (c) the coupling mechanisms is used to attach two modules to each other.

3.2.1 Structure and mechanisms

The first prototype of Mori is a flat robot of triangular shape. It is mobile on flat surfaces, can be attached to other modules of its kind and turn from quasi-2D shapes into 3D structures. Furthermore, the prototype is self-contained with on-board control, actuation, and sensor integration, with the exception of power supply. The robotic origami system achieves modularity through the coupling and actuation mechanisms, which in their combination account for the key characteristics of the robot, namely modularity and origami folding. Each side of a module contains both protruding and receiving elements of both mechanisms, allowing any side of one module to be connected to any side of another. The two genderless mechanisms are illustrated in Figures 3.4b and 3.4c.

As a low profile is necessary in origami robots to maximise the folding range, component selection focuses on minimising the overall thickness of the robot. The remaining dimensions are primarily defined by a minimal design that houses all necessary mechanisms and components at a minimum weight. Mori's main body has a thickness of 6 mm and the side-length of the equilateral triangle formed by the coupling axes is 80 mm. It is fabricated using a multi-jet 3D printer (Objet Connex 500). The total weight of Mori's prototype is 26 g, of which over two thirds are consumed by the actuation mechanisms in Figure 3.4b.

Actuation is provided by a stepper motor fixed in parallel to the coupling axis (Faulhaber FDM0620, 6 mm diameter, 0.25 mNm holding torque, 18° step angle). A stepper motor was chosen as it has a fixed step size, permitting open-loop position control, provides a holding torque, and can be free to rotate if necessary. A planetary gearhead with a ratio of 256:1 is attached to increase the effective torque and reduce the step size. A secondary gear system consisting of three spur gears with ratios 1:1:1.2 is installed to translate the actuation from the motor to the coupling axis. A slotted pivot is attached to the final gear in the transmission system, forming the active part of the actuation mechanism. This u-shaped pivot forms the counterpart for the insert, which is firmly attached to the housing. The engagement of actuation between two modules is denoted by ① in Figure 3.4b. The passive part of one module is inserted into the pivot of another such that when a torque is applied to the pivot it causes the two modules to fold up on one another, denoted by ② in the same figure.

The coupling mechanism, which is operated manually, consists of a spring-loaded pin that enters the socket of another module. The pin is first retracted, denoted by ① in Figure 3.4c, and the two engaging modules are brought together by aligning their coupling axes, denoted by ②. The pin is then released so that the spring-loaded mechanism locks the two coupling axes to one another, denoted by ③ in the same figure. A hinge is thereby formed, restricting motion radially and axially, so that only folding about the coupling axis is possible when two modules are connected.

3.2.2 Electronics and control

The unique concept behind Mori requires a special electronics design to account for the specific components and computational needs of the robot. In order to have full control over the behaviour of the three stepper motors, each motor requires 4 PWM channels that are transformed into the necessary signals for the motor windings through H-bridges. Furthermore, the on-board controller must be powerful enough to compute live kinematics and apply closed-loop control.

We use a 16-bit microcontroller, PIC24EP512GP806 from Microchip, with 64 leads and dimensions of 9 x 9 x 0.9 [mm] running at 3.3 V. It is configured to provide 12 PWM outputs (4/motor), two reconfigurable communication ports (UART, I2C, etc.), three digital input and three digital output pins, three analogue input pins and two status LEDs. The PWM channels are connected to three motor driver chips, Texas Instruments DRV8835. All electronic components are mounted on two triangular PCBs, placed on top of each other in the centre of Mori's body. The current prototype consumes around 600 mA when all three motors are active and requires four external connections to operate; two for power and two for serial communication. Current draw from the motors can be reduced by adjusting and optimising their on-time, which is necessary when incorporating internal power supply. Presently available batteries with a high current-drain that fit the current housing (with modifications to the PCB) can provide 50 mAh for a motor-runtime of 5 minutes with the current firmware at a weight of 1.2 g.

Application specific components, such as accelerometers and proximity sensors in Section 3.3.3, can easily be connected to the existing communication ports. The six digital pins are accessible but unconnected in the current version to allow for synchronisation and communication amongst neighbouring modules in the future. For this purpose a communication protocol needs to be established which synchronises actuation and provides information about neighbouring modules.

Mori's electronics allow for various forms of closed-loop control to be implemented depending on the task and configuration at hand. Angular position sensors can be added to provide position feedback of the motors or the folding pivots, other on-board sensors can provide position feedback based

on the device's kinematics, or external sensory systems can be implemented to provide the relevant control signals. The latter two methods are demonstrated in Section 3.3.3 in the form of an on-board accelerometer and a proximity sensor, as well as an external camera tracking system.

3.2.3 Performance

Each module is self-contained and has three separate actuation systems. The motor signals for each actuation system are updated at a frequency of 800 Hz resulting in a maximum motor speed of 200 steps/s (one step is 0.06°) or 2 rpm. The effective driving torque at the coupling axis of a module is around 30 mNm, accounting for gear ratios and transmission efficiencies. Therefore, when two modules are connected and their actuation is synchronised, the effective torque at the hinge is 60 mNm. Considering a weight of 26 g and a moment arm of 23 mm, the required torque to lift one module from a horizontal position is 5.9 mNm. Connecting two further modules to the remaining edges of the module being lifted, the torque required to lift them from a horizontal position rises to 30 mNm. Lifting a total of six modules connected in a hexagon from one of its external edges would require a total torque of 106 mNm per hinge, which exceeds the capabilities of the current system.

However, reconfiguration strategies can be adjusted to minimise the maximum torque experienced by each joint at any given time, increasing the likelihood of a target shape being achievable. For example, connecting three modules to a central one yields an equilateral triangle of double the side length, which is used in Sections 3.3.2 and 3.3.3. If all four modules are fully assembled, the total weight of the configuration is 104 g. The corresponding torque required to lift the central module from a horizontal position using only one of its neighbouring modules is 70 mNm, exceeding the capacity of the current system. However, this can be overcome by initially using multiple neighbouring modules to lift the centre and subsequently lowering the remaining joints until the target position is achieved. Thus, the possibility of transforming from a 2D or 3D configuration into another 3D shape is subject to optimisation.

3.3 Case studies

Reconfigurable modular robots are intended to provide system that can adapt their shape and function depending on a desired task [22]. Thus, a specific modular robot does not have a unique task it is designed for and it is difficult to evaluate the performance of such a system by means of a single function. This would diminish the significance of other potential tasks and thereby unjustly bias the robot's evaluation. By contrast, a singular modular robotic system can be evaluated by means of a number of different scenarios that demonstrate a multitude of functionalities, with specific attention to the set of key attributes of the robot.

The following three application-oriented implementations of our prototype were selected to demonstrate the versatility of the system and highlight the features that define it. The first implementation displays the robot's origami-inspired reconfigurability and modularity in the form of a reconfigurable modular surface, followed by a demonstration of its mobility on flat surfaces and manoeuvrability in small spaces. Finally, the prototype of our modular origami robot is integrated within a closed-loop manipulation experiment, where a ball is balanced on a floating three DoF platform assembled from the robot's modules.

3.3.1 Modular reconfigurable surface

The concept of a modular origami robot, as proposed in Section 3.1, combines both modular and origami robotics to enhance the system's flexibility and applicability. In the following demonstration the two defining aspects of Mori, namely modularity and origami, are highlighted. Six modules are connected in a closed chain, forming a *modular reconfigurable surface* in the shape of a hexagon, which then folds up on itself to create multiple structures. Two fully functional Mori prototypes are used along with four passive ones, which consist of Mori's frame and only have the components for the coupling mechanism embedded. This allows testing of the modularity and reconfigurability of the system without the need to produce larger quantities of fully functional robots. The two active modules are connected opposite one another in order to separate the two uncontrolled rotational joints, which become constrained through symmetric actuation of the active modules.

The connection sequence of the modular hexagon is shown in subset M1-M3 of Figure 3.5. This six-piece element forms the only possible configuration of modules around a single vertex that is entirely flat (valency equal to six) and can be extended indefinitely by adding further modules. It is thus the base element for reconfigurable surfaces made up of modular origami robots. Once connected, the surface is controlled manually to re-create three combinations of origami folds as shown in subset R1-R3 of Figure 3.5. R1 represents a simple mountain fold, R2 combines one mountain fold with two valley folds, and R3 shows a combination of three reverse folds. These configurations are examples of a large number of possible shapes that a reconfigurable surface of modular origami robots can assume.

We have hereby developed a modular robotic system that is capable of reproducing surfaces in 3D. While most physical displays capable of re-creating surfaces do so in 2.5D with protruding linear actuators, our robot is capable of producing surfaces in full 3D with a relatively low surface thickness. This can be used to interactively visualise computer generated surfaces and structures. Increasing the number of modules in the system improves the approximation of surfaces while altering the number of modules around a single vertex enables the re-creation of more complex and non-developable surfaces

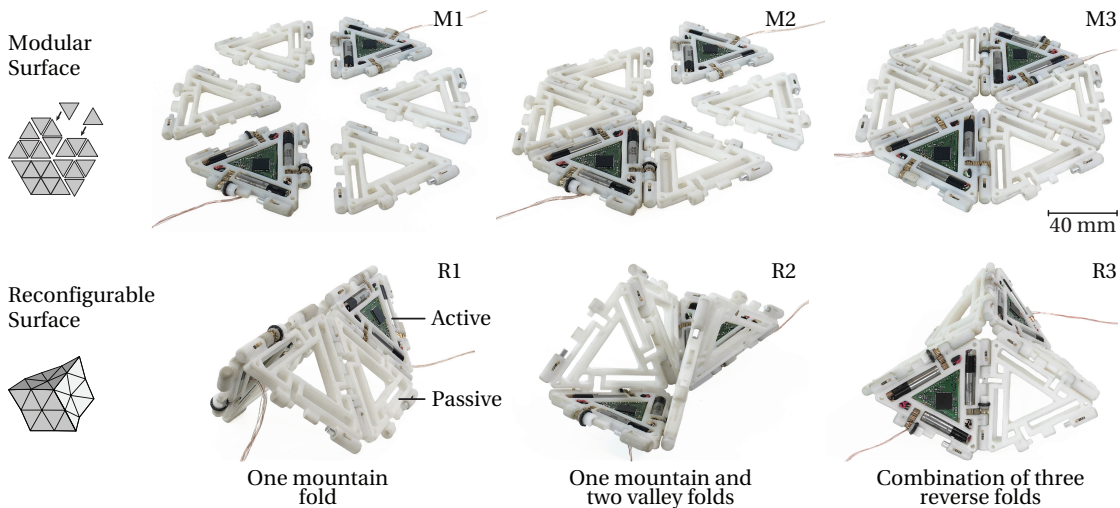


Figure 3.5 – Modularity and origami demonstration using two active modules along with four passive ones. The top row shows how the 6 pieces come together to form a modular reconfigurable surface in form of a hexagon. The bottom row shows three surface configurations that are achieved by the modular robotic system using the origami principle of folding surfaces to create 3D structures by manually controlling the active modules.

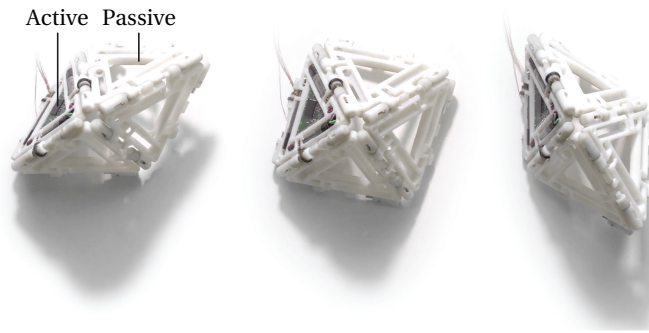


Figure 3.6 – A configuration of four Mori modules forming a pyramid. Three images with different angles between the modules are shown. The configuration has one active degree of freedom, such that one active module is enough to fully control the shape of the pyramid.

and structures. Figure 3.6 shows a configuration of four modules around a single vertex, forming a four-sided pyramid without a bottom face. As the number of effective degrees of freedom is reduced to one, a single active module is enough to fully control the configuration.

This demonstration emphasises the advantages gained by bringing together modularity and origami folding in our robot. Modularity allows the system to be assembled into any formation desirable while origami-inspired folding permits it to reconfigure from 2D modules into various 3D structures.

3.3.2 Mobility demonstration

Reconfigurable modular robots typically operate and fulfil tasks in collaboration with one another. However, it is also desirable for a single entity to be mobile, as this further increases the system's versatility and possible functions, as discussed in Section 3.1.2. The current prototype is turned into a mobile-type reconfigurable modular robot by incorporating rubber o-rings into each rotating pivot, turning them into wheels that slightly protrude the device's thickness. This allows a single module to drive in different directions on flat surfaces by using combinations of rotational speeds and directions of the three wheels, M1-M3, as illustrated in Figure 3.7. Initial tests of the robot's driving performance on a relatively smooth MDF surface showed a speed of around 3.5 mm/s.

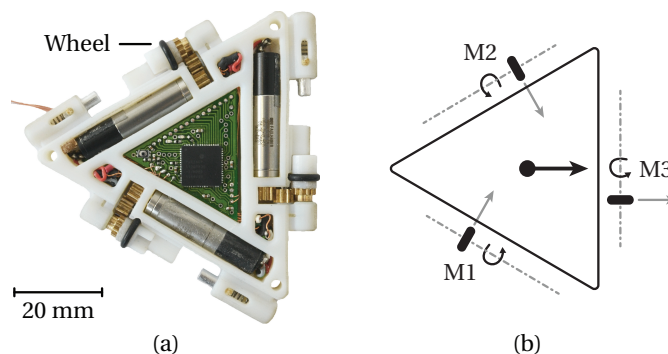


Figure 3.7 – Mori turns mobile – a single Mori module with three motors can travel across flat surfaces: (a) a rubber o-ring is attached to each rotating pivot and serves as a wheel; (b) a module can then travel between tasks or configurations by combining different rotational speeds and directions of the three wheels.

Being mobile not only allows a module to travel between locations where it is coupled and used as part of a larger structure, but also to access small spaces and perform manoeuvres within. As a result of its low thickness and quasi-2D profile, the robot is able to drive through gaps as small as 7×70 [mm]. We have prepared the following demonstration to highlight our prototype's mobility and manoeuvrability: A module enters a room through the gap underneath a door and is thereafter used to pick up an object, connect to three other modules, and reconfigure into a container.

The module is controlled using a joystick by a user who first steers the robot from one room into the other. The user subsequently drives the robot towards an object, in this case a Lego figure, which is considered to be located out of the user's reach, such as underneath a bed. The object is then moved onto the robot's surface using environmental constraints and driven towards three other, passive modules, which are attached by the user. The configuration of four modules is then folded up to form a modular container in form of a three-sided pyramid, a regular tetrahedron. Figure 3.8 shows a sequence of frames taken during the demonstration.

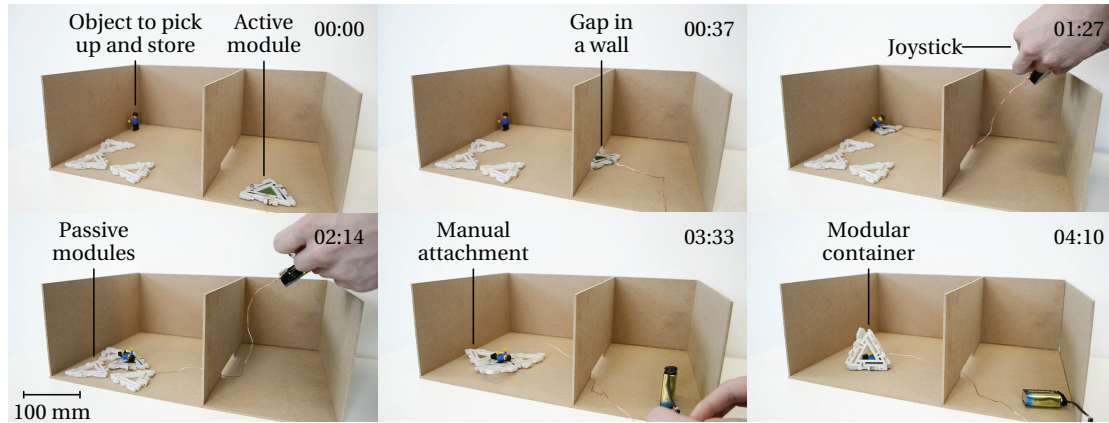


Figure 3.8 – Demonstration of Mori's mobility and manoeuvrability: A module is steered through a gap in a wall from one room into another and used to pick up an object from outside of the user's reach. The robot is subsequently driven towards three other modules, which are attached by the user. The four modules are then folded into a container in form of a regular tetrahedron. As seen in the images, the prototype is connected to an external joystick and a battery.

This implementation of our robot illustrates the importance of mobility in modular robotic systems and highlights the advantages of a modular origami robot in comparison with other types of robots. Due to its small size and low profile the prototype is able to pass through unknown and small openings while its modularity enables large volumetric expansions and dimensional reconfigurations.

3.3.3 Closed-loop manipulation

In the final implementation using our prototype, Mori is coupled with an external camera system to manipulate an object. This scenario provides an example of our modular origami robot being applied to a real-life situation where it is automatically controlled and interacts with its environment and objects within. For this purpose three passive modules are attached to a central active one and fold down such that the central module is lifted. A floating platform with three DoF is thereby formed which is then used to balance a ball on its surface. A kinematic analysis of the system is followed by a ball-balancing experiment using our current prototype.

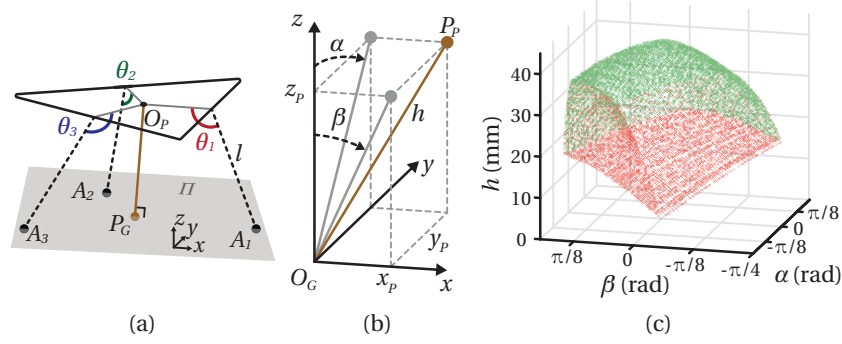


Figure 3.9 – Illustrations and notations used in the kinematic analysis of the floating three DoF platform. Due to the platform floating on a low-friction surface, forward and inverse kinematics use two different notations that are directly relatable. Please note that the figures in (a) and (b) are not to scale, nor do the two depictions represent the same set of variables. **(a)** In the forward kinematics the centre of the platform is the origin, O_P , and the three leg endpoints $[A_1, A_2, A_3]$ form the plane Π , which represents the floor but has no fixed frame of reference. **(b)** The inverse kinematics denote point P_P as the centre of the platform, which is defined by the three control parameters α , β , and h , and the origin O_G is the point where the normal to the platform connects point P_P to the ground. **(c)** The workspace of the platform shows the possible combinations of the three control parameters. Green points denote maxima and red points minima of the enclosed envelope.

Although conceptually similar to a simplified Stewart platform [80], its kinematics are distinctive due to the lack of a fixed frame of reference for the base. Therefore, the centre of the platform is taken to be the origin, O_P , for developing the forward kinematics, as shown in Figure 3.9a. The ground plane, Π , is formed by the endpoints of the legs, $[A_1, A_2, A_3]$, whose coordinates are given by Equation (3.2) in terms of the length of each leg, l , and the angles between the legs and the platform, $\theta_{i=1,2,3}$, where $90^\circ \leq \theta_i \leq 180^\circ$.

$$A_1 = \begin{bmatrix} l(1/3 - \cos(\theta_1)) \\ 0 \\ -l \sin(\theta_1) \end{bmatrix}, A_2 = \begin{bmatrix} (l/2)(-1/3 + \cos(\theta_2)) \\ (l\sqrt{3}/2)(1/3 - \cos(\theta_2)) \\ -l \sin(\theta_2) \end{bmatrix}, A_3 = \begin{bmatrix} (l/2)(-1/3 + \cos(\theta_3)) \\ (l\sqrt{3}/2)(-1/3 + \cos(\theta_3)) \\ -l \sin(\theta_3) \end{bmatrix} \quad (3.2)$$

The three parameters of interest for the kinematic analysis are α and β , the angles about the x- and y-axis respectively, as well as the height of the platform, h , which is the shortest distance between the origin and the plane Π . A plane equation for the plane Π can be found by determining the normal vector, $\vec{n} = [a, b, c]$, through the cross product of two lines between coordinates A_1 , A_2 and A_3 , yielding $ax + by + cz = d$, where $d = ax_i + by_i + cz_i$ and $i = 1, 2, 3$. The coordinates of the intersection point, P_G , of the line orthogonal to plane Π passing through the origin is then given by

$$P_G = \begin{bmatrix} 0 \\ 0 \\ 0 \end{bmatrix} + \vec{n}s = \begin{bmatrix} as \\ bs \\ cs \end{bmatrix} \quad (3.3)$$

where s can be found by substitution into the plane equation such that $s = d/(a^2 + b^2 + c^2)$. The three relevant kinematic parameters are then given by

$$\begin{aligned} \alpha &= \arctan(b/c), \\ \beta &= \arctan(a/c), \\ h &= \sqrt{(as)^2 + (bs)^2 + (cs)^2} \end{aligned} \quad (3.4)$$

In order to implement closed-loop control based on the position of the platform, the three kinematic parameters need to be inversely related to the three control output angles θ_1 , θ_2 and θ_3 . An arbitrary point on the ground plane is taken as the origin, O_G , to establish a fixed frame of reference for the ground. Given parameters α , β and h , the coordinates of point P_P , illustrated in Figure 3.9b, can be found by substituting x_p , y_p , and z_p for as , bs , and cs respectively in (3.4). Finding x_p , y_p , and z_p yields the plane equation for the platform, $x_px + y_py + z_pz = h^2$. Substituting the expressions for the coordinates of points A_i from (3.2) into this plane equation yields three equations for the three output angles θ_1 , θ_2 , and θ_3 , given by

$$\begin{aligned} x_pl(1/3 - \cos(\theta_1)) - z_pl \sin(\theta_1) &= h^2 \\ (x_pl/2)(-1/3 + \cos(\theta_2)) \\ + (y_pl\sqrt{3}/2)(1/3 - \cos(\theta_2)) - z_pl \sin(\theta_2) &= h^2 \\ (x_pl/2)(-1/3 + \cos(\theta_3)) \\ + (y_pl\sqrt{3}/2)(-1/3 + \cos(\theta_3)) - z_pl \sin(\theta_3) &= h^2 \end{aligned} \quad (3.5)$$

Given a set of desired variables α , β , and h , the bisection method can then be used to solve the expressions in (3.5) above to yield the three desired angles θ_1 , θ_2 , and θ_3 for closed-loop control, since the interval for its value is known. A workspace analysis has been performed, depicted in Figure 3.9c, showing the possible range of motion in terms of α , β , and h .

The practical implementation of this three DoF platform using our modular origami robot is shown in Figure 3.10. The control loop is closed by attaching an accelerometer to the top of the central module (ST LSM303D), returning angles α and β , and a proximity sensor to the bottom of the central module (ST VL6180X), returning height h . The platform is then coupled with a Simulink model and a camera to balance a ball on its surface. A 100 x 100 [mm] wooden plate is placed on the centre module to provide an even surface and slightly enlarge the balancing area.

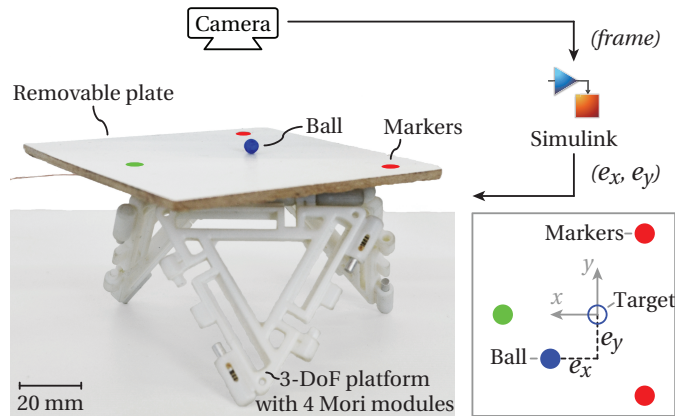


Figure 3.10 – Testing setup to evaluate the floating three DoF platform consisting of modular origami robots. One central module is connected to three passive ones and a flat plate is mounted with coloured markers; a camera feeds image frames into Simulink, which analyses the errors in x and y of the distance between the ball and the centre of the module. The errors are passed to the central module, which performs closed-loop control of the tilt angles to ensure the ball is balanced on the surface.

The Simulink model determines the location of the central module by tracking three coloured markers (one green and two red) as well as the location of a blue ball, depicted in Figure 3.10. The markers are identified by extracting a binary version of the input image with separate colour outputs of red, green, and blue, with auto-threshold and blob analysis in place. The model continues to calculate the distance of the ball to the centre of the module in terms of x and y , e_x and e_y respectively. The two resulting values are sent to the module via serial communication at a frequency of roughly 15 Hz.

The ball coordinates e_x and e_y are used by the module as the error signal for PD control, controlling the angle of the platform, in order to balance the ball on its surface. The height of the platform, h , is kept at a constant 25 mm and the angles of the platform are changed according to the position of the ball. The module calculates the change in angle of each leg based on a change in the angles of the platform by using the inverse kinematics described previously. Since the range of motion during balancing is within $\pm 5^\circ$ for both α and β , the change in leg angle relative to the platform angles is taken to be linear (real errors of a linear fit are less than 5%).

The following test validates the capabilities of the balancing platform: a ball is placed in one of the corners of the platform while it is even. The centre of the triangle, indicated by the three markers, serves as the target position and the platform moves the ball to the centre. Figure 3.11a shows the mean error and standard deviation of all ten repetitions while Figure 3.11b shows the recorded trajectory from five selected samples. An accepted error band of 15 mm was introduced, both in the control and in the figures, to account for a slight roughness of the surface and unevenness of the ball. The ball was successfully balanced on the surface in all ten repetitions of the test and reached the accepted error band in less than 7 s.

This ball-balancing experiment effectively demonstrates how our prototype of a modular origami robot can be configured to manipulate objects, further manifesting its ability to change shape and function depending on the task at hand. The incorporation of external sensing systems and additional on-board sensors into a closed-loop application highlights the versatility of the system towards a viable modular robotic framework that can tackle even more complex engineering problems. While its performance with respect to the balancing task cannot be compared with dedicated, single-purpose systems, it does show that our robot is highly reconfigurable towards a multitude of functions.

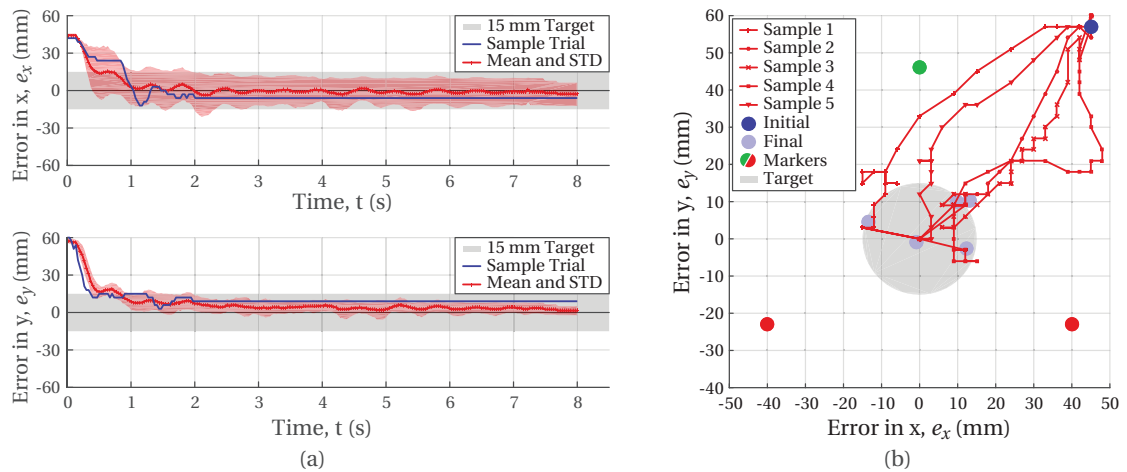


Figure 3.11 – Testing results of the modular origami robot platform balancing a ball: (a) errors e_x and e_y of one sample trial, mean and standard deviation, STD, of all trials and 15 mm target zone; (b) trajectory of five selected samples from starting point to final position in terms of errors e_x and e_y .

3.4 Discussion

In this chapter, we address the challenges of morphological flexibility in modular robots in terms of scalability, as well as design and control approaches. By studying the combination of the concepts behind both modular and origami robots, we demonstrate the enhanced versatility and applicability of modular origami robots and overcome their individual limitations. We provide a detailed analysis and implementation of the concept through a modular origami robot that is quasi-2D, light weight, and at the same time fully reconfigurable, modular, and mobile, greatly extending its potential use in various fields such as human-robot interaction.

Along with the conceptual introduction and analysis, we present Mori, a first prototype of a modular origami robot. Mori has a low-profile triangular structure with a manual coupling mechanism and a folding actuation mechanism at each edge. It is mobile on flat surfaces, can be attached to other modules of its kind and fold into any 3D configuration desirable. Three functional implementations using the current prototype are presented in order to demonstrate, analyse, and evaluate its key characteristics.

The first demonstration highlights the modularity and origami-inspired reconfigurability of the system by implementing it in form of a modular reconfigurable surface. Similarly, the demonstration of mobility highlights the advantages of modular systems being mobile and effectively uses modularity to achieve large volumetric expansions. The final experiment consolidates the versatility of the modular robot by configuring into a floating three DoF platform for object manipulation. Integrating on-board sensors and an external camera allows the robot to balance a ball on its surface and shows how this system consisting of relatively simple entities can realise more complex engineering solutions.

While the individual implementations of our robot may not match the performance of dedicated single-purpose systems, the potential of reconfigurable modular robots lies in the ability to change shape and function depending on the task at hand. Such systems are therefore best evaluated by considering how well they can adapt their functionality for different purposes and successfully accomplish a variety of tasks. This, however, bears the risk of overlooking the practicality of modular robots in real scenarios, as the ability to carry out a range of tasks does not imply general superiority over individual systems for each function. While the focus of this work is to study and analyse new methods and architectures for reconfigurable systems in order to promote their viability, the underlying limitations of each approach, and modular robots in general, must be carefully considered.

Although combining the concepts behind both modular and origami robots addresses a variety of challenges in reconfigurable systems, it is accompanied by new obstacles. The increased flexibility of the overall structure, transforming from 2D modules into 3D configurations, confines the possibilities in terms of mechatronic design and thereby the functional performance of the system. Merging the coupling mechanisms and kinematic joint between neighbouring modules, although it simplifies the fundamental structure, further complicates design and operational requirements. An equilateral triangular shape allows each edge of one module to connect to any other, but also limits possible shapes, configurations, and kinematic structures that the system can assume. Furthermore, some general restrictions of modular robots remain, such as requirements in terms of force, power, computation, and control, which limit the overall scalability of such systems.

These challenges and drawbacks confine the possibilities of our approach, and reconfigurable robots in general, while the underlying potential of systems that can address a wide range of tasks and functions prevails. The concept of a modular origami robot represents an advancement towards this

goal, simplifying the underlying architecture and improving the structural and functional versatility. This promising outlook calls for further work on such systems, including control strategies, analysis of the structural possibilities of the platform, as well as hardware extensions such as automated coupling and power autonomy.

4 Automatic coupling mechanisms for modular systems

A modular origami robot, as proposed in the previous chapter, addresses scalability and applicability of reconfigurable systems by merging the low profile, simplicity, and flexibility inherent to origami robots, with the versatility of modular robotic systems. In this chapter we further address the challenges associated with reconfigurable robots by studying the coupling between entities in a modular system. We analyse the overall requirements of automatic couplings and further explore the possibilities of modular origami robots by presenting a novel mechanism that greatly extends the system's capabilities and provides solutions to a number of key concerns in modular systems in general.

As modular robots are intended to fulfil tasks by combining multiple entities into specific structures, the mechanism by which modules connect to one another is one of the crucial aspects that define the system's characteristics and behaviour. The interface between modules must fulfil a multitude requirements to ensure the functionality of the overall system and thus poses significant challenges [22]. Given a particular architecture of the system, the coupling mechanism must address and cope with kinematic and kinetic constraints, embedded actuators and sensors, and the transfer of various mechanical and electronic interactions.

4.1 Coupling features

Couplings can either be gendered [81], with distinct sets of complementary features and reduced functionality, or genderless (hermaphroditic), such that any side of one module can connect to any side of another [82–84]. Genderless couplings greatly extend the reconfigurability of a modular system but are generally more bulky and complex due to the need to incorporate both male and female features into each interface. Bulky couplings reduce the range of motion of the robot and complex mechanisms elevate the demand for high precision. Various coupling methods have been proposed including mechanical [85], magnetic [49], solder-based [45], and pneumatic [86], with the majority utilising either mechanical or magnetic systems [23].

The material presented in this chapter has been adapted from the following publication:

[87] **C. H. Belke** and J. Paik, "Automatic Couplings With Mechanical Overload Protection for Modular Robots," *IEEE/ASME Transactions on Mechatronics*, vol. 24, pp.1420-1426, jun 2019, DOI: 10.1109/TMECH.2019.2907802

Magnetic connectors have been implemented as passive couplings using permanent magnets [88], as a guide during the reconfiguration process [89], and as active couplings using electromagnets [90]. To overcome the high power-consumption of electromagnets, semi-permanent magnets have been used as a semi-permanent interface [91]. Magnetic connectors are a relatively simple solution and fulfil various requirements of couplings such as automatic alignment. However, the low strength provided is oftentimes a disqualifying characteristic as it must be balanced with the ability to disengage modules and misalignment under load. Mechanical couplings are more common in *self*-reconfigurable systems [90] and are usually based on hooks or latches. While they are generally more complex than magnetic couplings, they offer more design freedom for the embedded mechanisms and their specifications. Their components are most commonly driven by DC motors although some systems utilise shape-memory alloy (SMA) actuators [92]. Many mechanical couplings also have self-alignment features that centre connectors during the docking process [93]. Some mechanical couplings are further able to perform single-sided disconnects when a module fails [83].

Besides a mere physical connection, couplings of modular robots provide the only physical interface to communicate with and sense neighbors. While many systems utilise wireless communication [90], a physical communication stream can provide a simple way to identify neighbors and their orientation [83]. Such a connection can also serve to synchronise neighbors and validate their status during locomotion of multiple modules [22] and when multiple units drive the same joint.

Each type of modular robot comes with a distinct set of challenges that depend largely on the overall design of the system and can vary greatly. In most modular robots the coupling mechanism is separated from any active DoF that changes the robots morphology. By contrast, in a system of light-weight quasi-two-dimensional (2D) modules that reconfigures by folding into three-dimensional (3D) structures [2, 68, 94] the coupling axis is also the active folding axis between two modules. The coupling mechanism must thus be fully integrated within the actuation mechanism of the folding link, while maintaining a compact, slender architecture. The mechanism presented herein has a specific design resulting from the unique requirements of a modular origami robot. Its functionalities and novel features, however, are applicable to a large spectrum of modular and reconfigurable systems.

Due to the large number of DoFs in modular robotic systems, individual modules are prone to damage as small forces are amplified through kinematic chains and singularities. More complex, single-purpose robots generally employ an abundance of sensors, both external and within the drive system, to ensure the system's limits are not exceeded. This, however, is not feasible in multi-robot systems due to the added complexity of individual modules, the necessary computational power, and the remaining danger from failure of the control system.

In this work we propose the use of mechanical overload protection features embedded in each active DoF of a module. Such a mechanism does not interfere with the robots functionality during normal operation and thus does not weaken the robot. Instead, it intervenes only when a force threshold is surpassed, outside of the normal operating conditions. Mechanical overload protection has previously been proven useful in human robot interaction [95] and damage prevention in humanoids [96]. Modular robots with magnetic interfaces automatically have some degree of overload protection built in, as the coupling disengages when magnetic forces are exceeded. There is, however, a trade-off between the strength of the coupling, and hence the ability to build larger structures, and the maximum force required to disengage modules. In this chapter we present a novel overload protection mechanism for mechanical couplings that does not interfere with the system during normal operation and at the same time ensures that no excessive forces are present.

4.2 System overview

Taking full advantage of modular robots requires each module to be equipped with an automatic coupling mechanism allowing the system to self-assemble and reconfigure into any desired configuration. The coupling must incorporate various features that ensure full functionality of the system such as sensing and actuation of the connection mechanism and any associated DoFs. Additional features may furthermore be required depending on the overall design of the modular robot and any imposed constraints. In this section we discuss a variety of coupling elements and present a design for a modular origami robot that fulfils these requirements while also providing the technological building blocks for a wide range of modular robotic systems. The design of the coupling is depicted in Figure 4.1.

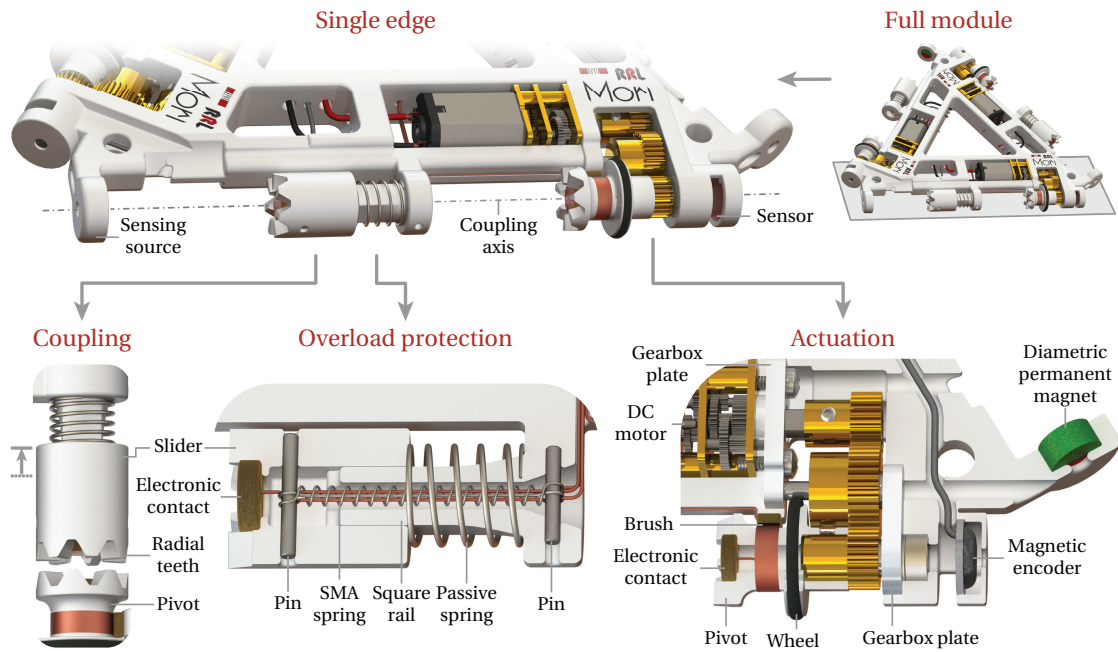


Figure 4.1 – Design overview of the automatic coupling mechanism with mechanical overload protection. Top: visualisation of a whole module (excluding internal components) and a single edge with one complete coupling mechanism. Bottom: visualisation of coupling, detailed section view of the overload protection, and actuation system.

4.2.1 Functional features

A modular robotic systems exhibits the greatest amount of flexibility in terms of reconfiguration and module allocation if any edge or face of one module can connect to any edge or face of another module. This can be achieved by incorporating both male and female coupling features (or other types of matching elements) into each edge or face, effectively making the coupling mechanism genderless (or hermaphroditic). Each edge in our design is identical and contains all functional features, as shown in the full module illustration in Figure 4.1, resulting in a genderless mechanism.

A modular origami robot has a quasi-2D structure with hinges that enable origami-like folding about the coupling axis. In order to maintain this low thickness, all components that must be aligned with the coupling axis (i.e. cannot be moved to the center of a module) must be contained within a cylinder

of a diameter equal to the device's thickness. This includes actuation elements of the coupling and of the rotational DoF, sensing of the angle, and electronic connections.

The design of the coupling mechanism incorporates various mechanical elements that greatly extend the capabilities of modular origami robots. In order to incorporate these features and to reduce the cost of a single module, the overall size compared to our previous prototype [2] is about 67% larger while maintaining the same slenderness ratio. The length of the coupling axis is 133 mm and the thickness of the design is 10 mm. The main body of a module is fabricated using a multi-jet 3D printer (Objet Connex 500), allowing us to incorporate detailed mechanical features into the body and to reduce the number of parts. The mechanical design of the coupling mechanism includes the following features.

Coupling mechanism

The first version of our modular origami robot was specifically designed to enhance flexibility and applicability, but could only be connected to other modules manually by retracting a spring-loaded pin, and only when modules were at 180° to one another. In this design we overcome these limitations by using a similar mechanism of connection, with a retractable element that engages with another module, as shown in the coupling illustration in Figure 4.1, but with a new approach to the method of retraction as well as additional features.

A retraction-based coupling mechanism switches between two states or positions during a coupling process, one state allows for coupling and decoupling, while the other ensures a steady connection between two modules. Since a module is likely to be in the latter state most of the time, whether it is connected to another module or not, an automatic coupling mechanism should be designed to minimise, or eliminate, power consumption in this state. In this design we employ an SMA spring, which provides a contractile force when heated, in order to retract the coupling element to an open state. The use of a joule-heated SMA actuator allows us to greatly simplify the retraction mechanism, minimise its size compared to traditional actuators, partly thanks to their high force-density, and eliminate power consumption when closed.

The coupling element, or slider, runs on a rail of square cross-section attached to the main body, with minimal clearance, which allows sliding along the coupling axis but forbids rotation. A passive spring placed around the square pin ensures the coupling element returns to a closed state once the SMA spring goes back to a cold state and loses its contractile force. The maximum extension is restricted by a string connecting the coupling element to the base of the square shaft. These design elements are depicted in the overload protection illustration in Figure 4.1.

The front face of the coupling element has specially designed radial teeth, the design of which are covered in more detail in Sections 4.2.1 and 4.3. The teeth of the coupling element engage with identical teeth on a pivot of another module and thus transmit the rotational actuation. A radial design not only ensures a smooth mesh during operation, it also makes the coupling elements self-centring. When the distance between the axes of the two opposing elements is within a certain error-band, the two axes automatically align during the engagement process. This misalignment tolerance is addressed in Section 4.4.

Actuation

In order to minimise the size of a module, the rotational actuator is embedded in the main body of the module, away from the coupling axis. Three gears transmit the torque from the motor to a pivot on the coupling axis. The actuator is a DC motor with a 297.92:1 reduction ratio from Pololu and the three gears have a module of M0.3 with 20, 30, and 20 teeth respectively.

The gearbox is precisely located and reinforced using two CNC-machined polyacetal (POM) plates, one on each side of the gears. The motor is mounted to one of the plates, which has a location boss for both the motor and the main body. The shaft of the middle gear is mounted between both POM plates, ensuring alignment along the drivetrain. The final gear is fixed to a cantilevered shaft that is held by two bearings, one of which is press-fit into the POM plate, the other into the main body. The pivot with radial teeth fits onto the hub of the final gear and is held in place by its grub screw. The actuation mechanism is shown in Figure 4.1.

A single module is furthermore mobile on flat surfaces when no other module is connected to it, thanks to a wheel incorporated into each pivot. Two modules can therefore drive towards one another, retract the coupling mechanisms, align their axes, and successfully couple without user intervention. When a configuration of multiple modules is assembled, the wheels of unconnected edges can also be used to make the overall assembly mobile.

Overload protection

Due to the high number of DoFs and kinematic constraints in modular robotic systems, modules and couplings are prone to damage. In order to protect the mechanical assembly of the modules from damage, and make them safer for human interaction, we have developed a mechanical overload protection mechanism. This mechanism disengages two connected modules when the coupling experiences a torque higher than a certain threshold. The threshold is defined by a number of design parameters of the coupling, introduced in Section 4.3, and can therefore be easily adjusted.

The overload protection mechanism is incorporated into the design of the coupling such that it shares most of the mechanical features with the retraction mechanism. The two engaging pieces of the coupling, namely the pivot and the slider shown in Figure 4.1, have radial teeth with angled faces such that a torque applied to the coupling also produces an axial force away from the coupling interface. When this axial force overcomes the frictional forces both on the teeth and between the slider and the square rail, the slider moves to an open state. A detailed analysis of this mechanism is presented in Section 4.3.

4.2.2 Electronics and control

An automatic coupling for modular robots not only requires an actuated mechanism to connect to another module, it must also be able to detect whether a connection is made, active, or lost. When coupled, a module must furthermore be aware of its state relative to the connected module. We propose the following solutions, implemented in our design, as follows.

Sensing

As soon as a connection between two modules is made, each module must be aware of the absolute angle between them. This means that the sensing source cannot be on the same module as the corresponding sensor as this would only provide information about the rotation of the pivot. A passive sensing source, such as a permanent magnet, is therefore ideal, as it reduces the number of electronic connections between modules. In our design we use a cylindrical, diametric magnet fixed inside the housing, with the same orientation in each module. An absolute magnetic encoder (AS5048B from AMS) on another module can then sense the angle between the two modules as soon as their axes are aligned.

Synchronisation

Since all sides of a module are identical, there are two actuators driving the same link when two modules are connected. If the actuation of these modules is not synchronised, there will be an increase in power consumption and potentially damage to the drive mechanism. It is therefore vital to synchronise the actuation of two such modules when driving the same link. In order to do so we have incorporated electronic connections into the coupling elements, the slider and the pivot, with one input and one output for each side of a module, as shown in Figure 4.1.

The electronic connection consists of a cylindrical sponge that compresses to ensure a stable contact and a copper layer glued to the surface. Since the pivot can rotate continuously, an additional brush is used to connect the electronic contact of the pivot to the controller. This brush also consists of a sponge and a copper layer, which is in contact with a copper strip attached to the outside of the pivot. A communication protocol based on interrupts has further been developed for these electronic contacts based on serial communication. This allows a module to detect when another module is connected or disconnected, as well as to synchronise the actuation of the link to control the angle between them.

4.3 Mechanical overload protection

The novel overload protection mechanism introduced in this work presents a simple and compact method of preventing damage to robotic joints. It is integrated into the coupling mechanism of our modular origami robot, requiring no additional components, and obtains its functionality from a special, parametric design. The mechanism automatically disengages the coupling between two robots when the applied torque exceeds a predefined threshold, which lies outside of the normal working conditions of the robot. This threshold can be modified through a single design parameter such that the mechanism is easily adjusted towards a multitude of applications, scales, and user groups. In this section we provide a detailed analysis of this overload protection mechanism by modelling its behaviour and testing multiple parameters, materials, and fabrication methods.

4.3.1 Modelling

The overall concept of the mechanism is based on a number of functional requirements and fuses existing mechanical features and functions. The actual coupling consists of two complimentary pieces with identical radial teeth that mesh to transmit rotational actuation. Below the predefined torque threshold the coupling behaves like a positive clutch, which couples two pieces by mechanical interference and cannot slip. Thus, the mechanism does not weaken the robot or hinder performance

during normal operation. When the torque threshold is reached, however, the slider retracts and causes the coupling to disengage. This effect comes from the angular design of the teeth producing an axial force on the slider, which overcomes frictional and spring forces at a threshold.

The design is centred around a variable torque threshold, τ_{thresh} , which is dependent on a number of design parameters. In the following analysis we develop an expression for τ_{thresh} such that it can be adjusted by modifying a single parameter. For this purpose we first consider the geometry of the radial teeth, depicted in Figure 4.2c. The teeth have similarities to those of a Hirth joint, a locked mechanical coupling for shafts, although with an altered design and a different purpose. The faces of each tooth span between two radial lines, resulting in a varying angle of the face along the radius, unlike a Hirth joint. This allows for a planar, rather than a conical, design of the coupling mesh. The varying angle of the face is one of the key factors determining the torque threshold and is dependent on the tooth arc angle, θ_{arc} , and the height of the tooth, h . The angle spanned by half a tooth, γ , is defined by the number of teeth, n , as $\gamma = \pi/n$, limiting the maximum value of θ_{arc} . The contact area between two teeth is then fully defined through the inner and outer radii, R_i and R_o respectively.

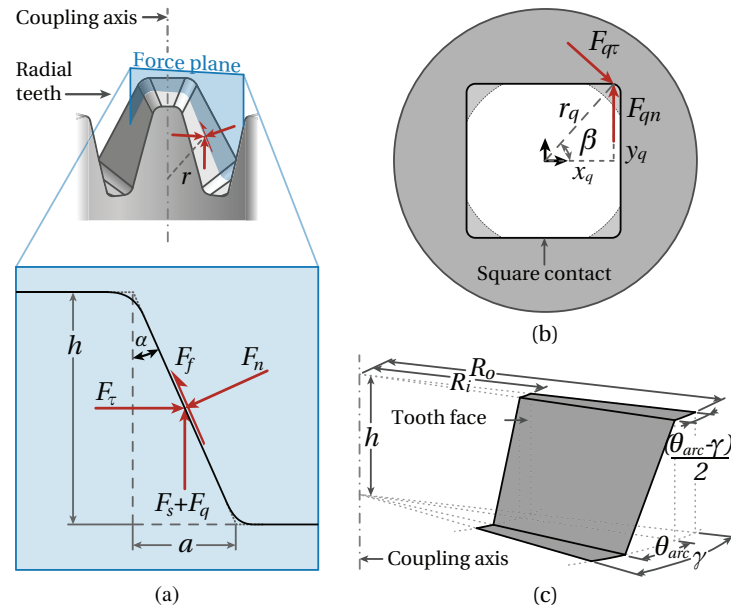


Figure 4.2 – Modelling diagrams for the two contact points in the overload protection model. (a) shows the force plane of a tooth face and the forces acting on it. (b) shows the contact forces between the slider and the square rail. (a) and (b) are used to calculate the torque threshold τ_{thresh} . (c) Radial tooth design schematic. The tooth face is the interaction surface between two teeth. The design parameters in this schematic can be altered to change the torque at which the coupling disengages.

Considering the overall geometry of the radial teeth we can establish a force plane, orthogonal to the radius, to evaluate the interaction forces between two teeth, illustrated in Figure 4.2a. The force plane creates a cross-sectional profile at radius r with an angle α between the face and the coupling axis given by $\tan(\alpha) = a/h$, where a is the distance between the two radial lines, fully defining the face at radius r . Using the equilibrium of forces both along the surface and orthogonal to the surface we can establish expressions for the frictional force between two teeth, F_f , given by

$$F_f = F_r \sin(\alpha) - (F_s + F_q) \cos(\alpha) \quad (4.1)$$

and the reaction force resulting from the opposite tooth, F_n , given by

$$F_n = F_\tau \cos(\alpha) + (F_s + F_q) \sin(\alpha) \quad (4.2)$$

where F_τ is the force orthogonal to the radius resulting from the torque, τ , applied to the coupling such that $\tau = rF_\tau$, F_s is the force exerted by the passive spring, and F_q is another frictional force resulting from a force on the square rail due to the applied torque.

The spring force, F_s , is given by $F_s = kx_s$, where k is the spring stiffness and x_s is the pre-loaded distance, while the frictional force from the square rail, F_q , can be determined as follows. Due to a small clearance between the slider and the square rail, the torque applied to the coupling can be translated to a force towards the corner of the square cross-section, $F_{q\tau} = (r/r_q)F_\tau$, as shown in Figure 4.2b, where r_q is the distance between the point where $F_{q\tau}$ is applied and the centre of the slider. The resulting reaction force, F_{qn} , creates a frictional force that resists the motion of the slider, F_q , which can be approximated using Coulomb friction as

$$F_q = \mu \frac{r}{r_q} F_\tau \cos(\beta) \quad (4.3)$$

where μ is the static coefficient of friction and β is the angle between the force $F_{q\tau}$ and the normal to the surface.

We can now find an expression for the torque threshold, τ_{thresh} , by relating Equations (4.1) and (4.2) using Coulomb friction and Equation (4.3), given by

$$\tau_{thresh} = \frac{F_s(\mu \sin(\alpha) + \cos(\alpha))}{\sin(\alpha) - \mu \cos(\alpha) - \lambda \cos(\alpha) - \mu \lambda \sin(\alpha)} \quad (4.4)$$

where the tooth arc angle θ_{arc} can be related to the torque threshold using the face angle $\alpha = \arctan(2r \sin(\theta_{arc}/2)/h)$ and $\lambda = \mu(r/r_q) \cos(\beta)$ is used for simplification.

We have chosen the tooth arc angle θ_{arc} as the key design parameter, keeping all other parameters constant. Given a desired torque threshold τ_{thresh} and specific design, we can adjust θ_{arc} to yield the required behaviour of the mechanism.

4.3.2 Testing

Given the above model we can design the overload protection mechanism by choosing parameters that meet the overall specifications of the robot and adjusting θ_{arc} to yield the desired torque threshold. The global design parameters established during the design process presented in Section 4.2 are presented in Table 4.1.

In order to verify both the feasibility of the overload protection mechanism and the model thereof we utilised two materials and fabrication methods to manufacture test pieces. One set of test pieces was made out of VeroWhite using a multi-jet 3D printer, while the other set was CNC-machined out of polyacetal (POM). The VeroWhite pieces were printed with a glossy finish and a layer height of 16 μm , and the POM pieces were CNC machined with a resolution of 15 μm . The remaining modelling parameters for the two materials measured after fabrication are given in Table 4.2.

We fabricated six test pairs and one square contact for each material with arc angles increasing in 2° intervals from 10° to 20°, as well as one final test pair that matches the desired torque threshold

4.3. Mechanical overload protection

Table 4.1 – Global design parameters for the mechanism incorporated into the automated coupling of a modular origami robot.

Parameter	Symbol	Value
Number of teeth	n	7
Tooth height	h	2 mm
Inner radius	R_i	2.5 mm
Outer radius	R_o	5 mm
Pre-load distance	x_s	5.4 mm
Spring stiffness	k	0.33 N mm ⁻¹

Table 4.2 – Material- and fabrication-dependent parameters for the model of the overload protection mechanism.

Parameter	Symbol	VeroWhite	POM
Friction coeff.	μ	0.25	0.19
Slider angle	β	50.6°	52.3°
Slider radius	r_q	2.95 mm	2.77 mm

using the 3D-printer with an arc angle of 15°. The samples were placed in a test frame that mimics the placement within a coupling with a manual drive wheel for the pivot. A torque sensor (ATI Nano 17) was attached to the pivot such that the torque could be gradually increased until the overload protection was triggered and the test pieces disengaged. This was repeated at least 20 times per sample set to obtain an average value for the real torque threshold.

Figure 4.3 shows the test results for the two sets of test pieces, the corresponding modelling results from Section 4.3, sample test pieces, and the testing set-up. The modelling results approach asymptotes at 13.08° and 9.76°, reflecting the self-locking condition that occurs when the axial force produced by the torque acting on the angled teeth can no longer overcome the frictional forces acting on the slider. This self-locking condition was confirmed during the test as the mechanism did not disengage up to the limit of the torque sensor (0.5 Nm) at arc angles of 10° and 12° for the 3D-printed test pieces. The machined test-pieces with an arc angle of 10° did expectedly also not disengage up to the limit of the torque sensor since the modelled threshold is several times larger. The remaining test pieces confirm the expected behaviour of the mechanism, disengaging at values close to the predicted torque thresholds. Although errors in the torque threshold of 10-20% are significant, the test validates the functionality and efficacy of the overload protection mechanism.

While these errors are acceptable in our implementation and can be accounted for in the design, some applications may demand more precise threshold values from the mechanism, which can be achieved in a number of ways. Errors become larger as the value for the arc angle approaches the self-locking condition, as small variations in geometry and surface finish have a bigger impact on the torque threshold. Therefore, designing the system such that the desired torque threshold occurs at an arc angle value significantly higher than the self-locking condition improves the effective precision. Alternatively, mechanical improvements can reduce errors such as tightening tolerances in the machining process, adjusting the CNC cutting profile to better reflect the path of moving elements, or using different materials for interfacing parts in order to improve sliding properties. 3D-printed pieces, although used by the authors in this instance for ease of manufacture, are less predictable due to the quality of the UV-cured, glossy surface finish.

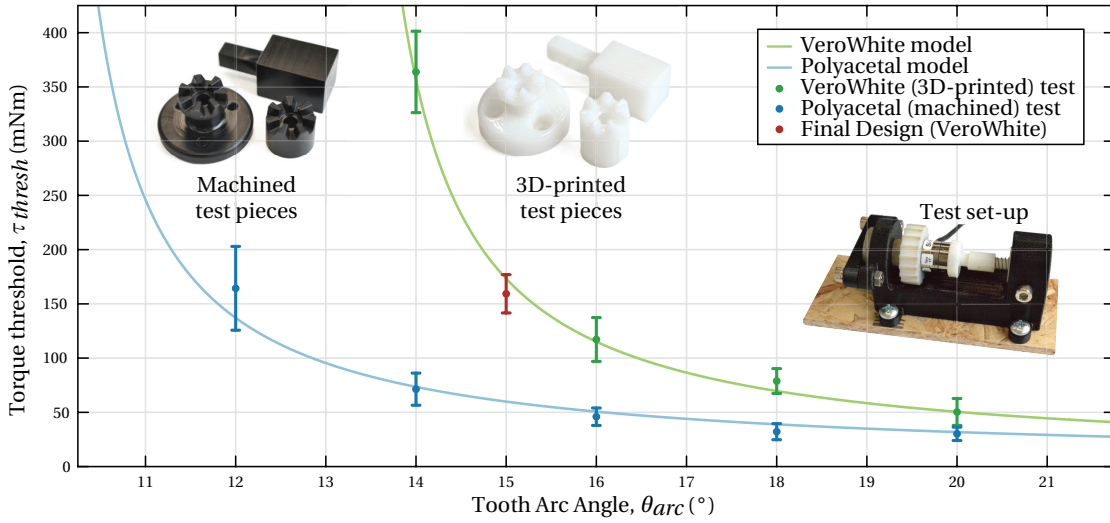


Figure 4.3 – Results from modelling the overload protection mechanism and from testing the model on two materials and fabrication methods. The torque at which the coupling disengages is plotted against the tooth arc angle, θ_{arc} , a design parameter of the radial teeth. VeroWhite was 3D-printed and used in the final design of the coupling mechanism, while the polyacetal pieces were CNC-machined.

The desired torque threshold for the final design of our modular origami robot is determined by the recommended maximum torque value of the DC motors, given as 25 oz-in (or 177 mNm) by the manufacturer. This corresponds to a tooth arc angle of 15° , which was verified during testing as shown in Figure 4.3. In case the intended application, user group, or motor specifications for the coupling change, the torque threshold can easily be adjusted by replacing the two coupling elements in each hinge of the robot.

4.4 Coupling demonstration

Following the modelling of our proposed overload protection mechanism this section presents our prototype of the automatic coupling for modular robots and a demonstration thereof. The design presented in Section 4.2 has been implemented in form of a functional prototype with features that greatly extend the capabilities of modular origami robots, as depicted in Figure 4.4. The features of the prototype fulfil the requirements of couplings for self-reconfigurable modular robots and can be extracted to fit a variety of designs and systems.

We have manufactured two identical prototypes of the coupling, each containing a single edge of a modular origami robot. This allows us to test all functions of the mechanism without manufacturing the full robot. Each prototype is controlled using an Arduino Uno running identical programs with no physical connections between them. The only communication between the two controllers occurs through the electronic contact within the coupling. This simulates the functionality of a fully mobile modular origami robot with no external connections.

During the testing of the coupling mechanism we place the two prototypes opposite one another such that the two edges are aligned, but a small distance away from each other. This ensures that the prototypes engage when moving forward since a single edge only has one degree of freedom while moving (a full module has three wheels such that it can manoeuvre freely on flat surfaces). Once aligned,

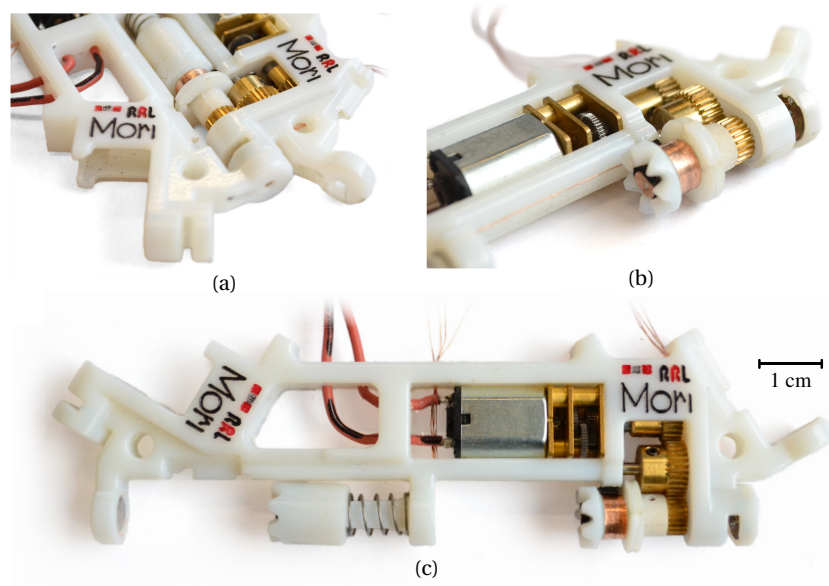


Figure 4.4 – Prototypes of the coupling mechanism with mechanical overload protection on modular origami robots. (a) Two modules with coupling mechanisms engaged. **(b)** Actuation mechanism and electronic brush system of a single mechanism. **(c)** One full edge of a modular origami robot with the automatic coupling mechanism.

we simultaneously command the two modules to initiate a coupling sequence consisting of retracting the slider, moving forward, and releasing the slider. If a connection is not detected immediately after releasing the slider, the pivots start rotating back and forth by small amounts until an electronic contact is made to ensure both couplings engage properly, which accounts for the flat face at the end of each tooth.

Once two modules are properly coupled and have confirmed that they are synchronised, both modules actively maintain the desired angle of the coupling through closed-loop control. In our test we ensure that both modules receive the same desired angle at all times by using a single potentiometer connected to both module controllers (and connecting grounds). The position of the potentiometer then determines the absolute angle of the coupling. This can be altered to other forms of angle input in the future, such as wireless communication, depending on the intended application and the global control system. In order to disengage the coupling we simultaneously command the prototypes to initiate a decoupling sequence consisting of returning to an absolute angle of zero, retracting the sliders, and moving away from each other. Figure 4.5 shows key frames from a single test that encompasses all of the coupling’s functionalities, as described above.

We further tested the mechanisms ability to account for misalignment of two couplings. Couplings should approach one another in a direction perpendicular to the coupling axis during the coupling process in order to avoid collisions, which is possible in most conceivable scenarios and configurations. For the purpose of testing misalignment tolerance during this process we place the two edges onto separate rigs and increase misalignment in both the radial and angular direction, the latter being the angle between the two coupling axes. The coupling process was repeated five times at each interval and the resulting misalignment tolerance stems from the largest misalignment where all trials were successful. The radial dimension was increased in steps of 0.5 mm and the angular dimension in steps of 1° .

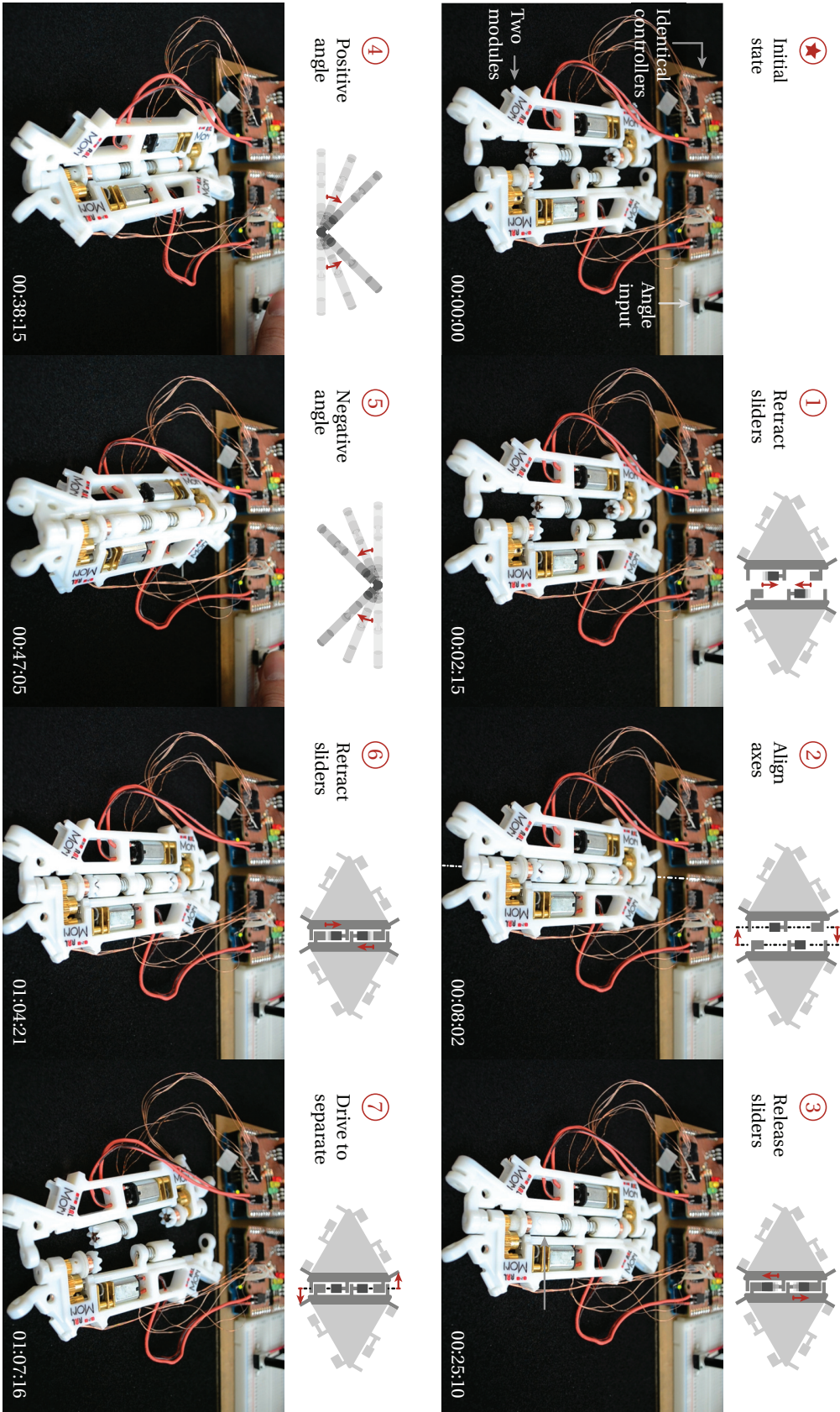


Figure 4.5 – Testing of the coupling mechanism with key frames showing the main steps in the process. The coupling sliders are first retracted and two modules drive towards one another to align the coupling axes. The coupling then engages and the angle between the modules is set using a potentiometer. During the uncoupling process the pins are again retracted and the modules drive away from each other.

Table 4.3 – Misalignment tolerance results obtained from testing the prototype of the automatic coupling.

Direction	Value	Percentage
Radial	± 2.5 mm	± 25 %
Axial	+1.2 mm, -0.5 mm	+1.1 %, -0.5 %
Angular	$\pm 3^\circ$	n/a

The testing results for the misalignment tolerances of our coupling are summarised in Table 4.3. The misalignment tolerance in the axial direction results from the travel of the slider creating a gap between the two coupling elements, and additional chamfers and clearances that guide the couplings. The relatively large misalignment tolerance of 25 % in the radial direction, the most critical for a modular origami robot, arises from self-centring design of the radial coupling teeth, as outlined in Section 4.3.

4.5 Discussion

The design of couplings for modular robots presents various challenges and requirements that must be solved and fulfilled to create fully functional reconfigurable systems. These comprise, amongst others, a robust mechanism design, actuation and sensing of the connection and associated DoFs, ease of coupling and alignment, as well as communication and synchronisation. In this chapter, we present a genderless automatic coupling mechanism with embedded mechanical overload protection that overcomes some of the challenges associated with modularity in a wide range of robotic systems. The coupling contains various unique features that can be applied to other systems individually or as a whole to improve the reconfigurability of robots.

The coupling utilises SMA actuators to automate the docking process and DC motors to actuate the rotational DoF. A special electronic connection embedded in the coupling not only enables each module to detect the state of the coupling and to gather information about the neighboring module, but also serves as a means of synchronisation. Mechanical overload protection incorporated into the coupling protects the robots from damage. It consists of a friction-based positive clutch mechanism that is triggered when a pre-defined torque threshold is reached. Thanks to a parametric, self-centring design this threshold can easily be adjusted to meet the varying requirements. Along with the design, modelling, and testing of the proposed coupling we present a working prototype thereof. Using a single edge of two modules we demonstrate a coupling process with automatic coupling and decoupling, detecting and synchronising the connection, as well as closed-loop control of the rotational DoF. We furthermore validate the self-centring design by testing misalignment tolerances.

While this chapter addresses some of the challenges in coupling modular robots, and in particular modular origami robots, there are several critical factors and difficulties that must be accounted for. As the coupling is one of the crucial elements that allow modular systems to function, its reliability and robustness affect the overall performance. Merging the coupling mechanism and the kinematic joint between neighbouring modules further escalates the physical and functional requirements that must be met. Mechanical strength, manufacturing tolerances, and other factors impacting the system's scalability were not addressed in the prototype presented in this chapter. The embedded overload protection mechanism relies on mechanical friction between components in the coupling and small changes in these properties can have a considerable impact on the torque threshold. Furthermore, as frictional forces increase under load, the ability to retract the coupling and disengage modules could

be affected, thereby limiting the system's ability to reconfigure in larger assemblies. These limitations must be taken into account and addressed in order to take full advantage of the potential benefits.

Despite these drawbacks, the coupling mechanism represents one of the advancements necessary to realise a fully functional modular origami robot. While the design of the mechanism is directed towards modular origami robots, our approaches to actuation, coupling, overload protection, sensing, and communication represent building blocks that can be used to incorporate modularity into other robotic systems.

5 Reconfiguration algorithms based on origami principles

In addition to functional and mechanical challenges in realising modular robots able to address a diverse set of tasks, controlling such systems is highly demanding. When planning and executing the reconfiguration process of modular assemblies, for instance, control, power, and computational requirements stemming from large numbers of individual entities and degrees of freedom must be overcome. In this chapter we address some of these challenges by developing algorithms for efficiently reconfiguring modular robotic structures.

Several approaches to optimising this process have been proposed thus far, which can be grouped into two main categories. The first category considers a target configuration by dividing the modular architecture into different sets of modules to simplify the reconfiguration process. A task-oriented optimisation has been implemented by minimising the number of DoFs of different types of modules in the configuration [97]. A multi-objective optimisation problem has been addressed with a concurrent design approach that splits the architecture into different levels [98], a neural network approach that finds the optimal design [99], as well as a genetic algorithm [100]. The relationship between morphological design and motion planning has been established and analysed by using the implicit function theorem to optimise design parameters [101]. The aforementioned approaches facilitate the optimal design of the final configuration for specific tasks, but do not address the dynamic reconfiguration procedure in modular robots.

The second category of optimising the reconfiguration process aims to minimise the number of connectivity changes when transforming from an initial shape into the desired configuration. The challenge of such a combinatorial optimisation problem lies in its inherent NP-completeness [102], even for chain-type modular robots [103], yielding the need for heuristic solutions with some guarantee of performance. A graph-based planning algorithm has thus been proposed to generate a near-optimal transforming sequence in polynomial time [104].

Although some of the above reconfiguration planners target a reduction in the number of connectivity changes, all of the approaches require some form of coupling and uncoupling between modules in

The material presented in this chapter has been adapted from the following publications:

[105] M. Yao, **C. H. Belke**, H. Cui and J. Paik, "A reconfiguration strategy for modular robots using origami folding," *The International Journal of Robotics Research*, vol. 38, pp.73-89, jan 2019, DOI: 10.1177/0278364918815757.

The original contributions of C. H. Belke were conceptual work, methodical development, result analysis, and partial writing.

the process. Connectivity changes complicate the overall transformation, are time-consuming, and can lead to failure resulting from commonly experienced alignment errors [106, 107]. Consequently, they cast high demands on control algorithms and hardware implementations to detect and overcome misalignments [108]. It is thus desirable to minimise or even remove any connectivity changes from the reconfiguration process.

This chapter introduces a planning algorithm for the reconfiguration of modular robots that does not require any connectivity changes during the transformation, but only before motion begins and after it is completed. For this purpose, we make use of the fact that in task-specific scenarios modular robots commonly transform from a collection of modules on a surface to a functional 3D configuration. We can therefore simplify the reconfiguration process by turning a 2D pattern into a 3D shape, given that a corresponding 2D pattern exists [109]. This process, in its conceptual form, can be related to the principles behind origami [12, 72, 110]. Furthermore, by also considering the inverse of this process we can find a way of transforming from one 3D configuration into another with an intermediate 2D phase during which all connectivity changes occur, greatly reducing the possibility of misalignment errors.

The optimised method for planning the reconfiguration of modular robotic systems introduced in this chapter draws similarities to the concept of folding in origami. While utilising origami principles to plan the reconfiguration process eliminates the need for connectivity changes during transformation, a remaining critical aspect for modular systems is energy consumption. Since most systems have an on-board power-supply, minimising power consumption is vital, particularly during the highly demanding reconfiguration process. The overall reconfiguration planning problem can thus be formulated as follows: given a desired 3D target configuration, find the 2D layout and the corresponding actuation sequence that will result in the lowest energy consumption.

The energy consumption during reconfiguration depends on the initial planar pattern as well as the actuation sequence of different modules, both of which are essential considerations in the field of computational origami [68], committed to designing algorithms that compute the folding process of origami structures. Computing the initial crease pattern of a sheet of paper, corresponding to an initial planar pattern of modular robots, has been optimised for paper models using tree-based algorithms [111], while the rigid foldability of objects, where only flat sections can exist between hinges, is subject to mathematical conditions [112]. The rigid origami model applies directly to our approach since it omits the properties of paper creases, allowing direct kinematic translations between tiles or modules [53, 113, 114].

While the aforementioned approaches assume zero thickness structures, additional constraints need to be applied when the folding object has a non-zero thickness [115, 116]. Automating the folding process of both zero and non-zero thickness structures requires planning the sequence of folding steps. This has been demonstrated by means of a robot capable of folding origami [117] as well as self-folding robotic sheets [118]. Previous approaches to modelling algorithms for folding origami structures consider a wide range of problems and scenarios, but they do not consider energy consumption during the reconfiguration process.

Here we present a new approach to reconfiguration for modular robotic systems inspired by origami principles, as well as the first algorithmic framework for planning an energy-optimal reconfiguration scheme of folding in modular robots. In our approach we determine an optimal initial planar configuration and an optimal actuation sequence, both NP-complete problems where the candidates of reconfiguration schemes grow exponentially with the number of modules in the system. Since the optimisation scheme cannot be validated without enumerating the search space, we develop an

automatic modelling algorithm for modular robots based on the work of [119–122], as well as a heuristic algorithm for generating energy-optimal folding schemes. The proposed methodology is validated by demonstration on the platform of the modular origami robot Mori.

5.1 Planning strategies

In this section, we address the complexities of reconfiguring modular robotic systems by presenting the first algorithmic framework for planning an energy-optimal reconfiguration scheme using origami principles, eliminating connectivity changes during reconfiguration. An overview of the method is shown in Figure 5.1 with the framework composed of two main approaches, an *automatic modelling algorithm* and a *heuristic algorithm*. A target 3D shape is given as an input to the algorithms, which can generally be achieved through a large number of different folding schemes, consisting of an initial planar layout and a folding sequence.

Due to the NP-completeness of the reconfiguration planning problem, enumeration processes are needed to search for an optimal solution. An intuitive and direct approach is to calculate the required torque of different folding schemes, and we propose an *automatic modelling algorithm* (Section 5.1.1) to follow through this approach. In this algorithm, joint motion is first computed for each module in the pre-folding pattern, considering constraints resulting from the physical structure of a module. The forward kinematics of the modular architecture is then automatically generated with its geometry modelled as a hierarchical structure of a rooted tree. The joint dynamics of the configuration is then derived using the recursive Newton–Euler (RNE) formulation, and energy consumption of the reconfiguration is calculated with the predefined folding sequence.

A less straightforward approach is to design a *heuristic algorithm* (Section 5.1.2) to evaluate the torque requirements of different folding schemes, by utilising some measure to assess energy consumption based on the derived joint dynamics. The proposed algorithm includes two heuristic planning procedures. The first is a two-step planning process to determine the pre-folding pattern with minimum energy consumption, by first defining a unified folding sequence eliminating the coupling effect of the actuation order and layout in the required torque, followed by an optimal layout planner. The second procedure determines the optimal folding sequence for the energy-optimal layout generated before, by implementing an optimal folding sequence planner. The output of the two approaches is an energy-optimal reconfiguration scheme with both an optimal layout and an optimal actuation order.

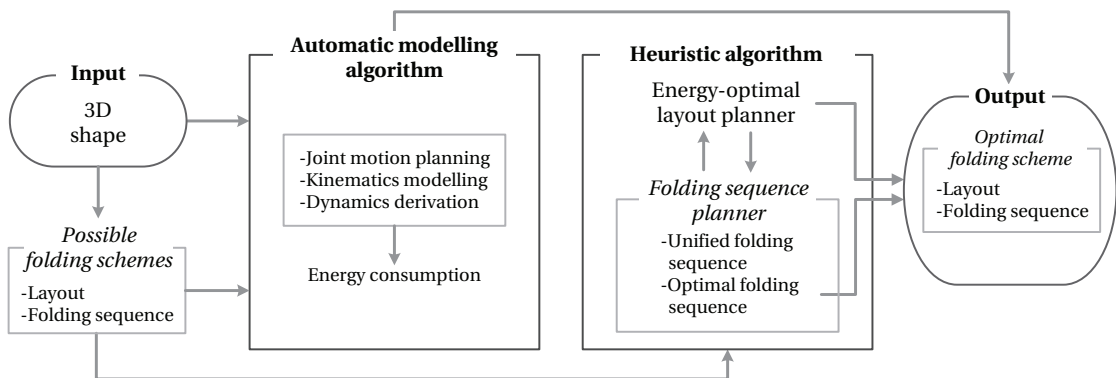


Figure 5.1 – Overview of our method for energy-optimal reconfiguration of modular robots. It consists of two two approaches, an automatic modelling algorithm and a heuristic algorithm, based on the principles of origami.

5.1.1 Automatic modelling

In modelling modular robotic systems the numerous approaches for fixed-structure robots cannot be applied directly as the number of configurations grows exponentially with the number of modules [123]. For this reason, automated modelling techniques have been proposed and developed to address the increased modelling complexity [120–122]. The dynamic model for modular robots is generally derived using the RNE method. Most approaches are based on Lie theory [124] where adjoint mapping is conducted on the Lie group $SE(3)$ of homogeneous transformations. The adjoint representation in the derived wrench and torque is a compact expression of a matrix, which complicates the derivation and estimation for energy consumption of joint actuators, usually in an integration form with time [34, 100]. In this section, we develop an *automatic modelling algorithm* for modular robots following [119] to calculate the energy consumption of folding schemes during the reconfiguration process. The overall procedure is shown in Algorithm 1 and the algorithmic inputs and step-by-step modelling techniques of the algorithm are explained in detail as follows.

Algorithm 1 Automatic modelling algorithm.

Input: 3D shape and folding scheme (pre-folding pattern and folding sequence);

Output: Energy consumption of the folding scheme;

- 1: Joint motion planning with angle constraints;
 - 2: Automatic kinematic modelling of the modular architecture;
 - 3: Automatic dynamic derivation of joint motion;
 - 4: Computation of energy consumption in folding sequence;
 - 5: **return** Energy consumption of the reconfiguration process.
-

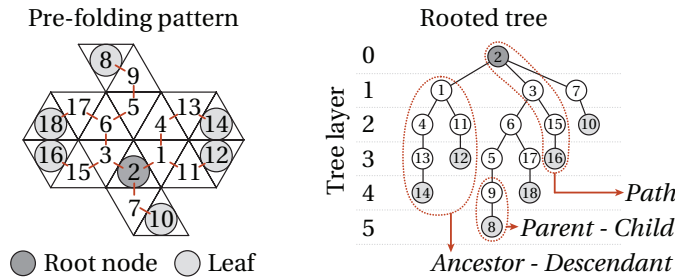


Figure 5.2 – A pre-folding pattern with a root node and its corresponding rooted tree. Left: a planar layout with a designated root node representing the base. Right: the rooted tree creates a hierarchical structure of the layout. Important components in the architecture include *leaf*, *path*, as well as *parent–child* and *ancestor–descendant* relations. The tree layer describes the distance between a vertex and the root node along its path.

Input shape

The inputs of Algorithm 1 are the mesh of the 3D target shape and a folding scheme consisting of a pre-folding pattern and a folding sequence. In general, there are numerous planar patterns that can fold into a given 3D configuration. The reciprocal process of reconfiguration, unfolding a 3D structure into 2D layouts [125], is used to generate the pre-folding patterns. The general procedure is to produce a graph representation of the 3D configuration, followed by spanning trees and corresponding rooted trees generated by the represented graph. A rooted tree stands for a pre-folding pattern of the 3D structure with a designated root and can be generated via traversal algorithms such as breadth-first search (BFS) and depth-first search (DFS). The connected structure of a rooted tree remains unchanged

during the reconfiguration as no connectivity changes are required in our approach. The rooted tree thus represents the intermediate quasi-2D shape and desired 3D configuration simultaneously. A pre-folding pattern with a root node and its corresponding rooted tree are shown in Figure 5.2. The root node is the ancestor of all other modules, shapes the unique tree structure in the kinematics modelling, and is the origin of the inertial frame in the dynamics derivation and torque computation. Different root nodes selected as the robotic base result in variations of the required torque and must thus be specified. The shape of a modular unit in the pre-folding pattern is secondary, and can be anything from cubic to hexagonal. In our analysis we use an equilateral triangular shape, the simplest regular polygon, to simplify the overall structure.

Joint motion planning

The first step of the algorithm is to plan joint trajectories for all modular units in time intervals consistent with the folding sequence. As the torque requirements vary with different joint motion profiles, even with the same folding scheme, we use a unified joint motion planner for every module in each time period to guarantee a fair comparison between different folding schemes. With the discussion on time periods and folding schemes detailed in Section 5.1.2, here we focus on the joint trajectory planning as follows.

To generate a joint trajectory passing through several path control points, predefined nodes on the trajectory, a series of polynomials are usually used to interpolate the path [126]. The joint angle $q_i(t)$ of module i varies from zero in the initial pattern to its final position $\hat{\theta}_i$ in time period $T_k \in [t_{k-1}, t_k]$, $k \in \mathbb{Z}^+$, as $q_i(t_{k-1}) = 0$ and $q_i(t_k) = \hat{\theta}_i$, with default zero boundary conditions for velocity and acceleration, $\dot{q}_i(t_{k-1}) = \dot{q}_i(t_k) = 0$ and $\ddot{q}_i(t_{k-1}) = \ddot{q}_i(t_k) = 0$ respectively. The folding angle $\hat{\theta}_i$ is the dihedral angle between module i and its *parent* in the 3D structure and can be computed using the algorithm presented in [127]. Since there are six path control points resulting from the boundary conditions, a fifth-order polynomial is needed for the interpolation.

The joint angle is restricted due to the non-zero thickness, d , of a module. The threshold value of the joint angle, the minimum dihedral angle, is denoted as ϑ and can be calculated using $\sin(\vartheta/2) = (d/2)/r$, where r is the radius of the hinge. The joint angle $q_i(t)$ is thus restricted by

$$\begin{cases} -\pi < q_i(t) < -\vartheta \\ \vartheta < q_i(t) < \pi \end{cases} \quad (5.1)$$

Kinematics modelling

The next step in the *automatic modelling algorithm* is to generate a kinematic model of the configuration and the folding motion for each module, including position, velocity, and acceleration, given a set of joint trajectories produced in Step 1 [122]. In a modular architecture modelled as a hierarchical structure defined by a rooted tree as shown in Figure 5.2, the kinematic transformation Φ starting from root node R to each of the *descendant* modules i in *path* j can be recursively formulated as

$$\Phi_i = A_{P_{j,1}}^{P_{j,2}}, A_{P_{j,2}}^{P_{j,3}}, \dots, A_{P_{j,s-1}}^{P_{j,s}} \quad (5.2)$$

where $A_k^{k'}$ is a 4×4 homogeneous matrix describing the relative pose of neighbouring modules (k, k') , and can be calculated as presented in [122]. P_j is the set of modules in the j th *path* of the rooted tree, and $P_{j,1} = R$, $P_{j,s} = i$.

Dynamics derivation

In Step 3 of the algorithm, the dynamics of the configuration is automatically derived using a modified RNE formulation and the required torque is calculated for each folding scheme. We assume zero ground interactions to simplify the mathematical derivation, common practice in related work [120–122]. The initialisation and backward recursion are similar to the standard RNE [119]. In backward recursion, where the generalised velocity and acceleration of each module are propagated from the root node to the *leaves* of all *paths*, the motion is not influenced by multiple connections due to the uniqueness of the *parent* module. In forward recursion, however, where forces and moments are propagated from the *leaves* to the root node R , multiple connections must be accounted for. The forward recursion forces and moments exerted on module i can be derived as:

$$\begin{aligned} \mathbf{f}_i &= \sum_{j=1}^{|C_i|} \mathbf{f}_{C_{i,j}} + \mathbf{F}_i \\ \mathbf{n}_i &= \sum_{j=1}^{|C_i|} (\mathbf{n}_{C_{i,j}} + \mathbf{p}_i \times \mathbf{f}_{C_{i,j}}) + \mathbf{N}_i + (\mathbf{p}_i + \mathbf{r}_i^*) \times \mathbf{F}_i \\ \tau_i &= \mathbf{z}_i \cdot \mathbf{n}_i \end{aligned} \quad (5.3)$$

where $\mathbf{F}_i = m_i \ddot{\mathbf{r}}_i$ and $\mathbf{N}_i = \mathbf{I}_i \dot{\boldsymbol{\omega}}_i + \boldsymbol{\omega}_i \times (\mathbf{I}_i \boldsymbol{\omega}_i)$. The remaining parameters are given in Table 5.1. In this formulation base coordinates are used as the reference frame, an implicit expression compared to the more commonly used link coordinates, considered to be more efficient. The formulation using base coordinates, however, reveals the direct relations between the required torque and the link motion, including position and orientation in the inertial frame. This helps in the evaluation and estimation of energy consumption in the *heuristic algorithm* design in Section 5.1.2.

Table 5.1 – Variable and parameter notations used in Sections 5.1.1 and 5.1.2.

Variables	
\mathbf{f}_i	Force exerted on module i by its <i>parent</i> ;
\mathbf{n}_i	Moment exerted on module i by its <i>parent</i> ;
τ_i	Input torque of the actuator along \mathbf{z}_i ;
\mathbf{z}_i	Actuating axis of module i , the coincident edge of module i and its <i>parent</i> ;
\mathbf{F}_i	Total external force on module i ;
\mathbf{N}_i	Total external moment on module i ;
\mathbf{p}_i	Vector from DH coordinate origin $i - 1$ to coordinate origin i ;
\mathbf{r}_i	Vector from the base coordinate origin to the centre of mass (CM) of module i ;
$\ddot{\mathbf{r}}_i$	Acceleration vector of \mathbf{r}_i ;
\mathbf{r}_i^*	Vector from DH coordinate origin i to CM of module i ;
\hat{r}_i	Distance between robotic base (root node R) and CM of module i , and $\hat{r}_i(t) = \mathbf{r}_i(t) $;
$\boldsymbol{\omega}_i$	Angular velocity of module i ;
$\dot{\boldsymbol{\omega}}_i$	Angular acceleration of module i ;
C_i	The set of <i>children</i> of module i , $ C_i $ is the number of components in C_i .
Module parameters	
l	Side length of each modular unit;
m_i	Mass of module i ;
\mathbf{I}_i	Inertia tensor of module i about its CM.
Other parameters	
λ_s	$s = 1, 2, 3, 4$, constants defined as $\lambda_1 = \ \mathbf{I}_i\ $, $\lambda_2 = \frac{l/2}{\sin(\pi/3)} m_i$, $\lambda_3 = m_i$, and $\lambda_4 = \mathbf{p}_i = 0$ or l ;
κ_s	$s = 1, 2, 3$, design parameters, $\kappa_s > 0$.

Energy consumption

The final step is to evaluate the energy consumption of the reconfiguration scheme, with modules folding in series. This depends on physical motor parameters and is expressed as the product of torque and angular velocity of each joint [100]. To simplify the computation, we assume that the total energy consumed by all motors is based on the accumulated value of torque input to all joints. We also assume that no energy is required to hold the position between two modules. The energy consumption of a folding scheme, ε , with n modules in the configuration, during folding time $t \in [t_0, t_p]$, is then given by

$$\varepsilon = \sum_{i=1}^n \frac{\int_{t_{k-1}}^{t_k} |\tau_i| dt}{t_k - t_{k-1}} = \sum_{i=1}^n \frac{\int_{t_0}^{t_p} |\tau_i| dt}{t_p - t_0} \quad (5.4)$$

5.1.2 Heuristic algorithm

The automatic modelling algorithm outlined above is a direct, but computationally heavy method of generating energy-optimal folding schemes. Here we propose a heuristic algorithm consisting of two planning processes: an optimal pre-folding pattern and a folding sequence of modules with minimum energy consumption.

Energy-optimal layout planner

Firstly, we aim to establish an initial planar layout of modules that will result in minimum energy consumption when folding into a 3D target shape. Inspired by a process for creating optimal cut-out sheets of 3D paper models [125, 128], where weight functions are put forward with some optimum criteria and assigned to edges of a representative graph, here we design a cost function that evaluates energy consumption of a pre-folding pattern during its reconfiguration.

In a rooted tree structure as depicted in Figure 5.2, the edge between a *parent* and a *child* can be assigned a weighted value measuring energy consumption of actuating the *child* to its final position. We define a weight function of edge $e_i : (i, i')$, where i' is the *parent* of module i , as $\omega(e_i)$. The overall energy consumption for a pre-folding pattern can be evaluated using a cost function, χ , the sum of weights of all edges in the rooted tree:

$$\chi = \sum_{i=1}^{n-1} \omega(e_i) \quad (5.5)$$

A measurement of energy consumption in actuation time $T_k \in [t_{k-1}, t_k]$ of module i can be realised by integrating $|\tau_i|$ twice with time, $\varepsilon'_i = \int_{t_{k-1}}^{t_k} \int_{t_{k-1}}^{t_k} |\tau_i| dt dt$. Using Eq. 5.3, this gives

$$\varepsilon'_i = \int_{t_{k-1}}^{t_k} \int_{t_{k-1}}^{t_k} \left| |\mathbf{z}_i| \cdot |\mathbf{n}_i| \cdot \cos(\varphi_i) \right| dt dt \quad (5.6)$$

where φ_i is the vector angle between \mathbf{z}_i and \mathbf{n}_i . The actuating axis \mathbf{z}_i can be written as $\mathbf{z}_i = \Phi'_i \mathbf{z}_0$, where Φ'_i is a orthonormal rotation matrix, the upper 3×3 of the kinematic transform matrix Φ_i . Here, $\mathbf{z}_0 = [0 \ 0 \ 1]$ is a unit vector in the z -direction, thus $|\mathbf{z}_i| = 1$. Using $\cos(\varphi_i) \leq 1$, Equation 5.6 can be written as

$$\varepsilon'_i \leq \int_{t_{k-1}}^{t_k} \int_{t_{k-1}}^{t_k} |\mathbf{n}_i| dt dt \quad (5.7)$$

Defining Λ_i as the upper limit of Equation 5.7, $\Lambda_i = \int_{t_{k-1}}^{t_k} \int_{t_{k-1}}^{t_k} |\mathbf{n}_i| dt dt$, and Γ_i as the double integral of force \mathbf{f}_i , $\Gamma_i = \int_{t_{k-1}}^{t_k} \int_{t_{k-1}}^{t_k} |\mathbf{f}_i| dt dt$, we can formulate an estimation of the energy metric as follows.

Theorem 1 *The energy metric of actuating module i to its final position $\hat{\theta}_i, \epsilon'_i$, can be estimated by Λ_i^* , defined as the maximum of Λ_i , and Λ_i^* is derived from Equation 5.3 as*

$$\Lambda_i^* = \sum_{j=1}^{|C_i|} (\Lambda_{C_{i,j}}^* + \lambda_4 \cdot \Gamma_{C_{i,j}}^*) + \lambda_1 \cdot (\kappa_2 |\hat{\theta}_i| + \kappa_3 |\hat{\theta}_i|^2) + \lambda_2 \kappa_1 |\hat{r}_i(t_k) - \hat{r}_i(t_{k-1})| \quad (5.8)$$

with Γ_i^* , the maximum of Γ_i , given by

$$\Gamma_i^* = \sum_{j=1}^{|C_i|} \Gamma_{C_{i,j}}^* + \lambda_3 \kappa_1 |\hat{r}_i(t_k) - \hat{r}_i(t_{k-1})| \quad (5.9)$$

Related variables and parameters are listed in Table 5.1 and a proof for this theorem can be found in Appendix A. Computation requires updated position data of the configuration, term $\hat{r}_i(t)$, which is determined by the actuation order detailed in Section 5.1.2).

This procedure is inherently a kinematic propagation rather than an integration of joint torque with respect to time as in Equation 5.6. Hence, the simplified estimation in Equation 5.8 substantially reduces computational costs. The energy metric, defined as the double integral of the torque magnitude, is equivalent with the energy consumption defined in Equation 5.4 when comparing and ranking different reconfiguration schemes. It allows us to derive its upper bound, Λ_i^* , and calculate it using variables such as joint angle and inertial distance, instead of their derivatives and second derivatives. This can significantly reduce computational loads and simplify the optimisation process. We can use Equation 5.5 to evaluate the energy consumption of a pre-folding pattern with $\omega(e_i) = \Lambda_i^*$, enumerate all possible layouts, and obtain the one with minimum cost.

Folding sequence planner

When planning the reconfiguration of an assembly, actuating all modules in a configuration simultaneously results in the shortest time. However, this is not necessarily an energy-optimal process. In this section we propose two algorithms with asynchronous folding sequences, a unified framework for generating the actuation order in different layouts and an energy-optimal sequence planner with time-saving consideration.

For a pre-folding pattern with n modules, there are $n - 1$ modules to be actuated with p folding steps in series. Each folding step spans from time t_{k-1} to t_k , in time period $T_k \in [t_{k-1}, t_k]$, $k = 1, 2, \dots, p$. We assume that the length of each time period is equal, Δt , so that $t_k = t_{k-1} + \Delta t$ and $t_p = t_0 + p\Delta t$. To save time overall, the number of modules folding up in each time period should be as large as possible. The goal of a folding sequence planner is to determine which n_k ($n_k > 0$) modules of a layout are to be folded up in time period T_k with minimum energy consumption and sequence number p . To simplify computation, we assume no collisions occur during reconfiguration.

We first present a unified sequence planner to decouple the effect of the folding sequence from the pre-folding pattern in terms of energy consumption. If modules are in the same *path*, the energy consumption of a single module can change depending on when it is folded relative to another. We therefore assume that modules in the same *path* of the rooted tree of a layout are actuated in separate

time periods. If module i is a *leaf*, then $|C_i| = 0$, the joint torque of module i can be simplified to

$$\tau_i = \mathbf{z}_i \cdot [\mathbf{N}_i + (\mathbf{p}_i + \mathbf{r}_i^*) \times \mathbf{F}_i] = \mathbf{z}_i \cdot [\mathbf{I}_i \dot{\boldsymbol{\omega}}_i + \boldsymbol{\omega}_i \times (\mathbf{I}_i \boldsymbol{\omega}_i) + (\mathbf{p}_i + \mathbf{r}_i^*) \times m_i \ddot{\mathbf{r}}_i] \quad (5.10)$$

which shows that torque τ_i is only determined by the movement and position of module i . Since the *leaves* of a rooted tree Υ , denoted as $leaf(\Upsilon)$, are in different *paths*, they can all be actuated in the first time period, T_1 . As they have now assumed their final position relative to their *parent*, they can be removed from Υ and a new rooted tree is obtained. In the next time period, T_2 , all new *leaves* of Υ are folded, and so on. The procedure is summarised in Algorithm 2.

Algorithm 2 Unified folding sequence planner.

Input: Rooted tree Υ of a pre-folding pattern;

Output: Sets of modules folding in series;

- 1: Initialisation: $k \leftarrow 1$, $n \leftarrow |\Upsilon|$, $\Omega_k \leftarrow \emptyset$;
 - 2: **while** $n > 1$ **do**
 - 3: $\Omega_k \leftarrow leaf(\Upsilon)$, *leaves* of Υ are modules to be actuated in time period T_k ;
 - 4: $\Upsilon \leftarrow \Upsilon - \Omega_k$, remove $leaf(\Upsilon)$ and obtain a new rooted tree;
 - 5: $n \leftarrow |\Upsilon|$
 - 6: $k = k + 1$
 - 7: **end while**
 - 8: **return** $\Omega_1, \Omega_2, \dots, \Omega_k, \dots, \Omega_p$
-

This unified sequence planner takes advantage of the independence of *leaves* in a rooted tree. For modules that are not *leaves*, however, the energy consumption is coupled with the configuration and position of its *descendants*. In order to determine the optimal folding sequence for a specific layout in terms of energy consumption, every possible folding sequence has to be evaluated.

Algorithm 3 Rearrangement of folding sequence.

Input: $S = [s_1, s_2, \dots, s_n]$;

Output: $\Omega_1, \Omega_2, \dots, \Omega_k, \dots, \Omega_p$;

- 1: Initialisation: $k \leftarrow 1$, $n \leftarrow |S|$, $\Omega_k \leftarrow \emptyset$;
 - 2: **while** $n > 1$ **do**
 - 3: $\Omega_k \leftarrow \Omega_k \cup \{s_1\}$
 - 4: **for** $i = 2 \rightarrow n$ **do**
 - 5: $P'_i \leftarrow \emptyset$
 - 6: **for** $j = 1 \rightarrow |\Omega_k|$ **do**
 - 7: $a \leftarrow \Omega_k(j)$
 - 8: $P'_i \leftarrow P'_i \cup \{a\}$
 - 9: **end for**
 - 10: **if** $s_i \notin P'_i$ **then**
 - 11: $\Omega_k \leftarrow \Omega_k \cup \{s_i\}$
 - 12: **end if**
 - 13: **end for**
 - 14: $k \leftarrow k + 1$
 - 15: $S \leftarrow S - \Omega_k$
 - 16: $n \leftarrow |S|$
 - 17: **end while**
 - 18: **return** $\Omega_1, \Omega_2, \dots, \Omega_k, \dots, \Omega_p$
-

Assuming *descendants* modules are locked, the motion of a module can be described as rigid-body rotation about the actuating axis under the influence of gravity. The actuation torque is thus given by

$$\tau_i = J_i \ddot{q}_i - M_{g,i}, \quad J_i \ddot{q}_i = \sum_{j=1}^{|D'_i|} I'_{j,i} \ddot{q}_i, \quad M_{g,i} = \left| \mathbf{r}_{g,i} \times \frac{\mathbf{z}_i \times \left(\sum_{j=1}^{|D'_i|} m_j \mathbf{g} \times \mathbf{z}_i \right)}{|\mathbf{z}_i|^2} \right| \quad (5.11)$$

where $D'_i = \{D_i, i\}$ is a set of modules including module i and its set of *descendants*, D_i , J_i is the moment of inertia of D'_i with respect to \mathbf{z}_i (fixed during movement of module i), $M_{g,i}$ is the moment due to gravity of D'_i relative to \mathbf{z}_i , $I'_{j,i}$ is the moment of inertia of module j with respect to \mathbf{z}_i , $\mathbf{g} = [0 \ 0 \ -9.8] \text{ m}^2/\text{s}$ is the gravitational acceleration vector, and $\mathbf{r}_{g,i}$ is a perpendicular vector from \mathbf{z}_i to CM of D'_i .

Applying the work-energy principle in terms of rotational kinetic energy, the net work of module i , W_i , is given by

$$W_i = W_{\tau,i} + W_{g,i} = \frac{1}{2} J_i \dot{q}_i(t_k)^2 - \frac{1}{2} J_i \dot{q}_i(t_{k-1})^2 \quad (5.12)$$

where $W_{\tau,i}$ and $W_{g,i}$ are the work due to τ_i and gravity during time period T_k , respectively, given by

$$W_{\tau,i} = \int_{q(t_{k-1})}^{q(t_k)} \tau_i(t) dq, \quad W_{g,i} = \left(\sum_{j=1}^{|D'_i|} m_j \right) (\mathbf{r}_{g,i}(t_k) \cdot \mathbf{g} - \mathbf{r}_{g,i}(t_{k-1}) \cdot \mathbf{g}) \quad (5.13)$$

Joint velocity at the beginning and end of each time period is zero, so that $W_i = 0$, and $W_{\tau,i} = -W_{g,i}$. The energy consumption of a folding sequence is therefore $W_\tau = \sum_{i=1}^n |W_{\tau,i}|$, and we can design an evaluation function, χ' , given by

$$\chi' = W_\tau = \sum_{i=1}^n |W_{g,i}| = \sum_{i=1}^n \left| \left(\sum_{j=1}^{|D'_i|} m_j \right) (\mathbf{r}_{g,i}(t_k) \cdot \mathbf{g} - \mathbf{r}_{g,i}(t_{k-1}) \cdot \mathbf{g}) \right| \quad (5.14)$$

to evaluate different folding schemes and find an optimal one through enumeration.

Since the motion of a module in a different *path* to module i does not affect the joint torque, energy consumption of various folding schemes will be identical. Modules in different *paths* can be actuated in the same time period without changing energy consumption. Although the number of permutations of the folding order of n modules in a layout are as many as $n!$, the number of schemes can be reduced significantly. Given an array of module sequences $\mathbf{S} = [s_1, s_2, \dots, s_i, \dots, s_j, \dots, s_n]$, $s_i, s_j \in \{1, 2, \dots, n\}$, $s_i \neq s_j$, it can be rearranged into p folding steps instead of n . The procedure for rearranging a vector of folding order into folding steps is presented in Algorithm 3, where the rearranged folding sequence is denoted as $\{\Omega_1, \Omega_2, \dots, \Omega_p\}$ and P'_i represents the set of modules in the same *path* as module i .

5.2 Simulation and results

To evaluate the performance of the proposed reconfiguration method for modular robots, we utilise different configurations of the modular origami platform introduced in Chapter 3. We apply both the *automatic modelling* and the *heuristic algorithm* to generate energy-optimal reconfiguration










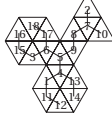

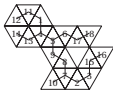
schemes and provide comparative results. The physical parameters for the simulation are taken from the first prototype of Mori, with a side length of 80mm, a thickness of 6mm, a weight of 26g, and the inertia tensor $I = 10^{-2} \times [-3.09, -3.09, -6.15, 0.67, 8.32 \times 10^{-2}, 2.30 \times 10^{-16}] g.mm^2$. The relevant Denavit-Hartenberg parameters are given in Table 5.2.

Table 5.2 – Denavit-Hartenberg parameters for the modular origami platform.

ζ_1	Offset along previous z to common normal of previous and new z	$\zeta_1 = 0$ or l
$\zeta_2(q)$	Angle about previous z , from old x to new x	Joint variable
ζ_3	Length of the common normal	$\zeta_3 = 0$ (axis intersection)
ζ_4	Angle about common normal, from old z to new z	$\zeta_4 = 60^\circ$

We have chosen three configurations, a tetrahedron, an octahedron, and a quadruped, representing two structural and one functional shape. All possible 2D layouts are generated through the unfolding process outlined in Section 5.1.1, some of which are depicted in Table 5.3. Different arrangements with the same 2D shape, such as tetrahedron L1 and L13, are taken as unique layouts due to the effect of the root node and the arrangement.

Table 5.3 – Target 3D configurations and corresponding pre-folding patterns.

3D shape	Possible layouts (L for Layout)		
			
Tetrahedron	Tetrahedron L1	Tetrahedron L7	Tetrahedron L13
			
Octahedron	Octahedron L1	Octahedron L160	Octahedron L320
			
Quadruped	Quadruped L35	Quadruped L70	Quadruped L105

5.2.1 Optimal layout

We first evaluate the proposed *heuristic* algorithm in terms of the torque requirements of the generated optimal layout compared to the *automatic* algorithm, which enumerates all possible layouts. The parameters used for Theorem 1 are $\lambda = [6.15 \times 10^{-11}, 0.0012, 0.026, 0 \text{ or } 0.08]$ and $\kappa = [3, 1, 2]$. The results are shown in Table 5.4, including a ranking that places the output of the *heuristic* algorithm among all possible layouts. The corresponding layout, rooted tree, and folding sequence are shown in Table 5.5.

To give a more realistic comparison of the two methods in terms of performance, we generate energy-optimal layouts on a Windows PC with Intel Core i7, 2.6 GHz, and 12GB RAM, and measure the computation time. We further use two performance indicators to compare the two methods, for each root node R among n modules, $R = 1, 2, \dots, n$. Firstly, we measure the equivalence of the *heuristic* algorithm in terms of optimality by taking the number of optimal layouts identical to those generated

Chapter 5. Reconfiguration algorithms based on origami principles

by the *automatic* algorithm, n_1 , and calculating $Rate\ 1 = \frac{n_1}{n} \times 100\%$. Secondly, we count the number of optimal layouts generated by the *heuristic* algorithm with less required torque than the median of all layouts with root node R , to calculate $Rate\ 2 = \frac{n_2}{n} \times 100\%$. The results are presented in Table 5.6.

Table 5.4 – Comparison between the energy-optimal layout generated by each algorithm in terms of required torque. The ranking places the heuristic algorithm among all automatically generated layouts.

3D shape	Method	Optimal layout	Torque [Nm]	Max. torque [Nm]	Ranking
Tetrahedron	automatic	L3 ($R = 1$)	0.016	0.321	—
	heuristic	L3 ($R = 1$)	0.016		1/16
Octahedron	automatic	L331 ($R = 5$)	0.240	2.328	—
	heuristic	L6 ($R = 5$)	0.294		14/384
Quadruped	automatic	L1 ($R = 5$)	0.990	4.892	—
	heuristic	L1 ($R = 5$)	0.990		1/108

Table 5.5 – Energy-optimal layouts generated by both algorithms, along with the corresponding rooted tree and the unified folding sequence.

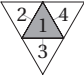
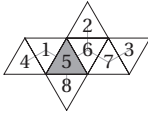
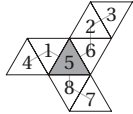
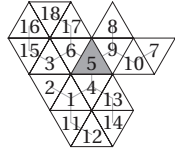
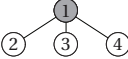
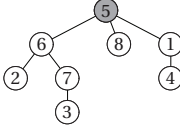
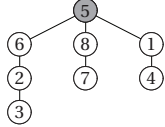
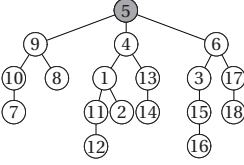
Tetrahedron L3 ($R = 1$)	Octahedron L331 ($R = 5$)	Octahedron L6 ($R = 5$)	Quadruped L1 ($R = 5$)
			
			
Ω_1 (2) (3) (4)	Ω_1 (2) (3) (4) (8) Ω_2 (1) (7) Ω_3 (6)	Ω_1 (3) (4) (7) Ω_2 (1) (2) (8) Ω_3 (6)	Ω_1 (2) (7) (8) (12) (14) (16) (18) Ω_2 (10) (11) (13) (15) (17) Ω_3 (1) (3) (9) Ω_4 (4) (6)

Table 5.6 – Performance comparison between the two methods to generate energy-optimal layouts in terms of computation time two performance indicators.

3D shape	Modules	Layouts	Method	Computation time (s)		Performance	
				Total	Layout	Rate 1	Rate 2
Tetrahedron	4	16	automatic	36	0.563	—	—
			heuristic	0.7	0.011	100%	100%
Octahedron	8	384	automatic	6435	2.090	—	—
			heuristic	12.5	0.004	0%	88%
Quadruped	18	108	automatic	13723	7.060	—	—
			heuristic	20	0.010	6%	61%

An increase in complexity of the 3D shape in terms of number of modules and layouts diminishes the performance of the heuristic algorithm. However, the computation time is reduced significantly, thanks to the estimation of the required torque, while still providing decent performance with respect to generating a layout with low energy consumption.

5.2.2 Optimal folding sequence

The optimal folding order for a 2D layout is generated by enumeration using Equation 5.14 and rearranged using Algorithm 3. The sequences for the optimal layouts generated by the *heuristic* algorithm are shown in Figure 5.3a, with the tetrahedron omitted as there is only one step for Layout L3. As the number of possible folding sequences for the modular origami platform is at least $(\lceil n/3 \rceil)!$, we use the Monte-Carlo method to verify the optimality of the generated folding sequences. Arrays of folding orders are generated randomly, rearranged, and the torque requirements calculated using Algorithm 1. We compare the performance of the folding sequence generated for the optimal layout, and the three layouts from Figure 5.3, with k randomly generated ones. Counting the number of randomly generated layouts with higher torque requirements, k_1 , we obtain a measure of performance for the optimal folding sequence, $Rate = k_1/k \times 100\%$. The results are plotted in Figure 5.3b.

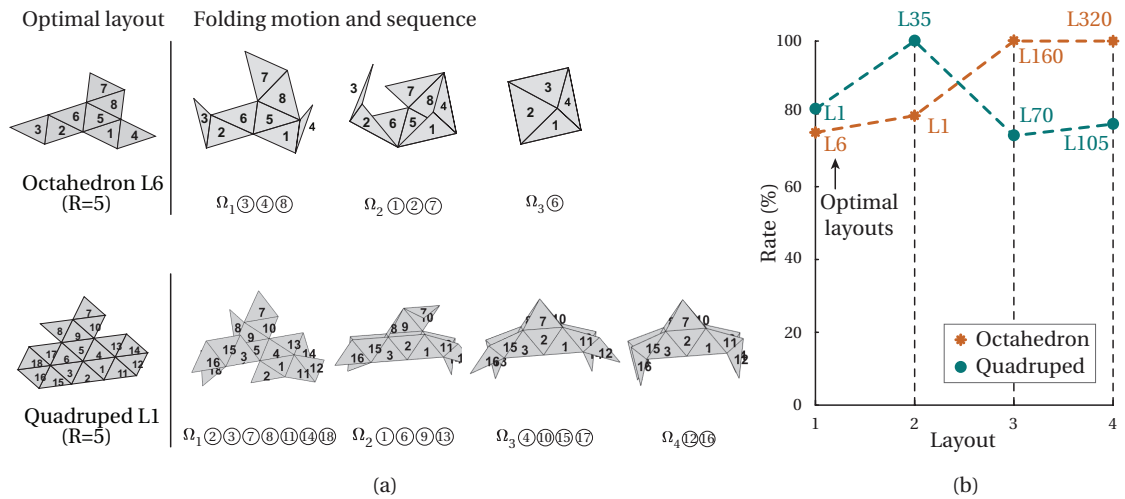


Figure 5.3 – Optimal folding sequence and performance for the optimal octahedron and quadruped layout. (a) shows the folding motion and folding sequence generated by the optimal folding sequence planner; (b) shows the performance rate of the folding sequence for the optimal layout and three more layouts compared to randomly generated folding sequence through the Monte-Carlo method.

5.3 Discussion

Planning and executing the reconfiguration process of modular robots, transforming from one functional configuration to another, is highly challenging due to the high number of individual entities and DoFs. A viable approach for practical systems must take into account physical limitations such as motor torques and misalignments, as well as limited resources such as power and computational capacity. In this chapter we address these challenges by proposing an algorithmic framework for the NP-complete reconfiguration planning problem utilising the concept of origami folding.

Given a target 3D shape of a modular robot, our approach consists of determining the optimal initial 2D layout and the optimal folding sequence of modules. We first present an automatic modelling approach as a baseline, which enumerates the energy consumption of all possible 2D layouts to determine the optimal one. We then propose a heuristic algorithm that uses several assumptions along with a cost function to evaluate energy consumption. Testing the approach by utilising the concept of a modular origami robot, the results obtained from simulating three structural and functional 3D shapes validate its performance, producing optimal or near-optimal reconfiguration schemes. Although the heuristic algorithm did not produce the absolute optimal solution in all cases, it consistently resulted in good performance with drastically reduced computation time.

Our approach to the reconfiguration process specifically focuses on minimising energy consumption during reconfiguration and reducing computational loads in the planning stage. Utilising origami principles to define the overall procedure removes connectivity changes during reconfiguration but also limits the type of relevant reconfiguration scenarios, primarily addressing the assembly of a collection of individual modules to 3D structures. Although it is possible to use our approach to reconfigure from one 3D shape to another, by unfolding to 2D, reorganising, and folding back to 3D, this is unlikely to represent an ideal process for all but a few unique cases. Furthermore, applying the concept of folding restricts the type of kinematic architectures of modular robots that can take advantage of it.

While these characteristics limit the scenarios and architectures that can be addressed, the overall methodology can be adapted and applied to wide range of systems. As the reconfiguration process is highly complex and yet crucial to enable fully functional implementations of modular robots, considerable effort is still required to address the multitude of remaining challenges.

Towards a Universal Robot **Part III**

6 Augmenting robotic reconfigurability through polygons

The previous part of this thesis studies several building blocks of reconfigurable robots and describes the initial conception of a robotic system based on quasi-2D modules that can assemble into a multitude of shapes and structures. Leveraging the concept of origami, folding 2D sheets into 3D shapes, and modularity, subdividing the system into stand-alone robots, the conceptual study of modular origami robots addresses some of the challenges associated with creating reconfigurable systems.

This chapter elaborates the initial concept into a new robotic paradigm for the development of robotic systems with an inherent morphological flexibility. By redefining the underlying structure of reconfigurable systems as shape-changing polygons, the paradigm enables the conception and creation of a wide range of multi-functional robots and structures. It proposes a framework for adopting and implementing the characteristic features at varying levels in order to address a spectrum of requirements, applications, and environments. The key features represent building blocks that, in combination, define the system's adaptability and can be adapted, extended, or reduced as required. The inherent ability to recreate a wide range of structural or functional 3D shapes results in an ideal candidate for assistive robots, human-robot interaction, and space exploration. The chapter begins with the background and motivation for the paradigm, focusing on morphological flexibility, followed by an in-depth description of the framework along with its challenges.

6.1 Morphological flexibility

In the context of robotics, morphological flexibility is the ability of a system to adapt its shape and structure to address different tasks or environments. This section begins with a general analysis of morphological flexibility in origami and modular robots and continues with a description of polygon meshing in this context.

6.1.1 Modular and origami robots

Origami robots utilise the concept of folding paper to create a single or multiple 3D shapes from quasi-2D structures. They are often made of multiple functional layers [57, 129] and regularly interface with additional functional components that are not embedded in the flat structure [130]. They use physical properties of living hinges and mechanical linkages created by folds and panels to achieve different functions [131, 132]. Some origami robots utilise the same configuration to achieve multiple

functions such as different types of locomotion [133], while others reconfigure into different functional shapes [58].

While the fabrication methods form one of the key benefits of origami robots, due to the low cost and simplicity of printing or stacking multiple layers, the morphological flexibility is determined in the design process and cannot be altered subsequently. Unlike a sheet of paper, which can be folded along infinitely many lines, robotic origami structures are limited to the fold lines and actuators embedded in advance. Furthermore, similar to a sheet of paper, the size and outline of the overall structure are fixed. One cannot simply enlarge parts of the robot or detach sections in one place and reattach somewhere else.

Although increasing the number of fold lines can make a structures more adaptable, managing these becomes evermore challenging. In order to take advantage of the structural flexibility arising from large numbers of living hinges, the resulting kinematic chains, whether closed or open, must be actively controlled, requiring numerous actuators and sensors, as well as significant power and computational capacities. Most origami robots therefore focus on a limited number of applications and structural or functional shapes, with the minimum number of components and embedded systems.

Modular robots, on the other hand, are based on the concept of attaching and detaching individual entities to form functional structures [134–136]. Their morphological flexibility is only partially defined in the design process through the number of ways modules can attach to each other as well as the number of degrees of freedom in each module. This flexibility can then be scaled by the number of entities in the overall system and is theoretically unlimited.

In practice, however, physical and computational restrictions apply to the morphological flexibility. This is in large part due to the system design and architecture of modular robots, requiring large numbers of entities to realise and assemble functional and structural 3D shapes. The architecture of an individual module commonly features a number of actuators that form a kinematic chain. The overall structure of those chains remains unchanged, so that the morphological flexibility of the system is limited to that of the kinematic chains formed in the configuration.

Furthermore, modular robots with sufficient functionality in terms of coupling, actuation, power, and control are generally bulky, heavy, and do not scale well beyond a small quantity. They most commonly resemble either tree-type links or cubic 3D pixels, greatly reducing the adaptability of more complex 3D assemblies.

6.1.2 Polygon meshing

The conceptual study of modular origami robots in Part II of this thesis begins to overcome the individual drawbacks of the two robotic concepts discussed above by creating a modular robot consisting of quasi-2D modules that can fold up on each other. However, the desired homogeneity of individual entities, resulting in equilateral triangles, limits the ability to approximate 3D shapes and thereby the flexibility of the system. Even with an increase in the number of units, singularities in the collection of closed chains contained in the system greatly reduces the adaptability of 3D structures. This has been shown with polygon meshes, used extensively in computational modelling and computer graphics.

Polygon meshing simplifies complex virtual 3D models to reduce computational loads [137]. Vertices are distributed across the 3D model, connected by edges to form polygon faces, which in turn constitute the 3D surface of the resulting mesh. Various meshing and remeshing algorithms have been developed

to address different needs in terms of computational requirements, accuracy, and graphical performance [138, 139]. Reducing the number of polygons generally reduces the accuracy of the resulting mesh but improves computational demands, and vice versa. This can be counteracted to an extent by increasing the density of vertices in critical regions and reducing it in areas with little variation.

When remeshing a model towards a set of homogeneous equilateral triangles, while maintaining the polygon count, the distortion of the resulting 3D mesh increases dramatically as the variation in edge length approaches zero. A small variation in edge length, however, can result in a smooth overall mesh that closely resembles the original model while only consisting of very similar triangles [140, 141]. The amount of variation necessary to maintain a close resemblance depends on the size of the triangles relative to the size of the model and its curvature range. This form of remeshing can be applied with a range of parameters to address different functional and morphological needs and forms the basis for the robotic paradigm proposed here.

6.2 A new robotic paradigm

Extending the initial concept of modular origami, this section elaborates the paradigm into its full form, incorporating polygon meshing and varying degrees of reconfigurability. Since, theoretically, any structure or shape can be represented by a polygon mesh in a virtual form, a robotic platform based on this concept could equally recreate any structure or shape in a physical form, although limited by physical and practical considerations. Merging the constituent polygons of such meshes with quasi-2D robotic entities leads to a framework for developing a new range of robotic systems that greatly advances the potential of morphological and functional flexibility.

The paradigm suggests a conceptual framework for a new class of robots by simplifying the underlying structure of the modular building blocks and approximating physical and functional structures through polygon abstractions. Depending on the range of intended applications of the system, different aspects of the paradigm can then be adopted and extended to suit the requirements and optimise the overall functionality. The inherent adaptability in terms of shape, structure, function, and application encompasses an approach towards developing a universal robot.

6.2.1 Characteristic features

The shapes of faces in a polygon mesh are defined by the edges connecting different vertices. Although polygons with higher numbers of edges are possible, they are most commonly triangles or quadrilaterals. Since any polygon can be divided into a number of triangles, it provides the base unit for a face in this paradigm. It can either be considered as a standalone entity, or individual edges that can be assembled into a number of different polygons. While some robotic platforms utilise extending edges and connecting nodes, such as the heterogeneous modular robot Odin [142], articulated meshes [85], and tensegrity structures [143], the underlying architecture limits their reconfigurability and applicability. Introducing a physical representation of polygon meshing, in form of quasi-2D, shape-changing modules that cover the area between edges, overcomes these limitations and results in an inherent morphological flexibility. The concept of this new paradigm is illustrated in Figure 6.1.

The shape of a robotic polygon can be fixed and homogeneous, as is the case with the modular origami robots considered in Part II, fixed and heterogeneous with an arbitrary number of different shapes, or flexible with edges of a polygon changing in length, maximising adaptability. The flexible shape of a

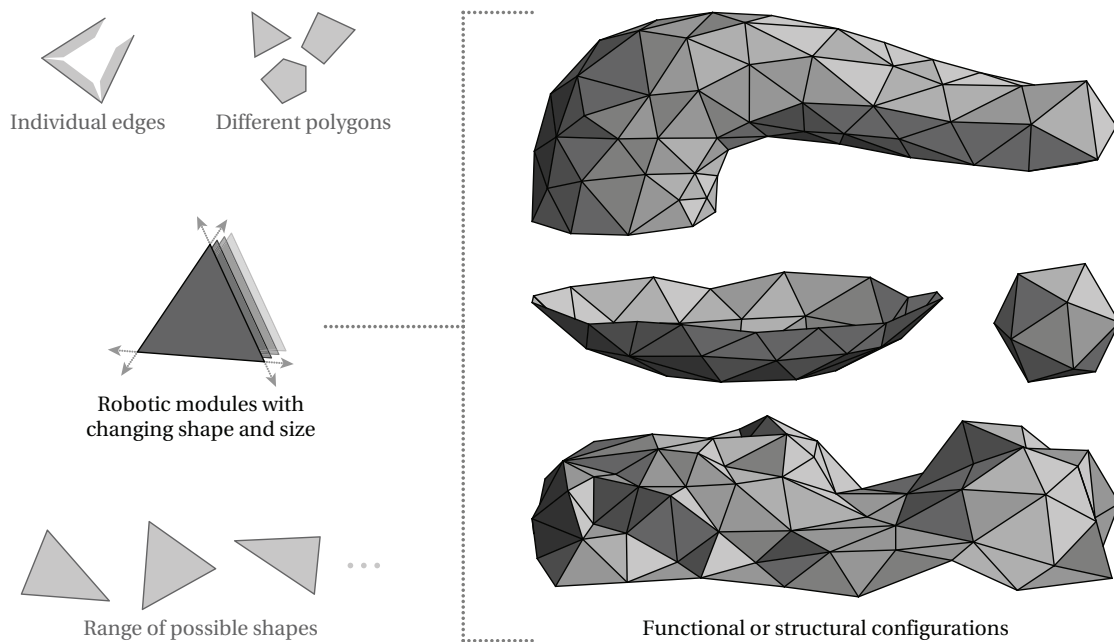


Figure 6.1 – Conceptual illustration of the new robotic paradigm. A reconfigurable modular robotic system based on polygons made up of individual edges able to alter in length, or any simplification or extension thereof. Approximating physical structures through polygon abstractions, similar to computer graphics, such systems can assume a wide range of structural or functional three-dimensional shapes.

polygon can be controlled actively or serve as a passive, compliant element, with any amount of active or passive modules contained in a system.

Connecting individual polygon robots or structures to one another at the edges forms a physical mesh in any desired shape or form. The connection between two polygons forms a rotary degree of freedom that can be actively controlled by one or both modules or left as a compliant hinge. The interface between two modules along the edge can be a passive or active coupling, as implemented in Chapters 3 and 4 respectively, or a pre-assembled hinge as part of a functional assembly. While polygon meshes generally consist of faces that are combined to form surfaces, where each edge of a polygon connects two faces, this could be extended by allowing potentially three or four polygon modules to connect on a single edge.

The aforementioned features define the architecture of the robotic structure, generating its morphological flexibility. They also have an impact on the functional flexibility as they determine the possible functional shapes that can be realised. The remaining functional factors are contained in the technological building blocks embedded in the system. These can include actuators, sensors, and controllers for the various degrees of freedom, power, computation and communication networks, additional end-effectors, and user interfaces.

The versatility of the framework can be further enhanced by incorporating various levels of modularity in the system, either extending or simplifying individual robots or the overall assembly. The architectural modularity, with individual edges making up polygonal modules, can be extended with technological or structural plug-ins. Systems can take advantage of heterogeneous modules with dedicated functions, creating modular computation, power, or sensing arrangements. Distributing

technological and algorithmic building blocks throughout the numerous entities of an assembly improves global performance and efficiency.

Overall, the paradigm provides a framework for creating a wide range of reconfigurable systems based on polygon meshes. They can be utilised to recreate 3D shapes through a polygon abstraction or arranged in functional structures taking advantage of the high degree of morphological flexibility.

6.2.2 Associated challenges

While this paradigm brings a new level of adaptability to robotic systems, realising them poses significant challenges and new approaches in terms of mechanical design, control, and electronics need to be established. The extent of these challenges encountered by a specific system depends on the range of intended applications, defining the complexity of the underlying structure. Advances in any of these areas will develop the integrity of the framework and enlarge the range of possible systems.

Along with the set of intended applications and environments, the physical and mechanical requirements for each module are defined by the number of modules within a system. Unlike traditional systems where only external factors change during operation, as the number of units in a reconfigurable structure grows, so do the forces and moments encountered. These need to be matched by the materials and mechanical properties of each module as well as the embedded actuators.

The physical structure of a single module, as well as the number of connected modules, determines the degrees of freedom in the overall structure. With fixed-shape polygons, every connection between two modules adds one degree of freedom, not considering closed chains and coupled hinges. By introducing flexibility in the shape of a polygon, an additional degree of freedom is added for each flexible edge in a module. Regardless of whether these degrees of freedom are active or passive, each of them needs to be incorporated into the body of a module with a suitable range of motion. Additionally, any misalignment in the structure is amplified through the large number of degrees of freedom, necessitating an intricate mechanical design and tight tolerances throughout.

The complexity introduced by large numbers of degrees of freedom also applies to the control of such systems, which is further complicated by the various closed chains constituting a polygon mesh. Adjusting just one vertex or edge in a mesh will often result in a large number of modules actively controlling their kinematic components. Firstly computing these kinematic chains and subsequently synchronising the system requires significant computational and communication capacities, whether distributed among the modules or aided by an external system. Due to the interconnected architecture, some active modules inevitably require more power, computation, and communication capacities than others. These systems must be further developed to account for the discrepancy and to allow for local and global synchronisation and distribution of resources.

Once the building blocks that allow a specific polygon-based robotic system to function and reconfigure have been established, it needs to be able to cope with a range of possible tasks. Each of these tasks will have a number of common and unique features, both computational and physical, that must be managed and controlled. Although some applications can make use of predetermined procedures, in order to take full advantage of the morphological flexibility, it must be complemented with a high degree of functional adaptability. For this purpose, modular control blocks and distributed networks need to be realised along with intelligent algorithms that are able to address new and varying tasks.

6.3 Discussion

The implementation of reconfigurability permits a single robotic system to address a multitude of applications, environments, and users. While the combination of two or more uni-functional robots into a single system can result in reconfigurable robots able to carry out multiple distinct tasks, such as a quadrotor tilting its propeller assembly to serve as wheels, they remain limited to functions actively incorporated in the design process. Reconfigurable modular robots address this constraint through the use of individual entities that can be assembled into a theoretically infinite number of formations. The underlying architecture of existing modular systems, however, greatly restricts the kind and scale of functional structures that can be realised as well as their adaptability once assembled.

This chapter proposes a new paradigm to reconfigurable robotics with an inherent morphological flexibility. By approximating physical structures through polygon abstractions, it enables the development of robots that can assume a wide range of structural or functional 3D shapes. Analysing the characteristic features and underlying challenges, we present a framework for developing a broad spectrum of robotic systems with varying degrees of modularity, adaptability, and applicability. This promising perspective of a universal robotic system calls for the development and study of implementations thereof, addressing the ample challenges outlined above and advancing the potential of reconfigurable robots in general.

While the proposed paradigm enhances the ability of robotic systems to change shape, configuration, and function, some of the fundamental drawbacks of modular robots remain. These need to be taken into account when developing, evaluating, and using such systems, in addition to the distinct challenges outlined in Section 6.2.2. As the number of individual entities in an assembly of modular robots increases, mechanical, electronic, and computational demands multiply, thereby diminishing the feasibility and performance of carrying out real tasks. This is further accentuated by the trade-off between the overall size of each entity and the embedded functionality. Although the simplified underlying architecture of this paradigm aims to improve the balance between reconfigurability and functional complexity, the ability to change the shape of each module potentially increases the complexity of planning and executing the overall reconfiguration process. In comparison to fixed-morphology modular robots, however, this added complexity is counteracted by the reduced number of entities needed for a given task resulting from the enhanced flexibility of shape-changing polygons.

7 A polygon-based modular robotic platform

Following the detailed description and analysis of the proposed paradigm, this chapter discusses the implementation of polygon-based robotic systems. It first covers a number of design considerations and possible ways of implementing such robots, before presenting the development of a modular robotic platform that addresses some of the key challenges. While the inherent morphological flexibility of the paradigm greatly enhances reconfigurability, it introduces a large amount of complexity in terms of mechanism and system design, electronics, and control. In addition to the already high number of entities and degrees of freedom in ordinary reconfigurable robots, the ability to change the shape of a module further increases the number of mechanisms working in tandem, demanding a precise and robust design. Moreover, the underlying architecture of an assembly of modules, similar to the concept of polygon meshing, is accompanied by kinematic dependencies that must be computed and controlled in synchronisation to ensure functionality of the overall system.

The robotic platform presented in this chapter provides a comprehensive solution to these issues and presents a sophisticated robot that closely resembles a highly automated implementation of the framework introduced in Chapter 6. It lays the groundwork for a versatile robotic system that can be applied to a wide range of tasks and scenarios, such as space exploration, personal robotics, or interactive 3D displays. It is intended to prove the viability of the paradigm and validate its underlying morphological and functional flexibility. The chapter outlines the mechanical advances and technological designs of the new robotic module, followed by results from initial functional testing. It further presents an experimental design consisting of application-oriented demonstrations, experiments, and testing procedures to validate the key characteristics of the platform in terms of functional adaptation, morphological flexibility, and optimisation.

7.1 Design considerations

The concept of polygon-based robots, as introduced in Chapter 6, utilises collections of morphologically flexible polygons to form robotic systems that are highly adaptable in shape and function. While Section 6.2.1 discusses the characteristic features of the paradigm and the range to which they can be adopted and extended, the physical implementation of such systems poses numerous challenges and can vary greatly. From largely passive systems with predefined configurations of fixed-morphology polygons to shape-shifting modules that autonomously assemble, the implemented features of the paradigm are defined by the intended range of functions and applications.

As the number of active features and components increases, so does the control over the resulting morphology as well as the mechanical and functional complexity of the robot. The main elements that are either active or passive include the length of each edge, the connection between polygons, and the hinge formed at each edge. The system can be designed with different numbers of edges per polygon and different numbers of distinct polygon types, determining the morphological adaptability and possible types of configurations. Changing the size or shape of a polygon alters the lengths of each edge as well as the angles between them. The adjustable edge length of a physical polygon represents a linear sliding joint along the axis of the edge, while the angle between edges forms a rotary joint around the connecting vertex with an axis perpendicular to the two edges. The six parameters making up a triangular polygon, three edges and two angles, can be fully described by defining three of those values. A polygon with four edges, on the other hand, requires defining five parameters to fully determine its shape and size, further increasing the mechanical complexity.

The implementation of a polygon-based robot requires careful analysis of the required functionalities and morphologies for a given set of applications. Each aspect of the paradigm comes with a range of possible approaches that determine the performance and flexibility of the underlying structure, while embedded technologies impact the functions and functionality of the overall system. For instance, actively shape-changing polygons can be controlled by telescopic edges or rotary hinges, with hydraulic, pneumatic, electromechanical, or piezo actuation, depending on the desired scale, range, and forces. The choice of passive elements, whether in a fully controlled or partially compliant robotic systems, completes and establishes the integrity of each polygon and the resulting physical mesh. Maintaining this mesh integrity over the entire flexible range of a system is crucial in enabling desired morphological changes.

The remainder of this chapter describes an implementation intended to validate the underlying morphological flexibility of the paradigm, while at the same time demonstrating a range of possible functions. It consists of a robotic platform of actively controlled reconfigurable polygons such that the overall system's morphology can be fully manipulated, widening the realm of applications. The design process and resulting choices for each aspect of the polygon robot are described in detail below.

7.2 System overview

The robotic platform embodies a modular system consisting of shape-changing, self-contained robotic triangles that can automatically connect to one another and assemble into a desired physical polygon mesh. Independent modules can automatically assemble into a configuration, while flat polygons with changing edge lengths enable the system to resemble and alter a wide range of 3D-shapes. This underlying morphological flexibility greatly enhances the applicability of the platform, as it can potentially realise a myriad of tools, structures, or mobile robots, provided that physical and practical limits are met. The mechanical and electronic design parameters were determined based on a number of planned experiments and demonstrations highlighting the potential of the paradigm, as outlined in Section 7.4.

Individual robotic modules are highly functional and incorporate many of the attributes introduced in Chapter 6. Various features are constructed to be expanded, reduced, or translated into a variety of other systems in the future with different applications and functions in mind. For instance, active modules can be combined with passive ones, reducing the number of actuators but maintaining some functionality, potentially featuring functional extensions. The system embodies a universal platform that can be adapted to suit a wide range of requirements.

7.2.1 Mechanical advances

The ability of this robotic platform to realise and alter polygon meshes in a physical form relies on the ability of each module to change its own polygonal shape. The range of possible shapes is defined by the relative change in length of each edge, which in turn defines the geometric and kinematic reconfigurability of the overall system. Adjusting the length of each edge requires a linear DoF along its axis as well as hinges that allow the angles to adjacent edges to change. As the vertices of coupled robots are shared, these hinges need to be offset from their rotary axis. This can be achieved through mechanical linkages or through arced features with the axis perpendicular to both edges as its centre.

To ensure a system of polygon modules remains functional at all times, no features of one module can protrude into the working range of an adjacent one in any state. This impacts the spectrum of possible shapes a module can assume, as widening the range of shapes implies an increase in the range of motion of the linear rails as well as the offset hinges. The larger the range of motion, the more space is taken up by the rotary hinges and linear rails, so that less space is available in the body of a module to house functional components. We have developed an implementation of a triangular module that addresses this trade-off between range of motion, morphological flexibility, autonomy, and functionality of the overall system. It integrates new approaches to mechanical design, electronics, and control, necessary to realise the framework introduced in Chapter 6. A render highlighting the overall module design and the main functional features and components is shown in Figure 7.2.

Individual modules have a triangular base shape with each edge able to independently increase in length, illustrated in Figure 7.1a. The three extending edges, Edge 1-3, and three hinges with axes through the vertices and perpendicular to the edges, R1-R3, form a kinematic chain with three degrees of freedom. Changing the length of any edge results in the three angles between the edges, α , β , and γ , to change without affecting the length of the other edges. Simultaneously increasing all three edge lengths at the same rate leaves the angles unchanged but increases the area of the triangle.

Once two modules, A and B, are connected, one edge of module A shares an axis with an edge of module B, Edge_{A2} and Edge_{B1} as illustrated in Figure 7.1b. The resulting rotational link between the modules is the reference for their relative position, controlled using the angle between any two hinge axes, e.g. R_{A2} and R_{B2}, denoted as δ . The dihedral angle between the two polygons is then $\pi - \delta$. When a module is not connected to another, it can move freely on flat surfaces using the same actuation that controls δ

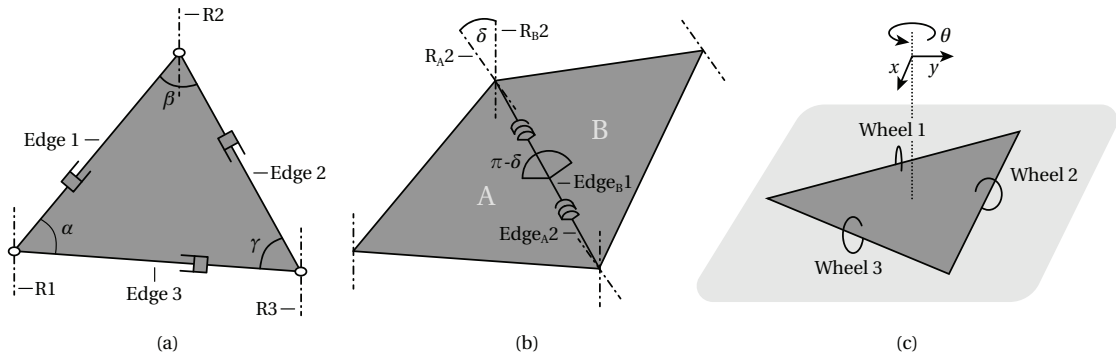


Figure 7.1 – Degrees of freedom and notations in different operational states of a module. (a) shows the kinematic chain of a single module formed by the three edges; (b) shows two coupled modules, the shared edge, and the resulting rotational joint; (c) shows the mobile degrees of freedom of a single module on flat surfaces resulting from the three wheels.

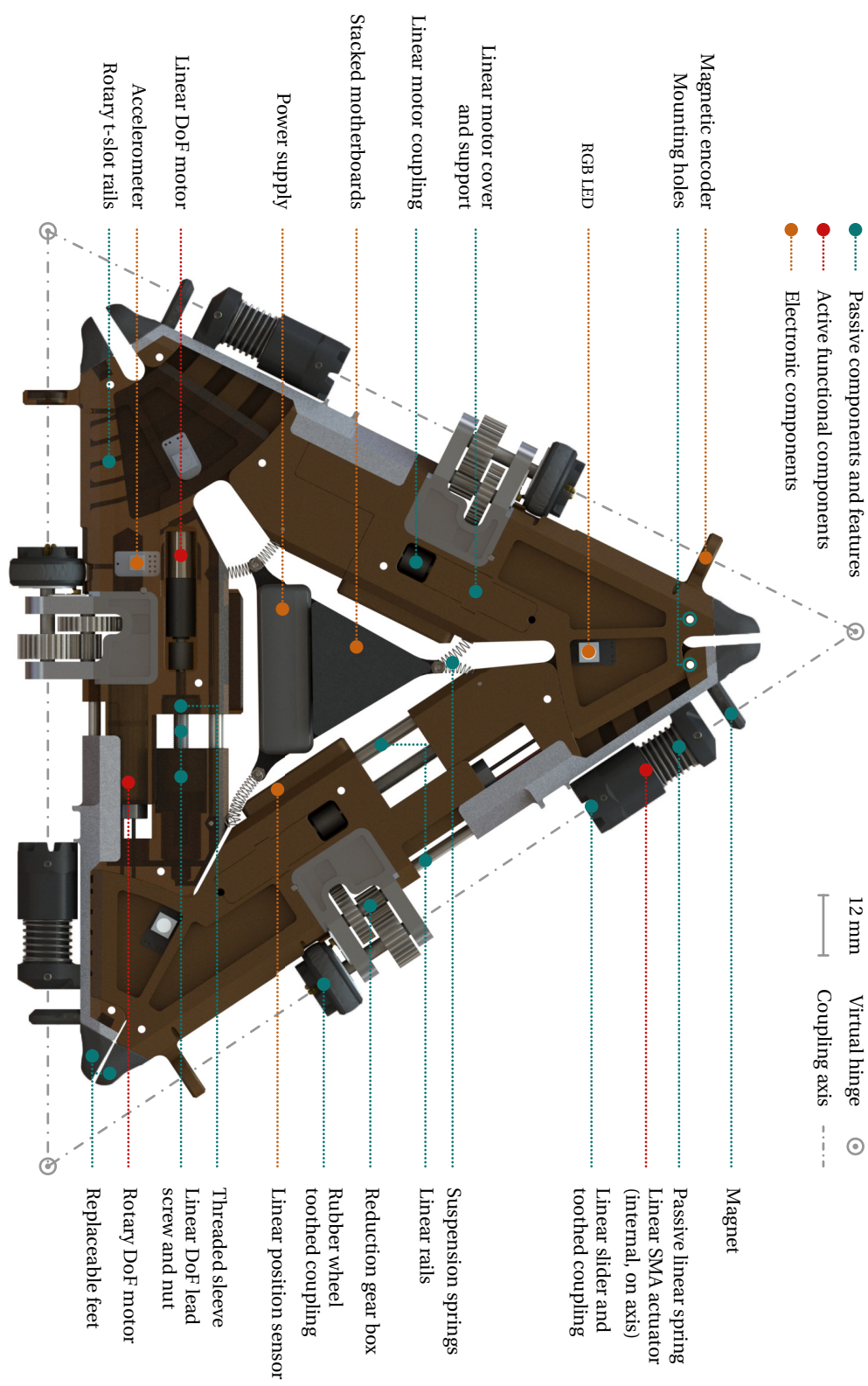


Figure 7.2 – Illustration of the design of a full polygon-based robotic module. The main functional components and features, active and passive, as well as electronic components are highlighted. Each edge in the design is identical and all components, except for the central electronics and the accelerometer, appear three times. The illustration shows three edges with different lengths, fully closed, extended half way, and fully open.

in a coupled state. As the lines from the contact points of the three wheels, Wheels 1-3 in Figure 7.1c, perpendicular to the edges, do not cross the centre of the polygon, a module has three translational degrees of freedom, x , y , and θ .

The integrity of a polygon mesh relies on the stability of vertices that are shared by connected polygons. For a physical implementation, the endpoints of two adjacent edges must remain connected at all possible angles and extension values. As the rotary axes between adjacent edges are shared by multiple modules, their hinges must be offset from vertex. We have developed a unique implementation that enables this shape change of a module, consisting of arced, interconnecting t-slots embedded in the two main pieces making up each edge, as shown in Figure 7.3. They provide a smooth hinge for the kinematic chain and rigidly couple the edges to each other. The two main pieces of a module are machined out of POM containing 13% PTFE to improve sliding properties for both the offset hinge and the linear rail. This t-slotted, sliding design reduces the mechanical complexity compared to other approaches, such as arced ball bearings, and provides a more rigid structure compared to mechanical linkages, although with a reduced range of motion.

The extension of each edge is guided by two linear steel shafts and additional features embedded in the main pieces. It is driven by an anti-backlash leadscrew assembly, Haydon Kerk NTG, coupled to a 6mm diameter DC motor with a reduction of 699.5:1, Precision Microdrives 206-108. A round, smooth disk mounted to the leadscrew axial sits in a cut-out on the main piece containing the motor and is held in place by a threaded POM sleeve, axially supporting the assembly. The motor itself is glued into a slot and supported by a cover that diagonally slides into place. Implementing a leadscrew provides a reasonable trade-off between force and speed that can be easily implemented into the mechatronic system compared to other telescopic approaches such as pistons or piezo actuators, although it is not backdrivable. The base length of each edge, the distance between two vertices, is 180 mm and can increase by 7.5%, limited to 6.7% when two edges are fully extended, while the overall thickness of the robot is 12 mm. One fully assembled module consisting of three edges and all functional and electronic components weighs 237 g in total.

Some unique design concepts are inherited from the two prototypes presented in Chapters 3 and 4. The coupling mechanism, featuring mechanical overload protection, and rotary actuation system, transferring motion from the body of the module to the edges, have been adapted to match the required precision, properties, and functionality of the new platform. The coupling mechanism consists of the same radial tooth design presented in Section 4.3 with a matching hexagonal sliding joint machined out of POM, greatly improving mechanical properties and tolerances, actuated by a joule-heated SMA

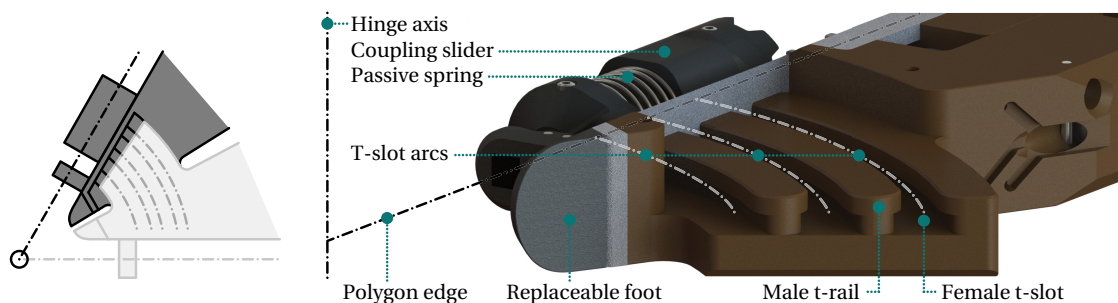


Figure 7.3 – Offset hinge design enabling the shape change of a polygon robot. It consists of arced, interconnecting t-slots that change the angle between two edges of a polygon, while maintaining the integrity of the mesh during morphological transformations.

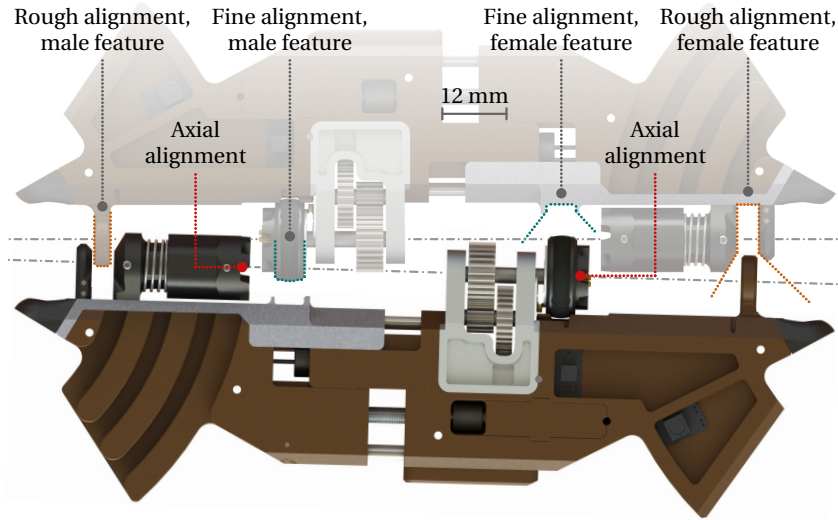


Figure 7.4 – Mechanical features addressing misalignment during the coupling of two modules. Rough alignment is achieved through protruding features holding electronic components. Final precise alignment is accomplished by the wheel of one module entering a curved slot in another module, shown in more detail in Figure 7.5.

spring. The mechanical, retraction-based coupling results in a robust connection between modules and does not require power in its closed state. SMA springs provide a high force to size ratio compared to DC motors and are easily incorporated compared to piezo actuators. Both opening and closing of the coupling takes less than 3 s at no load and room temperature.

The rotary component of the coupling joint is driven by a DC motor with a reduction of 256:1, Maxon DCX 8 M and GPX 8, connected to a custom gearbox consisting of two stages of 28:12, resulting in an overall reduction of 1393.8:1. The actuation system is used to both fold two connected modules, with a range of angles between them of $\pi - \delta = \pm 120^\circ$ as defined in Figure 7.1, and drive a single module or collection of modules across flat surfaces. The wheels incorporated into the rotary part of the coupling have a diameter 15 mm with a silicon insert, slightly protruding the device's thickness. This high reduction ratio of the gear train provides the required torque output in larger configurations but results in slow locomotion of individual modules.

The stability of the physical polygon mesh furthermore relies on the structural integrity of each module as well as the connection between them. In addition to the interconnecting t-slots that connect a polygon's edges, its mechanical features ensure that deflections and misalignments within the various mechanisms remain in an acceptable range even under high loads. All forces and moments acting on two connected modules are transferred solely through the coupling elements. The rotary part is coupled to the final shaft of the gear box, which sits firmly in one of the two main pieces. The retracting coupling assembly in turn is attached to an aluminium bracket that is glued and screwed to the other main piece, reinforcing the overall assembly and ensuring structural integrity under load. This aluminium bracket also provides the matching hole for one of the linear shafts, lubricated by a thin PTFE bushing, further strengthening the connection between the two main pieces, while the other shaft sits directly in the main piece.

To ensure successful coupling during the reconfiguration process, vital to the system's functionality, further mechanical elements have been incorporated into each edge to aid the alignment between two

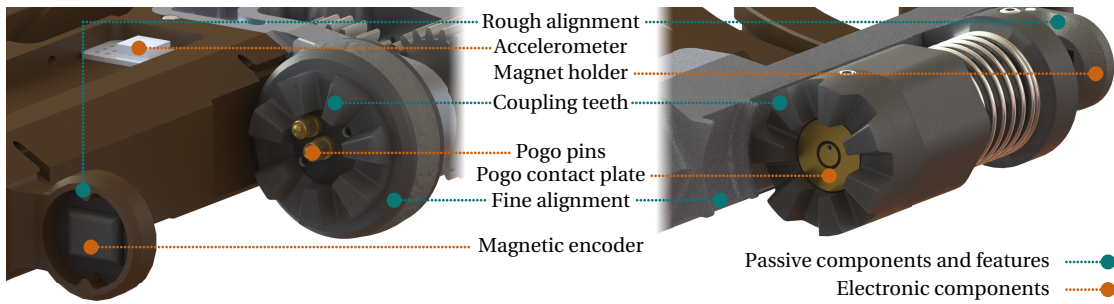


Figure 7.5 – Electronic and physical elements of the coupling mechanism of the polygon-based robot. It includes contact pins embedded in the coupling pieces, the absolute magnetic encoder, and the accelerometer. The physical coupling consists of a spring-loaded retracting element and a rotating pivot, both with radial, meshing teeth.

modules. Protruding features housing electronic components have angled features as a preliminary guide for larger offsets. The final precise alignment is accomplished through a rounded slot with angled ridges that the wheel of another module occupies when coupled. The self-centring design of the toothed coupling elements ensure slot and wheel engage during the coupling process. The alignment features are detailed in Figures 7.4 and 7.5, with testing results of the misalignment capabilities provided in Section 7.3.

The polygon mesh structure of the robot can inherently only feature two coupled modules per edge, and thus two closed surfaces cannot be joined at a single edge. However, the faces of two modules can be attached to one another to combine multiple surface meshes. Although this is not an automatic feature, the body of the robot contains mounting holes so that two modules can be fixed to one another at any distance or angle without using any of the couplings. These mounting holes, located near the three corners, can also be used to attach other physical features or interfaces to the face of a module. These corners also features attachment points for replaceable feet that can be adapted to a given application or locomotion mode.

7.2.2 Electronics and control

The polygon-based modules are designed to serve as a platform for the implementation of a variety of robotic polygon meshes. For the system to be adapted and its features to be adopted as required, the electronics and control systems must address the underlying morphological flexibility as well as promote and extend the various levels of modularity. We have addressed these challenges through an intricate electronics design that accommodates the higher numbers of DoFs, actuators, and interfacing components. Various control systems are integrated into the platform and are designed to study control and reconfiguration algorithms, with provisions in place for adaptations and extensions.

Each module holds a total of 24 individual PCBs connected by 81 wires and 17 physical contacts. The main electronics consist of two stacked PCBs that are located in the centre of a module, suspended by 6 extension springs. The bottom board contains the main micro-controller, a 16-bit Microchip dsPIC33EP512GM604, responsible for coordinating all functions of a module, motor, SMA, and LED drivers, a DAC, and the solder connections for all cables. The three Maxon motors are driven by two Texas Instruments (TI) DRV8834 chips and the maximum current output is set by a TI DAC5574. The three extension motors are driven by two TI DRV8836. The coupling SMAs are activated by an LED

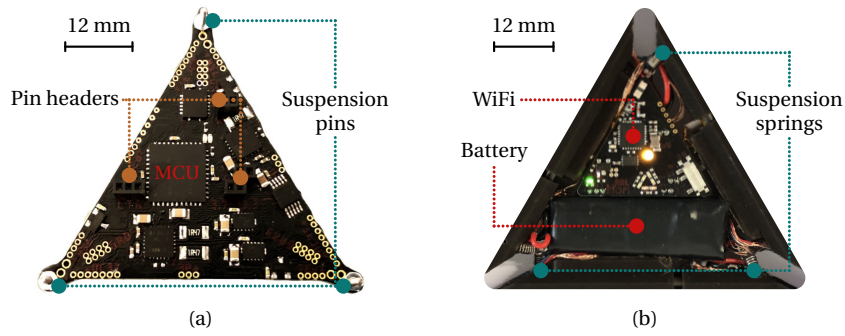


Figure 7.6 – Central electronic control boards of the polygon based robot. (a) shows the bottom PCB featuring the main controller, and motor and LED drivers, as well as all the solder points; (b) shows the top PCB including power and WiFi systems and the battery suspended in a module.

driver, TI TLC59208F, which also sets the colour and brightness of the six RGB LEDs located on both faces of a module. The top board is plugged into the bottom one with nine connections and contains the power and wireless communication electronics. A single cell, 150 mAh battery plugs into the top board resulting in a standby time of roughly 1.2 h and runtimes of around 25 m and 10 m under medium and maximum loads respectively. The battery provides 3.7V directly to the SMAs and the extension motors, a boost converter, TI TPS61030, supplies 5V to the three Maxon motors, and a MaxLinear SPX3819 regulates the 3.3V logic level. An Espressif ESP8266EX adds wireless communication and high-level control to each module. The electronics are depicted in Figure 7.6.

To account for a modular control architecture, several communication streams have been included in the design of the robotic platform that address the challenges associated with controlling and synchronising modules. Using the wireless chip, each module can communicate directly with another, as well as external computers providing global commands. In addition to this, electronic connections have been embedded in the coupling system. Spring-loaded pogo-pins in the centre of the rotary coupling element make contact with two rings on the sliding element of another module. As the rotary element can spin continuously, two spring-loaded levers are in turn used to connect it to the main body. They provide a ground connection shared by all modules and direct serial communication between neighbouring modules. Through a custom communication protocol, each module can interpret the commands directly, or pass them on until they reach the addressed module as instructed. These physical connections are also used to synchronise the actuation of the degrees of freedom shared by two neighbouring modules.

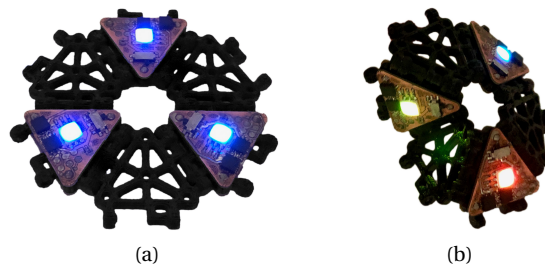


Figure 7.7 – Battery-powered plug-ins for passive modules with a fixed morphology. It features an accelerometer, a microcontroller, and an RGB LED to visualise the curvature profile of a surface. (a) the colours of the three LEDs are equal as all modules are horizontal. (b) three different colours resulting from different orientations.

The extension of each edge is measured by a linear potentiometer, ALPS RDC1014A09, coupled to one of the linear shafts. The angle between two connected modules is measured by an absolute magnetic encoder, AMS AS5048B, sensing the magnetic field of a permanent magnet on the coupled module. The two sets of three values are actively controlled by PI-loops running at 20 Hz and 100 Hz respectively. An accelerometer, NXP MMA8452Q, aligned to one of the edges, provides the static, spatial orientation of a module. This can be used to provide feedback on the overall configuration in an assembly and be fused with other sensor data to more accurately determine its state. For instance, in combination with the coloured LEDs on a module, the intensity of different wavelengths of light can change depending on the overall orientation of a module. We have demonstrated this by developing a simple battery-powered plug-in for passive modules of fixed morphology, resembling the architecture used in Part II, where the colour change visualises the curvature profile of a surface as illustrated in Figure 7.7.

When a module is not connected to another and the rotary coupling elements are used as wheels, the module computes the input to each motor based on a desired direction and trajectory. While the asymmetry of the wheels gives the robot an additional DoF, making the system holonomic and thereby greatly improving manoeuvrability, it also implies asymmetry in the speed it can achieve in different directions. Given a module drives in a direction perpendicular to one of the edges, following trajectories of the same radius to the left and to the right will result in different overall speeds. This must be taken into account when planning navigation profiles. We have developed a model to compute the wheel speeds for a given trajectory, taking the three extension values into account. It can translate user inputs of speed and steering angle to simplify user interactions, or combined with an external sensing system to automatically drive modules from one location to another. The model is derived as follows.

Given a triangular robot with vertices A , B , and C and opposing edge lengths a , b , and c , the angle between the vertices, α , β , and γ are given by

$$\alpha = \arccos \frac{b^2 + c^2 - a^2}{2bc}, \quad \beta = \arccos \frac{a^2 + c^2 - b^2}{2ac}, \quad \gamma = \pi - \alpha - \beta. \quad (7.1)$$

We take the edge opposing vertex A as the reference such that any trajectory of motion is tangent to the perpendicular at the centroid of the triangle. Taking the vertex with a fixed distance to the wheel on the edge opposing vertex A as the origin, the coordinates of the vertices and the centroid, P , are given by

$$A = \begin{bmatrix} b \cos \gamma \\ b \sin \gamma \end{bmatrix}, \quad B = \begin{bmatrix} a \\ 0 \end{bmatrix}, \quad C = \begin{bmatrix} 0 \\ 0 \end{bmatrix}, \quad P = \frac{A + B + C}{3}. \quad (7.2)$$

A wheel is located on each edge at a fixed distance d_w from the closest vertex clockwise and perpendicular to the edge. The coordinates of the three wheels, W_a , W_b , and W_c , are then given by

$$W_a = \begin{bmatrix} d_w \\ 0 \end{bmatrix}, \quad W_b = \begin{bmatrix} (b - d_w) \cos \gamma \\ (b - d_w) \sin \gamma \end{bmatrix}, \quad W_c = \begin{bmatrix} a - d_w \cos \beta \\ d_w \sin \beta \end{bmatrix}. \quad (7.3)$$

Each wheel exerts a force in a direction perpendicular to its edge when rotating, as shown in Figure 7.8. In order to compute the inputs for each wheel given a desired trajectory, we calculate the sum of moments about the centroid. To do so, we first find the shortest distances between the centroid and a

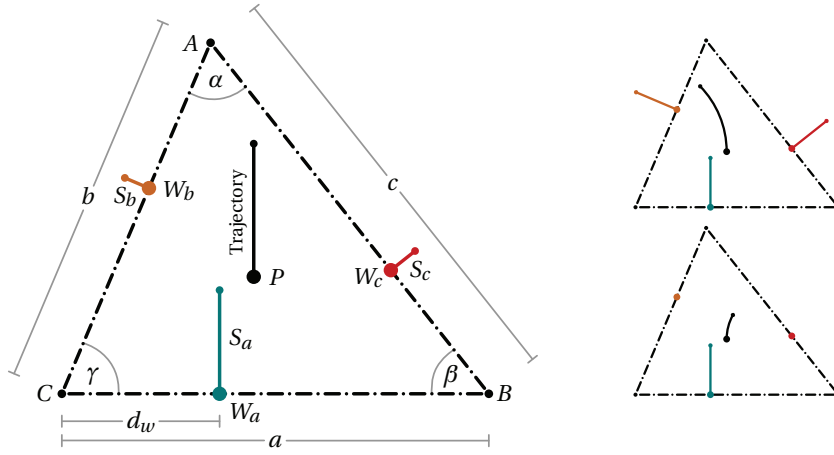


Figure 7.8 – Notations used in the derivation of the input speeds for the three motors given a desired trajectory. Left: the curved trajectory of a module, perpendicular to edge a at point P , is determined by a combination of relative rotational speeds S of the three wheels as well as the shape of the polygon. Right: maximum curvatures to the left and to the right.

line perpendicular to each edge going through its wheel coordinates, d_a , d_b , and d_c , given by

$$\begin{aligned} d_a &= |P_x - W_{a,x}|, \\ d_b &= \frac{|(\hat{W}_{b,y} - W_{b,y})P_x - (\hat{W}_{b,x} - W_{b,x})P_y + \hat{W}_{b,x}W_{b,y} - \hat{W}_{b,y}W_{b,x}|}{\sqrt{(\hat{W}_{b,y} - W_{b,y})^2 + (\hat{W}_{b,x} - W_{b,x})^2}}, \\ d_c &= \frac{|(\hat{W}_{c,y} - W_{c,y})P_x - (\hat{W}_{c,x} - W_{c,x})P_y + \hat{W}_{c,x}W_{c,y} - \hat{W}_{c,y}W_{c,x}|}{\sqrt{(\hat{W}_{c,y} - W_{c,y})^2 + (\hat{W}_{c,x} - W_{c,x})^2}} \end{aligned} \quad (7.4)$$

where \hat{W}_b and \hat{W}_c are arbitrary points on that line such as

$$\hat{W}_b = \begin{bmatrix} W_{b,x} - \cos(\pi/2 - \gamma) \\ W_{b,y} + \sin(\pi/2 - \gamma) \end{bmatrix}, \quad \hat{W}_c = \begin{bmatrix} W_{c,x} + \cos(\pi/2 - \beta) \\ W_{c,y} + \sin(\pi/2 - \beta) \end{bmatrix}. \quad (7.5)$$

As the interaction between the wheels and the ground is difficult to predict and changes significantly from surface to surface, we only aim to find a relationship between rotational speeds of the three wheels resulting in a given trajectory, adjusted through dimensionless factors to account for different conditions. We thus define relative input speeds to the wheels, S_a , S_b , and S_c , where $-1 < S < 1$, positive values result in forces away from the triangle, and negative values towards it. We assume that wheels on edges b and c are never stationary, $S_b \neq 0$ and $S_c \neq 0$. We can then use a virtual, dimensionless moment about the centroid, M , to relate the rotational speeds to a trajectory.

$$M = S_a d_a + S_b d_b + S_c d_c \quad (7.6)$$

Since we are interested in trajectories perpendicular to a reference edge, we can say that the virtual, dimensionless sum of forces, F , parallel to the reference edge is equal to zero.

$$\sum F_x = S_c \cos(\pi/2 - \beta) - S_b \cos(\pi/2 - \gamma) = 0 \quad (7.7)$$

Taking S_a as the reference value defining the overall speed of the robot, we can combine Equations 7.6 and 7.7 to give the required input for the other wheels resulting in a trajectory with a curvature determined by M as follows.

$$S_c = \frac{M - S_a d_a}{d_b \frac{\cos(\pi/2 - \beta)}{\cos(\pi/2 - \gamma)} + d_c}, \quad S_b = S_c \frac{\cos(\pi/2 - \beta)}{\cos(\pi/2 - \gamma)} \quad (7.8)$$

To account for different surfaces we can implement an offset, M_o to the virtual moment such that the input moment $M_i = M + M_o = 0$ results in a straight trajectory. The resulting relative speeds S_b and S_c can further be scaled by a multiplication factor to maximise the range of possible curvatures of a module.

7.2.3 An adaptable platform

The robotic module is designed as an implementation of a fully functional robotic platform utilising the proposed paradigm. Its various features can be adjusted, extended, or reduced to address a variety of applications and scenarios. The modules are constructed in a modular fashion so that individual parts, such as the couplings, electronics, or actuators, can be replaced easily. Mounting holes can be used to attach additional features or devices to individual modules, such as mechanical linkages, force-sensing plates for human interactions, or end-effectors for robotic arms.

Furthermore, the design itself is easily adaptable to produce varying modules with specialised functions. For instance, removing the rotary actuators and gearbox from a module retains the ability to alter the shape of the polygon and couple with another, while freeing up space in the centre. This reduces the torque of connections to fully functional modules by half and implies a loss of mobility. However, the added space can be used to produce specialised modules that can be distributed across an assembly featuring extra batteries, computational power, or additional sensors such as cameras. It can also interface with other technologies, such as fans to move around in micro-gravity environments or compressors to supply soft robotic actuators, all embedded within the same robotic framework.

Overall, the platform provides a fundamental system to study the potential of the proposed paradigm. The existing robot integrates the core features and functions to examine and further develop its core technologies including control schemes and reconfiguration algorithms. It is also designed to be extended to address the challenges of implementing such systems in a wide range of possible applications.

7.3 Functional testing

The robotic platform has been developed based on the framework presented in Chapter 6 and is designed to validate the morphological flexibility inherent to the new paradigm. In this section we verify the individual functional aspects of the robot including shape change and mobility. The adaptable morphology of an individual module provides the platform with its unique ability to physically resemble polygon meshes. Controlling the trajectory of individual modules travelling across flat surfaces augments the system's ability to assemble into any configuration and transform from a collection of individual 2D polygons into complex 3D shapes. By demonstrating these two functional aspects of the robot, we prepare for the validation and testing of the platform's morphological flexibility in application-oriented experiments.

7.3.1 Adaptable morphology

The shape of a polygon is defined by the number of edges and the length of each edge. The platform of robotic polygonal modules with adjustable edge lengths can change its own shape to address the requirements of its individual state or the overall physical mesh. Given the relative adjustability of each edge, the range of possible shapes of the resulting polygon can be determined, as shown in Figure 7.9a. We have tested the robotic module, utilising the combination of offset hinges and linear rails as highlighted in Figure 7.9b, to verify its adaptable morphology. Each edge of a module can extend the distance between its virtual vertices from 180 mm to 193.5 mm, or 192 mm when two edges are fully extended. The time for an edge to fully extend from a closed position is around 10 s, independent of any other edge. The motor driving the extension has been chosen to maximise the force exerted by the assembly along its axis, resulting in relatively slow movement. The resulting shapes of the polygon robot are depicted in Figure 7.9c.

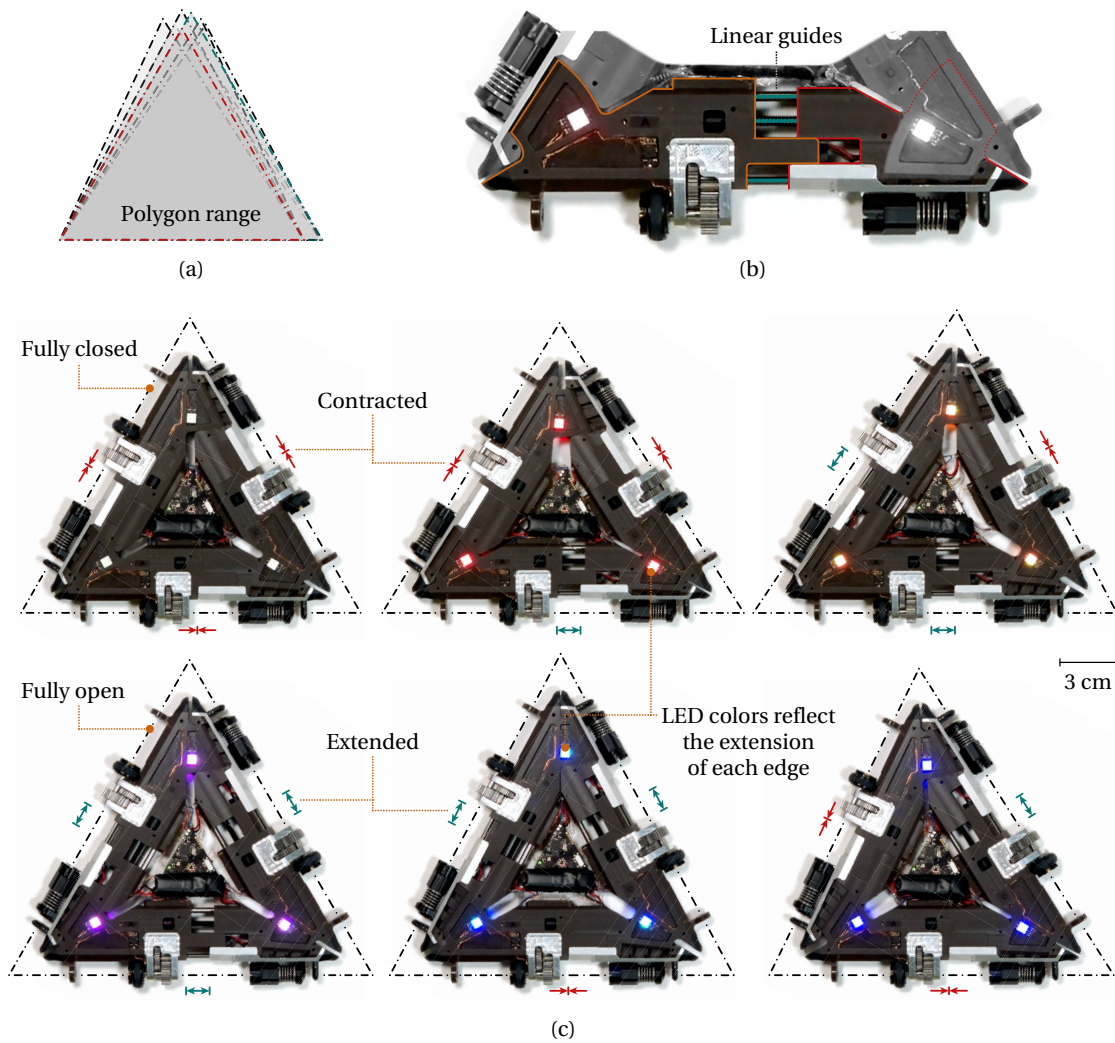


Figure 7.9 – Testing the adaptable morphology of the polygon-based robot. (a) shows the range of possible shapes of a polygon module; (b) shows an edge fully retracted and fully extended; (c) shows frames with maximum and minimum extension of edges in different combinations.

7.3.2 Mobility

A modular robotic system consisting of mobile entities results in enhanced reconfigurability due to the ability to automatically detach individual modules from an assembly and reattach elsewhere without the need for manual intervention. The polygon-based robotic platform obtains its mobility from the rotational DoFs at each edge, translating to three translational DoFs on flat surfaces. We have tested and verified the module's mobility as well as the control over its trajectory utilising the model presented in Section 7.2.2. The wheels of the module feature a silicon insert to improve frictional properties. This insert can be replaced to suit different environments and surfaces encountered in a given set of applications. We have tested a smooth silicon insert using DragonSkin 30 on a smooth surface to evaluate its performance. The results of our test and the corresponding model are visualised in Figure 7.10.

The test features eight combinations of wheel speeds tested on a module with equal extension values. The primary wheel, A, rotates at maximum speed and the wheels B and C are varied across the range. As the length of each edge is the same, wheels B and C rotate at the same speed. The module travels along a trajectory perpendicular to edge A, tracked using a green marker at the centroid of the triangle. Three trials were carried out at each combination with the position recorded at 10-second intervals and plotted alongside the modelled trajectory.

The difference in the range of possible radii between trajectories to the right and to the left is a result of the position of wheels along the edge. All wheels are shifted away from the centre of each edge in a clockwise direction, resulting in an additional DoF as well as an asymmetric trajectory range, as discussed in Section 7.2.2. As a module can rotate about its centroid and the drive model is primarily intended to improve controllability with an external tracking system, the model is simplified by ignoring resistance due to friction, resulting in diminished performance at smaller radii.

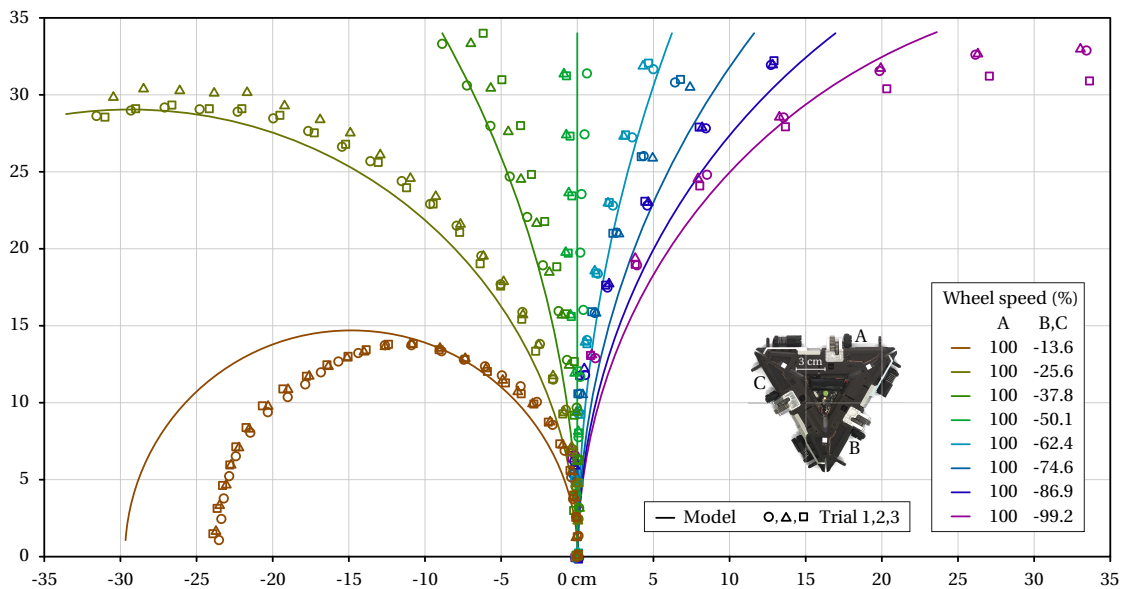


Figure 7.10 – Modelling and testing results of a module's mobility on a smooth surface using silicon inserts. The modelled trajectory for different combinations of wheel speeds is plotted alongside tracking points of three trials with positions recorded at 10-second intervals.

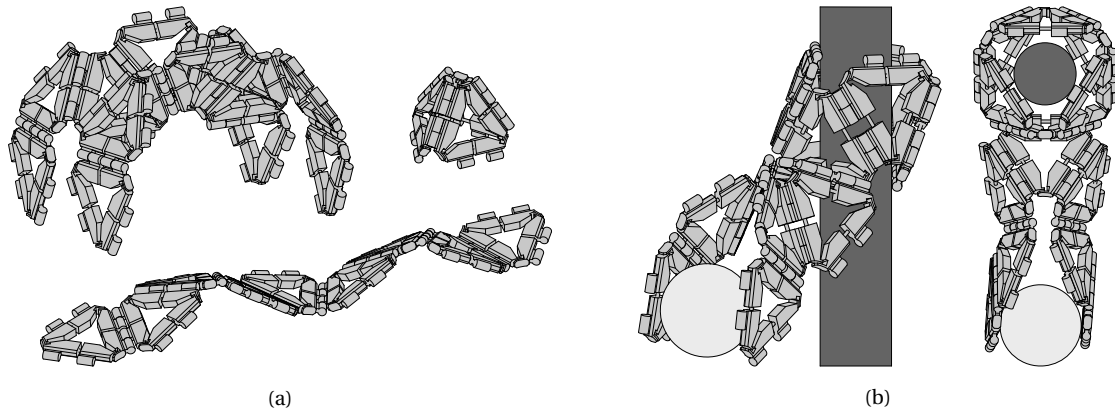


Figure 7.11 – Illustrations of the functional and structural configurations in the proposed experiments. (a) shows examples of locomotion assemblies including a four-legged robot, a snake, and a pyramid using the wheels of three unconnected edges; (b) shows two robotic arms branching off a closed chain of modules wrapped around a pole.

7.4 Proposed experiments

The functional testing outlined above verifies the core functionality of the robotic platform. In this section we propose a number of application-oriented demonstrations, experiments, and testing schemes that highlight the advanced level of reconfigurability inherent to the paradigm. They are designed to focus on and validate the key characteristics of the robotic system while highlighting the advantages and potential of the platform. All of the experiments that follow are possible with the robotic platform presented above, while they can also be used to validate other systems based on the paradigm.

7.4.1 Functional adaptation

In order to show the platform's ability to fulfil a variety of functions, we propose demonstrations in which a number of modules transforms from one functional state to several others, followed by experiments and testing procedures that validate the system's performance. These experiments focus on the two core functions of robots in general, namely locomotion and manipulation.

Locomotion

To demonstrate the system's adaptability in terms of locomotion, the following scenario highlights a number of distinct locomotion types that may be required during operation. A number of modules is tasked with retrieving an object from a distant location inside a habitable structure. At first, modules individually drive out of a room through a small gap under the door. Once on the other side, modules connect to one another and transform into a four-legged assembly. The quadruped makes its way down a hallway towards the object, located on top of a table. Once arrived, the systems transforms into a long chain, allowing it to climb onto the table. Several modules form an enclosure around the object and interface with mobile assemblies to carry it to the desired location. The quadruped, snake, and track are illustrated in Figure 7.11a.

The various types of locomotion can be selected and altered depending on a number of environmental and functional requirements such as terrain or speed. Additional types include, amongst others, closed

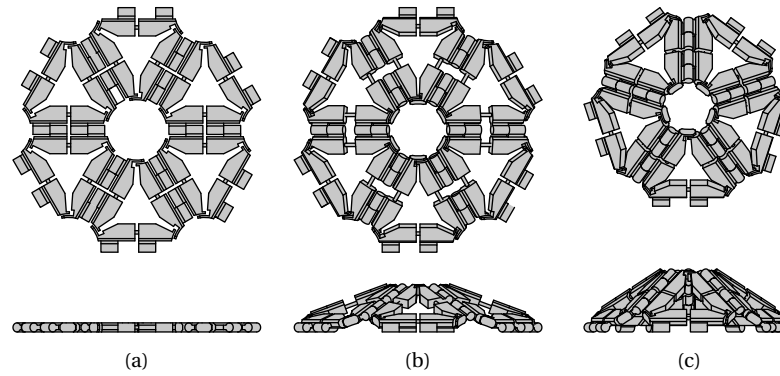


Figure 7.12 – Illustrations of modules around a single vertex transforming from a flat to a 3D surface. (a) shows six modules of equilateral shape around a single vertex; (b) shows the same modules with the inner edges extended to form an out-of-plane curvature; (c) shows a larger curvature after one module is ejected.

polygon assemblies morphing and shifting the centre of gravity in order to roll, and closed chains of varying width forming tracks that propel themselves. In order to classify these locomotion schemes we intend to test each of them on various types of terrain and compare their performance based on power consumption, speed, the ability to carry loads, and the number of entities. Additional specifications, such as control complexity and communication requirements, can be evaluated to produce a database of all parameters, simplifying the decision process during operation. We further plan to study the impact on the overall performance of altering the shape of polygons in order to fine-tune different locomotion schemes.

Manipulation

To demonstrate the platform's ability to address a range of different manipulation tasks, the following scenario features a user working in a remote environment assisted by a collection of modules. The modules assemble into a chain and wrap around a rigid object such as a tree or lamp post, closing the chain to ensure a tight grip. Additional modules form a second chain and attach to this now fixed reference frame, resulting in a robotic arm that assists the user. A single chain attached to the frame first serves as an extra contact point holding onto object the user is installing. Additional chains attach to the frame to form two end effectors that independently position an object as per the user's request. Further modules form branches on existing arms to support their weight or form kinematically constraining linkages. An example of two robotic arms attached a closed chain wrapped around a pole is illustrated in Figure 7.11b.

To assess the platform's performance in such scenarios we propose to compare the ability to wrap around differently sized and shaped objects, considering open and closed chains, power consumption, and surface properties. The workspace of robotic arms with different numbers of entities can further be evaluated, both with fixed-shape and adjustable modules, as well as the interference between multiple arms working in tandem.

7.4.2 Morphological flexibility

While in the previous two scenarios the shape-change of polygons can improve the performance of otherwise possible tasks, with the exception of closed, morphing polygon assemblies, the following

scenario relies entirely on that ability. A user is manipulating a polygon mesh through a computer interface, such as virtual or augmented reality, while a collection of polygon modules recreates the shape in a physical form. As individual vertices are modified in the virtual environment, the shapes of polygons alter to reflect that change. For instance, six modules connected in a chain around a single vertex is flat when all polygons are regular, while extensions of the inner edges result in a concave shape. When the maximum extension is reached, the system can eject one or more modules in order to increase the effective curvature of the resulting shape, thereby greatly increasing the accuracy of the represented mesh. This process is illustrated in Figure 7.12. Similarly, as the virtual model is extended or reduced, modules are automatically added or removed.

This general approach can be applied to wide range of scenarios where modular polygons assemble into any desired functional or structural shape. We propose to assess the performance of the platform at recreating such physical polygon meshes by comparing the ability to approximate 3D shapes of modules with varying ranges of possible shapes. This can further be compared to the performance of other types modular robotic systems in order to prove the versatility and superiority of the polygon-based platform.

7.4.3 Extensions and optimisation

In addition to experiments analysing the functional and morphological flexibility of the platform, several extensions and alterations of modules along with optimisation of key elements can be implemented and tested, further improving its overall performance. Different modules are likely to have vastly different power requirements in specific functional assemblies, such as the body of a quadruped versus its limbs. We plan to study power-sharing systems and algorithms to optimise the operational time of a group of modules. These can be tested in different configurations and application scenarios to compare and optimise the overall power usage of the system.

The robotic platform has several communication streams embedded in the system, such as global wireless and local serial communication, with different specifications and performance. Local serial communication has low latency and is used to synchronise modules and exchange information about their neighbours, while global wireless communication can address a range of modules and subsets, and allow distant modules to communicate. We intend to study these communication streams, along with different data-transfer protocols, and test different combinations and implementations to optimise overall information exchange based on different applications and morphologies.

Integrating extensions and specialised modules, as outlined in the Section 7.2.3, can greatly improve performance and applicability of the overall system. There are is wide range of additional components and dedicated modules that can be incorporated and we propose to verify the general benefit of this approach through a variety of general scenarios and specific components. Modules with extra battery packs, processing power, or sensors, although reduced general functionality, should be tested at different densities within configurations, evaluating the overall loss of functionality versus operation and computing time. Supplementary components attached to fully functional modules can further be assessed in distinct scenarios such as force plates and displays for human-robot interaction, or end effectors for manipulation tasks.

7.5 Discussion

Despite the promising potential of multi-functional robots, increasing reconfigurability and versatility poses various conceptual, functional, and engineering challenges. Following the introduction of a new robotic paradigm that provides a framework for addressing these challenges in Chapter 6, this chapter covers the implementation of such systems and details the development of a polygon-based modular robotic platform based on the paradigm. The platform's novel architecture, based on polygons, holds the potential to recreate a wide range of polygon meshes in a physical form, greatly surpassing the potential of existing self-reconfigurable modular robots. While specific sets of intended tasks and operations may require distinct scales, features, and technologies, the underlying framework yields a versatile reconfigurable tool that can service a myriad of applications.

The prototype of the platform presented in this chapter is designed to study and validate the versatility of the new paradigm. It addresses various challenges associated with it in terms of mechanical design, as well as power, communication, and control architectures. Triangular modules can transform their own shape, attach to other modules and assemble into structural and functional configurations. Initial functional testing of the prototype verifies its flexible morphology and mobility. A selection of proposed demonstrations and testing procedures is further provided to validate the functional and morphological flexibility of the platform and analyse further extensions and optimisations.

Due to the versatile nature and objective behind self-reconfigurable modular robots, the sheer quantity of unique aspects in each system renders a direct quantitative comparison ineffective. However, a qualitative analysis of the overall possibilities contained within each system in terms of reconfigurability, versatility, and applicability can provide a comparative overview of their potential. Table 7.1 summarises the characteristic features of a select number of such systems with distinct architectures, highlighting the differences of the polygon-based robotic platform, Mori 3.

First and foremost, the architecture of this new modular robot sets it apart from any existing system in terms of morphological and functional adaptability. It balances the complexity of a highly reconfigurable modular robot with six DoFs in each entity with a simplified kinematic architecture of adjustable polygons. While most self-reconfigurable modular robots are based on a lattice or tree-type designs, whose kinematic linkages limit their ability to alter the shape of an assembly, Mori 3 is only restricted by the range of possible polygon shapes, the need for continuous surfaces, and physical limits. The correlation to polygon meshing not only results in a larger range of how a collection of modules can configure and connect to one another, it also implies that an assembly of modules can change shape without impacting its kinematic chains.

In addition to the unique architecture, the polygon-based module incorporates essentially all features of the most sophisticated systems, such as Smores-EP, to combine its morphological flexibility with a high degree of applicability. In contrast to some systems that are primarily intended to showcase and study the process of reconfiguration such as 3D M-Blocks, Mori 3 is designed to carry out a range of functional tasks and operations as described in Section 7.4. It resembles an approach towards a universal robotic framework that can assume a wide range of structural or functional shapes and fulfil diverse tasks.

Although this system provides a new level of morphological and functional flexibility, several limitations and drawbacks remain, some of which are inherent to modular robots in general while others are unique to this platform. The design of the polygon modules is based around a number of experiments and demonstrations intended to highlight the potential and versatility of the paradigm, demanding

Table 7.1 – Comparison of different self-reconfigurable modular robotic systems. The comparison features a select number of distinct architectures by year of inception, highlighting the differences of the polygon-based robotic platform, Mori 3. Coupling features, mechanical properties, and communication streams complete the comparison.

Architecture								
Robot	Year	Module	System	DoFs ^a	Description ^b		Mobility ^c	
ATRON [144]	2005	Sphere	FC cubic lattice ^d	1	One R separating hemispheres		-	
M-TRAN III [106]	2008	Double cube	Tree-type	2	Two parallel R at centre of gendered cubes		1D	
Roombots [47]	2010	Double cube	Cubic lattice	3	Two diagonal R, one R between cubes		-	
ModRED [145]	2010	Chain	Chain-type	4	Three R (two parallel, one lengthwise), one L		2D	
UBot [146]	2011	Cube	Cubic lattice	1	Diagonal R for both gendered modules		-	
3D M-Blocks [89]	2015	Cube	Cubic lattice	0	Inertial flywheel to reconfigure and move		3D	
Smores-EP [91]	2016	Cube	Tree-type	4	Three R faces, one with extra R about centre		2D	
Mori3	2020	Triangle	3D polygon mesh	6	One R and one L at each edge		2D	
Robot	Type	Actuation	Gender ^e	Size (mm)	Vol. (cm ³)	Mass (g)	Local	Global
Coupling								
ATRON [144]	Hook	DC motor	G	∅ 110	697	850	Infrared	-
M-TRAN III [106]	Hook	DC motor	G	65 x 65 x 130	549	420	-	Bluetooth
Roombots [47]	Hook	DC motor	H	110 x 110 x 220	2662	1400	-	Bluetooth
ModRED [145]	Latch	Solenoid	H	368 x 114 x 119	4992	3170	-	Radio
UBot [146]	Hook	DC motor	G	80 x 80 x 80	512	350	Electronic contact	WiFi
3D M-Blocks [89]	Magnet	-	H	50 x 50 x 50	125	150	-	Bluetooth
Smores-EP [91]	EPM	Current pulse	H	80 x 80 x 80	512	500	Magnetic induction	WiFi
Mori3	Latch	SMA	H	△ 180 x 12 ^f	182	235	Electric contact	WiFi

^a number of actuated joints/linkages in a single module; ^b rotational joints/linkages are denoted as R and linear joints/linkages are denoted as L; ^c spatial mobility of a single module; ^d FC refers to a cubic lattice that is face-centred; ^e gendered systems are denoted as G, while hermaphroditic (or genderless) systems are denoted as H; ^f edge length and thickness of a triangle.

specific levels of performance from individual elements. These performance factors define the physical and functional limits of the platform such as the number of modules that can be manipulated under the influence of gravity, the range of possible shapes an assembly can reach, the time a collection of modules can operate for, or the maximum speed of different kinematic linkages. Reducing the functionality with respect to some applications or functions may allow a wider range of possibilities in another.

The architecture based on physical polygon meshes increases the flexibility of assembled structures, but greatly complicates the control of individual modules and the overall configuration due to the increased kinematic dependencies. This is further complicated by the high accuracy needed to maintain the integrity of individual polygons and the resulting meshes. While some demonstrations and experiments can be carried out using simplified models, any convoluted shapes or larger assemblies require sophisticated algorithms and considerable computational power. Some practical applications may take advantage of distributed compliant elements that replace otherwise active joints to reduce the redundancy in larger assemblies, but this limits autonomy and the number of possible reconfigurations.

The fundamental 2D structure of each module and resulting 3D surface meshes restrict the ability to create complex volumetric configurations. While cubic modular robots, for example, are less flexible in larger structures, the ability to connect modules to one another at different interfaces in 3D implies a larger range of possible volumetric configurations. Although this can be circumvented by merging two polygon modules at their face, or using additional connecting structures, the primary geometric reconfigurability is bound to continuous surfaces.

Once a larger surface of polygon modules is assembled, replacing or adding modules away from the edge of the configuration becomes more difficult. For instance, adding a number of modules to the centre of a dome-shaped assembly requires opening the surface at several locations by decoupling two edges of select modules to provide anchor points that can pass modules across. This may impact the structural integrity of the assembly and must be accounted for when planning the reconfiguration process. Furthermore, each module only features sensors to detect its neighbours, their relative position, and its own absolute orientation in space. Configurations of modules are thus fully aware of their own state and can pass modules from one border module to another, while separated modules or structures require additional sensors to assemble or connect.

The development of Mori 3 lays the groundwork for exploring the potential and studying the efficacy of the polygon-based paradigm. It introduces a new type of modular robotic system to the field that has distinct advantages over other approaches and addresses various aspects of reconfigurable robotics. While the creation of such systems constitutes a significant achievement, applying, testing, and implementing them remains a considerable challenge. This chapter provides a blueprint for an implementation of the paradigm, which we aim to validate through experiments and demonstrations in the near future. We hope that it encourages further work in the community in order to bring us closer to robotic systems that are not bound to specific tasks, environments, and users.

Towards a Robot Universe **Part IV**

8 Conclusion and outlook

The overarching objective of this thesis, and reconfigurable robotics in general, is the development of robotic systems that are not bound by a fixed morphology and not bound to a unique set of environments and tasks. Adapting the shape of a single robot can allow it to cope with different surroundings and fulfil multiple functions. Changing the configuration of different parts or modules of a robotic system can alter its behaviour and capabilities to address vastly different applications. Adjusting physical and mechanical properties of different joints, actuators, or links can shape the way a robot handles and interacts with its environment. Controlling and managing these properties, configurations, and shapes using varying methodologies provides the final building block to enable such versatile robotic systems.

While reconfigurable robots are designed to address a multitude of use cases, they are not intended to replace or compete with dedicated, single purpose systems. When designing a robot to operate in a unique environment and carry out a single, pre-defined task, the development can focus on reducing the system to a minimum that achieves the best possible result. Conversely, incorporating the technologies and features required to obtain flexibility in terms of form and function increases the overall complexity and potentially lowers accuracy and efficiency. This flexibility, however, is highly desirable in situations where the form and requirements of a task are not known in advance, or where the use of a different robot for each and every task is impractical.

Several approaches towards reconfigurability in robotics have been presented and studied in literature, such as origami and modularity, addressing a number of functional needs of a wide range of systems. Origami robots utilise the transformation of 2D structures into multiple 3D shapes to achieve particular behaviours. Reconfigurable modular systems employ a number of self-contained entities to assemble various structures with specific objectives. These approaches highlight the potential of embedding multiple functions into a single system. The fundamental architecture of existing reconfigurable robots, however, greatly limits their morphological and functional flexibility.

This thesis aims to overcome these limitations through the development of a new paradigm for highly versatile systems, taking advantage of both origami and modular robots, reconfigurable mechanisms, and polygon meshing. It provides a framework for the development of a new class of robotic systems with an inherent morphological and functional flexibility. These advances are validated through studies of various building blocks of reconfigurable robots and different prototypes thereof. The thesis presents a new approach towards reconfigurability in robotics and provides a robotic platform embodying its key characteristics to further study and take advantage of it. This chapter provides a summary of the work presented in this thesis, including the novel concepts it introduces, the challenges it addresses,

and the contributions it holds, followed by a discussion thereof and an analysis of the future potential. The main contributions of the thesis can be summarised as follows.

- Geometric and functional analysis of the challenges and potential of incorporating reconfigurability in robotic systems, addressing morphological and functional flexibility, complexity, and scalability.
- Study and development of key building blocks of reconfigurable modular systems, including reconfiguration mechanisms and algorithms through prototypes and simulation.
- Introduction and analysis of a novel reconfigurable robotic platform with an inherent morphological flexibility, merging the concepts of modular and origami robotics with polygon meshing.

8.1 Summary and contributions

Providing the first conceptual analysis towards the new paradigm, we studied two fundamental approaches in reconfigurable robotics, modular and origami robots. Both reconfigurable systems in their own right, they encompass a multitude of concepts for changing the morphology of a robotic system. Modular robots have been developed to assemble a variety of functional structures from a set of self-contained entities, while origami has been utilised to change the shape of a robot for different purposes. A first combination of these two approaches in literature, the initial version of the Mori robot combines various features of the two approaches and overcomes some of their individual limitations.

Utilising this unique system we analysed conceptual challenges in reconfigurable systems, such as scalability, control methods, and necessary features. We studied the feasibility of modular origami robots and validated its functional versatility through three distinct demonstrations and experiments that address the requirements of modular systems. By assembling different numbers of active and passive Mori modules in various configurations, we showed the first example of a true 3D representation of a modular reconfigurable surface. We further demonstrated a modules mobility with three translational DoFs in a mission-based scenario, highlighting the benefits of the quasi-2D design. We finally showed how this relatively simple architecture, compared to other modular robots, can be used in complex applications through closed-loop object manipulation, balancing a ball on a floating platform with three DoFs. Using this first prototype of Mori, we addressed and studied several challenges of reconfigurable systems in terms of design and control approaches, as well as functional versatility.

Following the initial conception of a modular origami robot, we further studied mechanical requirements and functional challenges in the automatic coupling of modular robots. Due to the high number of degrees of freedom, the increasing loads in larger assemblies, and the distribution of mechatronic and control systems, accounting for the failure of any constituent element and unexpected events is crucial. We developed the first mechanical overload protection mechanism for modular robots, which guards both the robotic system and any subject or object it interacts with from excessive forces. Designing and modelling a parametric, self-centring design of this mechanism results in an adjustable torque threshold and an ideal candidate for a multitude of modular robots and systems.

To complete the conceptual study of modular reconfigurable robots, we focused on the challenges associated with planning and executing the reconfiguration process. Due to the large number of entities and degrees of freedom in modular systems, determining how to assemble into a given 3D shape is computationally demanding and time-consuming. In order to optimise this process, we devised reconfiguration methods based on origami, determining optimal 2D layouts of modular robots and finding optimal folding sequences to achieve a target 3D shape. Our unique approach eliminates connectivity changes during the reconfiguration process, reducing the risk of failure due to

misalignment. We verified this procedure by simulating different structural and functional shapes and comparing results to automatic modelling schemes relying on enumeration. Although the performance, in terms of optimality, diminished with larger numbers of modules and possible 2D layouts, the viability of our methods for real-time reconfiguration planning was validated through dramatically reduced computation time along with above-average performance.

Following the conceptual study of various challenges in reconfigurable robotics, we elaborated the new robotic paradigm from an initial concept into its full form, incorporating polygon meshing and reconfigurability at varying degrees. We analysed morphological flexibility in modular and origami robots as well as in virtual polygon meshing to highlight the underlying possibilities and limitations. We then provided a detailed description of the proposed paradigm with its characteristics and associated challenges. By approximating physical structures through polygon abstractions, a system of shape-changing polygons can be devised that is able to assume a wide range of structural or functional 3D shape. It provides a universal framework for polygon-shaped modular systems with an inherent morphological and functional flexibility that surpasses existing concepts due to the underlying architecture.

The development of the new paradigm culminated in the development of new robotic platform of shape-changing polygonal modules. The system incorporates the core features of the framework with an inherent morphological flexibility and underlying architecture based on polygon meshing, distinct from any existing self-reconfigurable modular robots. The robotic platform provides a new degree of structural and functional reconfigurability that surpasses the possibilities of any existing system. Self-contained robotic modules can alter their own triangular shape, drive towards and attach to each other, and transform into functional three-dimensional configurations. It is designed as a platform to further study the building blocks necessary to fulfil its functional flexibility, such as control methods, reconfiguration algorithms, and power and communication networks. The different components of the platform can be extended, reduced, and interfaced with additional and complementary systems to address a variety of application-specific needs. It resembles an approach towards a universal robotic system that can assume a myriad of structural or functional shape and fulfil a variety of different tasks.

8.2 Discussion

The combination of modularity and origami, studied from the outset of this work, overcomes some of the limitations of the two underlying robotic concepts. It advances the functional versatility of origami robots and provides a new level of morphological flexibility in modular robots. At the same time, however, some of their unique advantages are lost due to necessary compromises when fusing the two systems. For instance, conventional origami robots utilise the concept of folding more accurately and effectively than is possible in a modular origami robot. Flexible and compliant hinges, although their behaviour is not as straight-forward to predict and control, result in kinematic joints with a larger range of motion and can frequently be folded flat. These are commonly combined with smart material actuators that lead to unique capabilities. Layer-by-layer, 2D construction is furthermore rapid and much less costly compared to traditional subtractive or additive manufacturing. Moving away from flexible hinges towards fixed axes facilitates the implementation of modularity, but complicates production. It does, however, enable an automatic coupling process and provides a clearly defined kinematic joint to reconfigure and control assemblies of modules.

In comparison to existing modular robots, the combination of modularity and origami improves the range of motion between modules and simplifies the kinematic structure and underlying architecture.

It promotes the functional versatility, already with small numbers of modules, but also limits the ways in which modules can be attached to one another, and thereby the resulting possible shapes. Moving from rigid triangular modules to shape-changing polygons greatly enhances the overall morphological flexibility of such systems and overcomes some of the tight kinematic constraints. The additional DoFs, however, complicate construction and highlight one of the key limitations and challenges of modular robots. While traditional, fixed-morphology robots can be constructed with functional requirements such as force and accuracy that match a desired task, these factors limit the scalability of modular systems. As the number of entities, and thus DoFs, grows, overall misalignments, force and power requirements, and computational loads escalate, raising costs and limiting applicability. Furthermore, the fundamental trade-off between the range of possible functions of modular robotic system and their performance at each individual task remains and must be taken into account.

8.3 A reconfigurable future

The robotic framework proposed in this thesis provides a new perspective on reconfigurability in robotics. By studying various features associated with such systems and addressing some of their challenges, we lay the groundwork for developing universal robotic systems based on polygon meshes. The platform introduced in Chapter 7 is designed to initially verify the inherent morphological flexibility and to subsequently study and develop various technological and scientific areas in the field. Although the robotic platform is an ideal tool for this purpose, advances can equally be made using theoretical and simulative analyses as well as practically using other robots and platforms that share the conceptual basis.

First and foremost, the reconfiguration process is the most essential factor in realising and utilising these robots. It is not only required for most functional configurations that take advantage of the adaptable morphology, but also for assembling any such configuration and transforming from one functional state into another. Initial studies with small numbers of modules can be carried out using manual and hard-coded procedures, but as the number of modules increases, automated models and controllers are inevitable. The reconfiguration process needs to be planned, controlled, and executed, for all of which new strategies and approaches are required to address the large number of degrees of freedom, not just resulting from the joints between modules, but also from the adaptability of modules themselves.

Building up on an established reconfiguration scheme, whether theoretical or with a functional platform, extensions to the system and its functionality can greatly enhance flexibility and efficiency. Modules with adapted functions and features in a heterogeneous system should be examined, such as extra sensors, computing power, communication systems, passive modules, or interfaces for other technologies. Distributing these modules in a configuration can result in different behaviour profiles and localised properties. Distributing non-physical elements, such as power and computation, can also improve overall performance and intelligence in the system. Physical and virtual interfaces such as coupling points or camera systems can be added to provide an improved infrastructure in specific environments.

Addressing these conceptual and functional challenges will pave the way towards practical implementations of the paradigm. We envision a universal robotic framework of shape-changing polygon modules at various scales and complexities. Based on the ability to recreate a wide range of 3D shapes or structures in the form of a physical polygon mesh, the realm of possible applications is vast. In personal robotics for instance, it ranges from a 3D computer display that users can physically interact

with to a universal assistive system that transforms into locomotion structures, robotic arms, or other tools as desired. Similarly, in space exploration it can serve as the architectural building block for any mobile, stationary, or functional system. Depending on the intended set of functions, the embedded technologies and features of a robotic system can vary greatly, while the underlying structure remains the same, providing an inherent morphological flexibility.

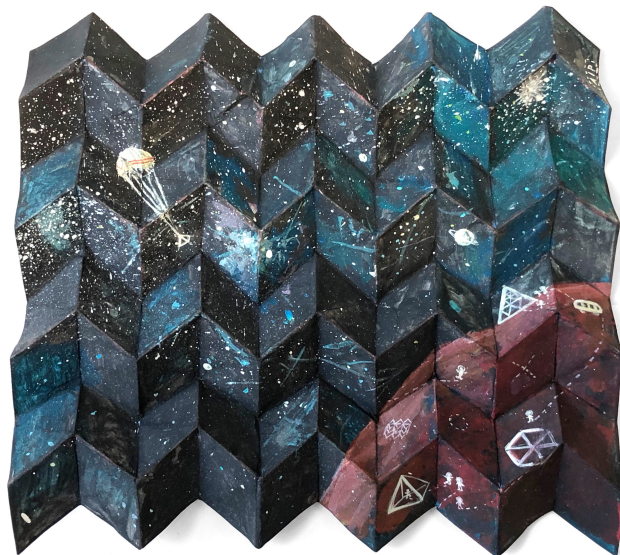


Figure 8.1 – An artist's rendition of a system of modular origami structures used on an extraterrestrial body. It is drawn in acrylic on a sheet of paper folded into the miura-ori origami pattern © Anna I. Popescu.

A Energy metric derivations

1. Derivation for *leaf* modules

If module i is *leaf*, then $|C_i| = 0$, from Eq. 5.3 the dynamic terms f_i and n_i are written as

$$\begin{aligned} f_i &= F_i = m_i \ddot{r}_i \\ n_i &= N_i + (p_i + r_i^*) \times F_i = I_i \dot{\omega}_i + \omega_i \times (I_i \omega_i) + (p_i + r_i^*) \times F_i \end{aligned} \quad (A.1)$$

Integrate $|f_i|$ twice with time, Γ_i is written as

$$\begin{aligned} \Gamma_i &= \int_{t_{k-1}}^{t_k} \int_{t_{k-1}}^{t_k} |m_i \ddot{r}_i| dt dt = m_i |\bar{\ddot{r}}_i| (t_k - t_{k-1})^2 \\ &= m_i \kappa_1 ||r_i(t_k) - r_i(t_{k-1})|| = m_i \kappa_1 |\hat{r}_i(t_k) - \hat{r}_i(t_{k-1})| \end{aligned} \quad (A.2)$$

where $|\bar{\ddot{r}}_i|$ is average value of $|\ddot{r}_i(t)|$ in time $t \in [t_{k-1}, t_k]$, and $\kappa_1 > 0$ is a constant. Integrate n_i twice with time, Λ_i is written as

$$\begin{aligned} \Lambda_i &= \int_{t_{k-1}}^{t_k} \int_{t_{k-1}}^{t_k} |n_i| dt dt \\ &\leq \int_{t_{k-1}}^{t_k} \int_{t_{k-1}}^{t_k} |I_i \dot{\omega}_i| dt dt + \int_{t_{k-1}}^{t_k} \int_{t_{k-1}}^{t_k} |\omega_i \times (I_i \omega_i)| dt dt + \int_{t_{k-1}}^{t_k} \int_{t_{k-1}}^{t_k} |(p_i + r_i^*) \times m_i \ddot{r}_i| dt dt \end{aligned} \quad (A.3)$$

For each term in Eq. A.3,

$$\begin{aligned} \int_{t_{k-1}}^{t_k} \int_{t_{k-1}}^{t_k} |I_i \dot{\omega}_i| dt dt &\leq \|I_i\| \cdot \int_{t_{k-1}}^{t_k} \int_{t_{k-1}}^{t_k} |\dot{\omega}_i| dt dt \\ &= \|I_i\| \cdot |\bar{\dot{\omega}}_i| (t_k - t_{k-1})^2 = \|I_i\| \cdot \kappa_2 ||\theta_i(t_k) - \theta_i(t_{k-1})|| \end{aligned} \quad (A.4)$$

where $|\bar{\dot{\omega}}_i|$ is average value of $|\dot{\omega}_i(t)|$ in time $t \in [t_{k-1}, t_k]$ and $\kappa_2 > 0$ is a constant; and $\theta_i(t)$ is the vector of generalised joint coordinates. The term

$$\begin{aligned} \int_{t_{k-1}}^{t_k} \int_{t_{k-1}}^{t_k} |\omega_i \times (I_i \omega_i)| dt dt &= \int_{t_{k-1}}^{t_k} \int_{t_{k-1}}^{t_k} ||\omega_i| \cdot |I_i \omega_i| \cdot \sin(\varphi_{i,1}) \cdot \hat{n}_{i,1}| dt dt \\ &\leq \int_{t_{k-1}}^{t_k} \int_{t_{k-1}}^{t_k} |\omega_i| \cdot |I_i \omega_i| dt dt \leq \|I_i\| \cdot \int_{t_{k-1}}^{t_k} \int_{t_{k-1}}^{t_k} |\omega_i|^2 dt dt \end{aligned} \quad (A.5)$$

where $\varphi_{i,1}$ and $\hat{n}_{i,1}$ are vector angle and normal vector of ω_i and $I_i \omega_i$.

Appendix A. Energy metric derivations

To derive the term $\int_{t_{k-1}}^{t_k} \int_{t_{k-1}}^{t_k} |\boldsymbol{\omega}_i|^2 dt dt$, reminding \dot{q}_i as angular velocity of module i rotating about \mathbf{z}_i , and $|\dot{q}_i| = |\boldsymbol{\omega}_i|$, with unified joint motion planning (Sec. 5.1.1), it is deduced that

$$\dot{q}_i(\xi_1) \cdot \dot{q}_i(\xi_2) \geq 0, \xi_1, \xi_2 \in [t_{k-1}, t_k] \quad (\text{A.6})$$

then it can be derived as

$$\begin{aligned} \int_{t_{k-1}}^{t_k} |\boldsymbol{\omega}_i|^2 dt &= \int_{t_{k-1}}^{t_k} |\dot{q}_i(t)|^2 dt = |\dot{q}_i(\xi)| \int_{t_{k-1}}^{t_k} |\dot{q}_i(t)| dt \\ &= |\dot{q}_i(\xi)| \cdot ||q_i(t_k)| - |q_i(t_{k-1})||, \xi \in [t_{k-1}, t_k] \end{aligned} \quad (\text{A.7})$$

and

$$\begin{aligned} \int_{t_{k-1}}^{t_k} \int_{t_{k-1}}^{t_k} |\boldsymbol{\omega}_i|^2 dt dt &= \int_{t_{k-1}}^{t_k} \int_{t_{k-1}}^{t_k} |\dot{q}_i(t)|^2 dt dt \\ &= |\dot{q}_i(\xi)| \cdot (t_k - t_{k-1}) \cdot ||q_i(t_k)| - |q_i(t_{k-1})|| \end{aligned} \quad (\text{A.8})$$

Since $\dot{q}_i(\xi)$ is a constant with predefined joint motion, define $\bar{\omega}_i$ as average angular velocity of \dot{q}_i in time $t \in [t_{k-1}, t_k]$, then

$$|\dot{q}_i(\xi)| \cdot (t_k - t_{k-1}) = \kappa_3 |\bar{\omega}_i| \cdot (t_k - t_{k-1}) = \kappa_3 ||q_i(t_k)| - |q_i(t_{k-1})|| \quad (\text{A.9})$$

where κ_3 is a constant and $\kappa_3 > 0$. Therefore it is derived that

$$\int_{t_{k-1}}^{t_k} \int_{t_{k-1}}^{t_k} |\boldsymbol{\omega}_i|^2 dt dt = \kappa_3 ||q_i(t_k)| - |q_i(t_{k-1})||^2 \quad (\text{A.10})$$

then Eq. A.5 can be expressed as

$$\begin{aligned} \int_{t_{k-1}}^{t_k} \int_{t_{k-1}}^{t_k} |\boldsymbol{\omega}_i \times (\mathbf{I}_i \boldsymbol{\omega}_i)| dt dt &\leq \|\mathbf{I}_i\| \cdot \int_{t_{k-1}}^{t_k} \int_{t_{k-1}}^{t_k} |\boldsymbol{\omega}_i|^2 dt dt \\ &= \|\mathbf{I}_i\| \cdot \kappa_3 ||q_i(t_k)| - |q_i(t_{k-1})||^2 \end{aligned} \quad (\text{A.11})$$

Since for each module, $|(\mathbf{p}_i + \mathbf{r}_i^*)| = \frac{l/2}{\sin(\pi/3)}$ is constant as, and another term in Eq. A.3, $\int_{t_{k-1}}^{t_k} \int_{t_{k-1}}^{t_k} |(\mathbf{p}_i + \mathbf{r}_i^*) \times m_i \ddot{\mathbf{r}}_i| dt dt$, is derived as follows, according to Eq. A.2

$$\begin{aligned} \int_{t_{k-1}}^{t_k} \int_{t_{k-1}}^{t_k} |(\mathbf{p}_i + \mathbf{r}_i^*) \times m_i \ddot{\mathbf{r}}_i| dt dt &= |(\mathbf{p}_i + \mathbf{r}_i^*)| \cdot \int_{t_{k-1}}^{t_k} \int_{t_{k-1}}^{t_k} |m_i \ddot{\mathbf{r}}_i| dt dt \cdot \sin(\varphi_{i,2}) \cdot \hat{\mathbf{n}}_{i,2} \\ &\leq \frac{l/2}{\sin(\pi/3)} m_i \kappa_1 |\hat{r}_i(t_k) - \hat{r}_i(t_{k-1})| \end{aligned} \quad (\text{A.12})$$

where $\varphi_{i,2}$ and $\hat{\mathbf{n}}_{i,2}$ are vector angle and normal vector of $\mathbf{p}_i + \mathbf{r}_i^*$ and $\ddot{\mathbf{r}}_i$.

With $|\boldsymbol{\theta}_i(t)| = |q_i(t)|$ and the boundary conditions of $q_i(t_{k-1}) = 0$ and $q_i(t_k) = \hat{\theta}_i$, Λ_i^* defined as the maximum of Λ_i can be expressed as

$$\begin{aligned} \Lambda_i^* &= \left| \int_{t_{k-1}}^{t_k} \int_{t_{k-1}}^{t_k} \mathbf{I}_i \dot{\boldsymbol{\omega}}_i dt dt \right| + \left| \int_{t_{k-1}}^{t_k} \int_{t_{k-1}}^{t_k} \boldsymbol{\omega}_i \times (\mathbf{I}_i \boldsymbol{\omega}_i) dt dt \right| + \left| \int_{t_{k-1}}^{t_k} \int_{t_{k-1}}^{t_k} (\mathbf{p}_i + \mathbf{r}_i^*) \times m_i \ddot{\mathbf{r}}_i dt dt \right| \\ &= \|\mathbf{I}_i\| \cdot \kappa_2 |\boldsymbol{\theta}_i(t_k) - \boldsymbol{\theta}_i(t_{k-1})| + \|\mathbf{I}_i\| \cdot \kappa_3 ||q_i(t_k)| - |q_i(t_{k-1})||^2 + \frac{l/2}{\sin(\pi/3)} m_i \kappa_1 |\hat{r}_i(t_k) - \hat{r}_i(t_{k-1})| \\ &= \|\mathbf{I}_i\| \cdot (\kappa_2 |\hat{\theta}_i| + \kappa_3 |\hat{\theta}_i|^2) + \frac{l/2}{\sin(\pi/3)} m_i \kappa_1 |\hat{r}_i(t_k) - \hat{r}_i(t_{k-1})| \end{aligned} \quad (\text{A.13})$$

2. Derivation for non-leaf modules

For modules that are not *leaves*, Γ_i and Λ_i are derived as

$$\begin{aligned}\Gamma_i &= \int_{t_{k-1}}^{t_k} \int_{t_{k-1}}^{t_k} \left| \sum_{j=1}^{|C_i|} \mathbf{f}_{C_{i,j}} + \mathbf{F}_i \right| dt dt \\ &\leq \sum_{j=1}^{|C_i|} \Gamma_{C_{i,j}} + \int_{t_{k-1}}^{t_k} \int_{t_{k-1}}^{t_k} |m_i \ddot{\mathbf{r}}_i| dt dt \leq \sum_{j=1}^{|C_i|} \Gamma_{C_{i,j}}^* + m_i \kappa_1 |\hat{\mathbf{r}}_i(t_k) - \hat{\mathbf{r}}_i(t_{k-1})|\end{aligned}\quad (\text{A.14})$$

thus Γ_i^* is written as

$$\Gamma_i^* = \sum_{j=1}^{|C_i|} \Gamma_{C_{i,j}}^* + m_i \kappa_1 |\hat{\mathbf{r}}_i(t_k) - \hat{\mathbf{r}}_i(t_{k-1})| \quad (\text{A.15})$$

Since

$$\begin{aligned}\int_{t_{k-1}}^{t_k} \int_{t_{k-1}}^{t_k} \left| \sum_{j=1}^{|C_i|} \mathbf{p}_i \times \mathbf{f}_{C_{i,j}} \right| dt dt &\leq \sum_{j=1}^{|C_i|} |\mathbf{p}_i| \cdot \int_{t_{k-1}}^{t_k} \int_{t_{k-1}}^{t_k} |\mathbf{f}_{C_{i,j}}| dt dt \cdot \sin(\varphi_{i,j}) \cdot \hat{\mathbf{n}}_{i,j} \\ &\leq \sum_{j=1}^{|C_i|} |\mathbf{p}_i| \cdot \Gamma_{C_{i,j}}\end{aligned}\quad (\text{A.16})$$

where $\varphi_{i,j}$ and $\hat{\mathbf{n}}_{i,j}$ are vector angle and normal vector of \mathbf{p}_i and $\Gamma_{C_{i,j}}$. Λ_i can be written as

$$\begin{aligned}\Lambda_i &\leq \sum_{j=1}^{|C_i|} \Lambda_{C_{i,j}} + \int_{t_{k-1}}^{t_k} \int_{t_{k-1}}^{t_k} \left| \sum_{j=1}^{|C_i|} \mathbf{p}_i \times \mathbf{f}_{C_{i,j}} \right| dt dt + \int_{t_{k-1}}^{t_k} \int_{t_{k-1}}^{t_k} |\mathbf{N}_i + (\mathbf{p}_i + \mathbf{r}_i^*) \times \mathbf{F}_i| dt dt \\ &\leq \sum_{j=1}^{|C_i|} \Lambda_{C_{i,j}} + \sum_{j=1}^{|C_i|} |\mathbf{p}_i| \cdot \Gamma_{C_{i,j}} + \int_{t_{k-1}}^{t_k} \int_{t_{k-1}}^{t_k} |\mathbf{N}_i + (\mathbf{p}_i + \mathbf{r}_i^*) \times \mathbf{F}_i| dt dt \\ &\leq \sum_{j=1}^{|C_i|} (\Lambda_{C_{i,j}}^* + |\mathbf{p}_i| \cdot \Gamma_{C_{i,j}}^*) + \|\mathbf{I}_i\| \cdot (\kappa_2 |\hat{\theta}_i| + \kappa_3 |\hat{\theta}_i|^2) + \frac{l/2}{\sin(\pi/3)} m_i \kappa_1 |\hat{\mathbf{r}}_i(t_k) - \hat{\mathbf{r}}_i(t_{k-1})|\end{aligned}\quad (\text{A.17})$$

Define $\lambda_1 = \|\mathbf{I}_i\|$, $\lambda_2 = \frac{l/2}{\sin(\pi/3)} m_i$, $\lambda_3 = m_i$, and $\lambda_4 = |\mathbf{p}_i| = 0$ or l , and the maximum of Λ_i can be expressed as

$$\Lambda_i^* = \sum_{j=1}^{|C_i|} (\Lambda_{C_{i,j}}^* + \lambda_4 \cdot \Gamma_{C_{i,j}}^*) + \lambda_1 \cdot (\kappa_2 |\hat{\theta}_i| + \kappa_3 |\hat{\theta}_i|^2) + \lambda_2 \kappa_1 |\hat{\mathbf{r}}_i(t_k) - \hat{\mathbf{r}}_i(t_{k-1})| \quad (\text{A.18})$$

with the maximum of Γ_i written as

$$\Gamma_i^* = \sum_{j=1}^{|C_i|} \Gamma_{C_{i,j}}^* + \lambda_3 \kappa_1 |\hat{\mathbf{r}}_i(t_k) - \hat{\mathbf{r}}_i(t_{k-1})| \quad (\text{A.19})$$

Therefore, the estimation of torque consumption $\varepsilon'_i = \int_{t_{k-1}}^{t_k} \int_{t_{k-1}}^{t_k} |\tau_i| dt dt$ can be represented by Λ_i^* as in Eq. A.18.

List of Figures

1.1	Conceptual vision of the new paradigm in form of a universal assistive system for space.	6
1.2	Conceptual vision of the new paradigm in form of a universal extraterrestrial exploration system.	7
2.1	Examples of structural and functional shapes utilising the new robotic paradigm.	14
3.1	Conceptual illustration of a modular origami robot.	18
3.2	Structural elements for analysing scalability with respect to torque requirements of modular origami robots.	19
3.3	Schematic illustration highlighting the core requirements of a modular origami robot. .	20
3.4	The first functional prototype of Mori, a modular origami robot.	21
3.5	Modularity and origami demonstration using two active modules along with four passive ones.	24
3.6	A configuration of four Mori modules forming a pyramid.	25
3.7	Mori turns mobile – a single Mori module with three motors can travel across flat surfaces.	25
3.8	Demonstration of Mori’s mobility and manoeuvrability.	26
3.9	Illustrations and notations used in the kinematic analysis of the floating three DoF platform.	27
3.10	Testing setup to evaluate the floating three DoF platform consisting of modular origami robots.	28
3.11	Testing results of the modular origami robot platform balancing a ball.	29
4.1	Design overview of the automatic coupling mechanism with mechanical overload protection.	35
4.2	Modelling diagrams for the two contact points in the overload protection model.	39

List of Figures

4.3	Results from modelling the overload protection mechanism and from testing the model on two materials and fabrication methods.	42
4.4	Prototypes of the coupling mechanism with mechanical overload protection on modular origami robots.	43
4.5	Testing of the coupling mechanism with key frames showing the main steps in the process.	44
5.1	Overview of our method for energy-optimal reconfiguration of modular robots.	49
5.2	A pre-folding pattern with a root node and its corresponding rooted tree.	50
5.3	Optimal folding sequence and performance for the optimal octahedron and quadruped layout.	59
6.1	Conceptual illustration of the new robotic paradigm.	66
7.1	Degrees of freedom and notations in different operational states of a module.	71
7.2	Illustration of the design of a full polygon-based robotic module.	72
7.3	Offset hinge design enabling the shape change of a polygon robot.	73
7.4	Mechanical features addressing misalignment during the coupling of two modules. . .	74
7.5	Electronic and physical elements of the coupling mechanism of the polygon-based robot.	75
7.6	Central electronic control boards of the polygon based robot.	76
7.7	Battery-powered plug-ins for passive modules with a fixed morphology.	76
7.8	Notations used in the derivation of the input speeds for the three motors given a desired trajectory.	78
7.9	Testing the adaptable morphology of the polygon-based robot.	80
7.10	Modelling and testing results of a module's mobility on a smooth surface using silicon inserts.	81
7.11	Illustrations of the functional and structural configurations in the proposed experiments.	82
7.12	Illustrations of modules around a single vertex transforming from a flat to a 3D surface.	83
8.1	An artist's rendition of a system of modular origami structures used on an extraterrestrial body.	95

List of Tables

4.1	Global design parameters for the mechanism incorporated into the automated coupling of a modular origami robot.	41
4.2	Material- and fabrication-dependent parameters for the model of the overload protection mechanism.	41
4.3	Misalignment tolerance results obtained from testing the prototype of the automatic coupling.	45
5.1	Variable and parameter notations used in Sections 5.1.1 and 5.1.2.	52
5.2	Denavit-Hartenberg parameters for the modular origami platform.	57
5.3	Target 3D configurations and corresponding pre-folding patterns.	57
5.4	Comparison between the energy-optimal layout generated by each algorithm in terms of required torque.	58
5.5	Energy-optimal layouts generated by both algorithms, along with the corresponding rooted tree and the unified folding sequence.	58
5.6	Performance comparison between the two methods to generate energy-optimal layouts in terms of computation time two performance indicators.	58
7.1	Comparison of different self-reconfigurable modular robotic systems.	86

Bibliography

- [1] A. Bicchi, A. Fagiolini, and L. Pallottino, "Towards a Society of Robots," *IEEE Robotics & Automation Magazine*, vol. 17, pp. 26–36, dec 2010.
- [2] C. H. Belke and J. Paik, "Mori: A Modular Origami Robot," *IEEE/ASME Transactions on Mechatronics*, vol. 22, pp. 2153–2164, oct 2017.
- [3] D. Brugali, R. Capilla, and M. Hinchey, "Dynamic variability meets robotics," *Computer*, vol. 48, no. 12, pp. 94–97, 2015.
- [4] R. W. Brennan, M. Fletcher, and D. H. Norrie, "An agent-based approach to reconfiguration of real-time distributed control systems," *IEEE Transactions on Robotics and Automation*, vol. 18, no. 4, pp. 444–451, 2002.
- [5] N. Chakraborty and K. Sycara, "Reconfiguration algorithms for mobile robotic networks," *Proceedings - IEEE International Conference on Robotics and Automation*, pp. 5484–5489, 2010.
- [6] M. Guo and D. V. Dimarogonas, "Multi-agent plan reconfiguration under local LTL specifications," *The International Journal of Robotics Research*, vol. 34, pp. 218–235, feb 2015.
- [7] M. Sugi, Y. Maeda, Y. Aiyama, T. Harada, and T. Arai, "A holonic architecture for easy reconfiguration of robotic assembly systems," *IEEE Transactions on Robotics and Automation*, vol. 19, no. 3, pp. 457–464, 2003.
- [8] J. Sun and J. Zhao, "An Adaptive Walking Robot With Reconfigurable Mechanisms Using Shape Morphing Joints," *IEEE Robotics and Automation Letters*, vol. 4, pp. 724–731, apr 2019.
- [9] Z. Tang, P. Qi, and J. Dai, "Mechanism design of a biomimetic quadruped robot," *Industrial Robot*, vol. 4, no. April, pp. 512–520, 2017.
- [10] M. A. Robertson, M. Murakami, W. Felt, and J. Paik, "A Compact modular soft surface with reconfigurable shape and stiffness," *IEEE/ASME Transactions on Mechatronics*, vol. 24, no. 1, pp. 16–24, 2019.
- [11] N. Tan, R. E. Mohan, and K. Elangovan, "A Bio-inspired Reconfigurable Robot," in *Mechanisms and Machine Science*, vol. 36, pp. 483–493, 2016.

- [12] Z. Zhakypov, C. H. Belke, and J. Paik, "Tribot: A deployable, self-righting and multi-locomotive origami robot," *IEEE International Conference on Intelligent Robots and Systems*, vol. 2017-Septe, pp. 5580–5586, 2017.
- [13] S. Banisadr and J. Chen, "Infrared actuation-induced simultaneous reconfiguration of surface color and morphology for soft robotics," *Scientific Reports*, vol. 7, p. 17521, dec 2017.
- [14] D. Zarrouk and L. Yehezkel, "Rising STAR: A highly reconfigurable sprawl tuned robot," *IEEE Robotics and Automation Letters*, vol. 3, no. 3, pp. 1888–1895, 2018.
- [15] Z.-c. Jiang, Y.-y. Xiao, X. Tong, and Y. Zhao, "Selective Decrosslinking in Liquid Crystal Polymer Actuators for Optical Reconfiguration of Origami and Light-Fueled Locomotion," *Angewandte Chemie International Edition*, vol. 58, pp. 5332–5337, apr 2019.
- [16] G. Chirikjian, "Kinematics of a metamorphic robotic system," in *Proceedings of the 1994 IEEE International Conference on Robotics and Automation*, pp. 449–455, IEEE Comput. Soc. Press, 2002.
- [17] X. Cui, J. Sun, X. S. Zhang, S. J. Xu, and J. S. Dai, "A Metamorphic Hand with Coplanar Reconfiguration," *2018 International Conference on Reconfigurable Mechanisms and Robots (ReMAR)*, pp. 1–7, 2018.
- [18] M. Minami, Y. Kobayashi, T. Matsuno, and A. Yanou, "Dynamic Reconfiguration Manipulability for Redundant Manipulators," *Journal of the Robotics Society of Japan*, vol. 34, no. 4, pp. 272–279, 2016.
- [19] R. Ghrist and V. Peterson, "The geometry and topology of reconfiguration," *Advances in Applied Mathematics*, vol. 38, pp. 302–323, mar 2007.
- [20] K. Tomita, S. Murata, E. Yoshida, H. Kurokawa, and S. Kokaji, "Reconfiguration Method for a Distributed Mechanical System," in *Distributed Autonomous Robotic Systems 2*, pp. 17–25, Tokyo: Springer Japan, 1996.
- [21] M. Yim, W.-M. Shen, B. Salemi, D. Rus, M. Moll, H. Lipson, E. Klavins, and G. S. Chirikjian, "Modular Self-Reconfigurable Robot Systems [Grand Challenges of Robotics]," *IEEE Robotics & Automation Magazine*, vol. 14, no. 1, pp. 43–52, 2007.
- [22] K. Støy, "Reconfigurable Robots," in *Springer Handbook of Computational Intelligence*, pp. 1407–1421, Berlin, Heidelberg: Springer Berlin Heidelberg, 2015.
- [23] H. Ahmadzadeh, E. Masehian, and M. Asadpour, "Modular Robotic Systems: Characteristics and Applications," *Journal of Intelligent & Robotic Systems*, vol. 81, pp. 317–357, mar 2016.
- [24] T. Fukuda, S. Nakagawa, Y. Kawauchi, and M. Buss, "Self Organizing Robots Based on Cell Structures - CEBOT," in *IEEE International Workshop on Intelligent Robots*, (Tokyo, Japan), pp. 145–150, IEEE, 1988.
- [25] K. C. Wolfe, M. S. Moses, M. D. M. Kutzer, and G. S. Chirikjian, "M3Express: A low-cost independently-mobile reconfigurable modular robot," in *2012 IEEE International Conference on Robotics and Automation*, (Saint Paul, MN), pp. 2704–2710, IEEE, 2012.
- [26] M. Rubenstein, A. Cornejo, and R. Nagpal, "Programmable self-assembly in a thousand-robot swarm," *Science*, vol. 345, pp. 795–799, aug 2014.

-
- [27] R. Groß, M. Bonani, F. Mondada, and M. Dorigo, "Autonomous Self-Assembly in Swarm-Bots," *IEEE Transactions on Robotics*, vol. 22, pp. 1115–1130, dec 2006.
- [28] H. Wei, Y. Chen, J. Tan, and T. Wang, "Sambot: A Self-Assembly Modular Robot System," *IEEE/ASME Transactions on Mechatronics*, vol. 16, pp. 745–757, aug 2011.
- [29] A. Castano, A. Behar, and P. M. Will, "The Conro Modules for Reconfigurable Robots," *IEEE/ASME Transactions on Mechatronics*, vol. 7, no. 4, pp. 403–409, 2002.
- [30] C. Wright, A. Johnson, A. Peck, Z. McCord, A. Naaktgeboren, P. Gianfortoni, M. Gonzalez-Rivero, R. Hatton, and H. Choset, "Design of a modular snake robot," in *2007 IEEE/RSJ International Conference on Intelligent Robots and Systems*, (San Diego, CA), pp. 2609–2614, IEEE, 2007.
- [31] M. Yim, D. Duff, and K. Roufas, "Walk on the wild side [modular robot motion]," *IEEE Robotics & Automation Magazine*, vol. 9, pp. 49–53, dec 2002.
- [32] R. Thakker, A. Kamat, S. Bharambe, S. Chiddarwar, and K. M. Bhurchandi, "ReBiS - Reconfigurable Bipedal Snake robot," in *2014 IEEE/RSJ International Conference on Intelligent Robots and Systems*, (Chicago, IL), pp. 309–314, IEEE, sep 2014.
- [33] K. Støy, W.-m. Shen, and P. M. Will, "Using Role-Based Control to Produce Locomotion in Chain-Type Self-Reconfigurable Robots," *IEEE/ASME Transactions on Mechatronics*, vol. 7, no. 4, pp. 410–417, 2002.
- [34] A. Kamimura, H. Kurokawa, E. Yoshida, S. Murata, K. Tomita, and S. Kokaji, "Automatic Locomotion Design and Experiments for a Modular Robotic System," *IEEE/ASME Transactions on Mechatronics*, vol. 10, no. 3, pp. 314–325, 2005.
- [35] A. Pamecha, I. Ebert-Uphoff, and G. S. Chirikjian, "A useful metrics for modular robot motion planning," *IEEE Transactions on Robotics and Automation*, vol. 14, no. 4, pp. 531–545, 1997.
- [36] K. Kotay, D. Rus, M. Vona, and C. McGray, "The self-reconfiguring robotic molecule," in *1998 IEEE International Conference on Robotics and Automation*, vol. 1, pp. 424–431, IEEE, 1998.
- [37] W.-M. Shen, M. Krivokon, H. Chiu, J. Everist, M. Rubenstein, and J. Venkatesh, "Multimode locomotion via SuperBot reconfigurable robots," *Autonomous Robots*, vol. 20, no. 2, pp. 165–177, 2006.
- [38] D. Brandt, D. J. Christensen, and H. H. Lund, "ATRON Robots: Versatility from Self-Reconfigurable Modules," in *2007 International Conference on Mechatronics and Automation*, (Harbin), pp. 26–32, IEEE, 2007.
- [39] L. Zhao, H. Wang, T. Lin, G. Chen, and L. Kong, "Conceptual Design and Kinematic Analysis of the Diamobot: A Homogeneous Modular Robot," in *Advances in Reconfigurable Mechanisms and Robots II*, vol. 36, pp. 693–703, Springer International Publishing, 2016.
- [40] A. H. Lyder, K. Støy, R. F. M. Garcíá, J. C. Larsen, and P. Hermansen, "On Sub-modularization and Morphological Heterogeneity in Modular Robotics," in *Advances in Intelligent Systems and Computing*, vol. 193, pp. 649–661, Springer Berlin Heidelberg, 2013.
- [41] S. Bonardi, M. Vespignani, R. Moeckel, and A. J. Ijspeert, "Collaborative manipulation and transport of passive pieces using the self-reconfigurable modular robots roombots," in *2013 IEEE/RSJ International Conference on Intelligent Robots and Systems*, (Tokyo), pp. 2406–2412, IEEE, nov 2013.

- [42] S. Murata and H. Kurokawa, "Self-reconfigurable robots," *IEEE Robotics & Automation Magazine*, vol. 14, pp. 71–78, mar 2007.
- [43] Y. Terada and S. Murata, "Automatic Modular Assembly System and its Distributed Control," *The International Journal of Robotics Research*, vol. 27, pp. 445–462, mar 2008.
- [44] K. Gilpin, A. Knaian, and D. Rus, "Robot pebbles: One centimeter modules for programmable matter through self-disassembly," in *2010 IEEE International Conference on Robotics and Automation*, (Anchorage, AK), pp. 2485–2492, IEEE, may 2010.
- [45] J. Neubert, A. Rost, and H. Lipson, "Self-Soldering Connectors for Modular Robots," *IEEE Transactions on Robotics*, vol. 30, pp. 1344–1357, dec 2014.
- [46] L. Brodbeck and F. Iida, "An extendible reconfigurable robot based on hot melt adhesives," *Autonomous Robots*, vol. 39, pp. 87–100, jun 2015.
- [47] A. Sprowitz, S. Pouya, S. Bonardi, J. Den Kieboom, R. Mockel, A. Billard, P. Dillenbourg, and A. J. Ijspeert, "Roombots: Reconfigurable Robots for Adaptive Furniture," *IEEE Computational Intelligence Magazine*, vol. 5, pp. 20–32, aug 2010.
- [48] V. Zykov, E. Mytilinaios, M. Desnoyer, and H. Lipson, "Evolved and Designed Self-Reproducing Modular Robotics," *IEEE Transactions on Robotics*, vol. 23, pp. 308–319, apr 2007.
- [49] M. Pacheco, R. Fogh, H. H. Lund, and D. J. Christensen, "Fable II: Design of a modular robot for creative learning," in *2015 IEEE International Conference on Robotics and Automation*, (Seattle, WA), pp. 6134–6139, IEEE, may 2015.
- [50] M. Yim, D. G. Duff, and K. Roufas, "Modular Reconfigurable Robots, An Approach To Urban Search and Rescue," in *1st International Workshop on Human-friendly Welfare Robotics Systems*, (Taejon, Korea), pp. 69–76, 2000.
- [51] L. Mahadevan and S. Rica, "Self-Organized Origami," *Science*, vol. 307, pp. 1740–1740, mar 2005.
- [52] E. D. Demaine, M. L. Demaine, and J. S. B. Mitchell, "Folding flat silhouettes and wrapping polyhedral packages: New results in computational origami," *Computational Geometry*, vol. 16, pp. 3–21, may 2000.
- [53] T. Tachi, "Origamizing Polyhedral Surfaces," *IEEE Transactions on Visualization and Computer Graphics*, vol. 16, pp. 298–311, mar 2010.
- [54] H. Okuzaki, T. Saido, H. Suzuki, Y. Hara, and H. Yan, "A biomorphic origami actuator fabricated by folding a conducting paper," *Journal of Physics: Conference Series*, vol. 127, no. 1, 2008.
- [55] J. Ma and Z. You, "Energy absorption of thin-walled beams with a pre-folded origami pattern," *Thin-Walled Structures*, vol. 73, pp. 198–206, dec 2013.
- [56] E. Rodriguez Leal and J. S. Dai, "From Origami to a New Class of Centralized 3-DOF Parallel Mechanisms," in *Volume 8: 31st Mechanisms and Robotics Conference, Parts A and B*, no. October 2016, pp. 1183–1193, ASME, 2007.
- [57] D. Rus and M. T. Tolley, "Design, fabrication and control of origami robots," *Nature Reviews Materials*, vol. 3, pp. 101–112, jun 2018.

-
- [58] E. Hawkes, B. An, N. M. Benbernou, H. Tanaka, S. Kim, E. D. Demaine, D. Rus, and R. J. Wood, "Programmable matter by folding," *Proceedings of the National Academy of Sciences*, vol. 107, pp. 12441–12445, jul 2010.
- [59] E. Vander Hoff, Donghwa Jeong, and Kiju Lee, "OrigamiBot-I: A thread-actuated origami robot for manipulation and locomotion," in *2014 IEEE/RSJ International Conference on Intelligent Robots and Systems*, (Chicago, IL), pp. 1421–1426, IEEE, 2014.
- [60] S. Miyashita, S. Guitron, S. Li, and D. Rus, "Robotic metamorphosis by origami exoskeletons," *Science Robotics*, vol. 2, no. 10, pp. 1–7, 2017.
- [61] D.-Y. Lee, S.-R. Kim, J.-S. Kim, J.-J. Park, and K.-J. Cho, "Origami Wheel Transformer: A Variable-Diameter Wheel Drive Robot Using an Origami Structure," *Soft Robotics*, vol. 4, no. 2, pp. 163–180, 2017.
- [62] D.-Y. Lee, G.-P. Jung, M.-K. Sin, S.-H. Ahn, and K.-J. Cho, "Deformable wheel robot based on origami structure," in *2013 IEEE International Conference on Robotics and Automation*, (Karlsruhe), pp. 5612–5617, IEEE, may 2013.
- [63] S. Miyashita, S. Guitron, M. Ludersdorfer, C. R. Sung, and D. Rus, "An untethered miniature origami robot that self-folds, walks, swims, and degrades," in *2015 IEEE International Conference on Robotics and Automation (ICRA)*, (Seattle, WA), pp. 1490–1496, IEEE, may 2015.
- [64] C. D. Onal, M. T. Tolley, R. J. Wood, and D. Rus, "Origami-Inspired Printed Robots," *IEEE/ASME Transactions on Mechatronics*, vol. 20, pp. 2214–2221, oct 2015.
- [65] J.-S. Koh and K.-J. Cho, "Omega-Shaped Inchworm-Inspired Crawling Robot With Large-Index-and-Pitch (LIP) SMA Spring Actuators," *IEEE/ASME Transactions on Mechatronics*, vol. 18, pp. 419–429, apr 2013.
- [66] C. D. Onal, R. J. Wood, and D. Rus, "An Origami-Inspired Approach to Worm Robots," *IEEE/ASME Transactions on Mechatronics*, vol. 18, pp. 430–438, apr 2013.
- [67] Z. Zhakypov, M. Falahi, M. Shah, and J. Paik, "The design and control of the multi-modal locomotion origami robot, Tribot," in *2015 IEEE/RSJ International Conference on Intelligent Robots and Systems*, (Hamburg), pp. 4349–4355, IEEE, sep 2015.
- [68] E. A. Peraza-Hernandez, D. J. Hartl, R. J. Malak Jr, and D. C. Lagoudas, "Origami-inspired active structures: a synthesis and review," *Smart Materials and Structures*, vol. 23, p. 094001, sep 2014.
- [69] S. Miyashita, S. Guitron, K. Yoshida, S. Li, D. D. Damian, and D. Rus, "Ingestible, Controllable, and Degradable Origami Robot for Patching Stomach Wounds," in *2016 IEEE International Conference on Robotics and Automation*, (Stockholm), IEEE, 2016.
- [70] J. Shintake, S. Rosset, B. E. Schubert, D. Floreano, and H. R. Shea, "A Foldable Antagonistic Actuator," *IEEE/ASME Transactions on Mechatronics*, vol. 20, pp. 1997–2008, oct 2015.
- [71] H. Shigemune, S. Maeda, Y. Hara, N. Hosoya, and S. Hashimoto, "Origami Robot: A Self-folding Paper Robot with an Electrothermal Actuator Created by Printing," *IEEE/ASME Transactions on Mechatronics*, vol. PP, no. 99, pp. 1–1, 2016.
- [72] A. Firouzeh and J. Paik, "Robogami: A Fully Integrated Low-Profile Robotic Origami," *Journal of Mechanisms and Robotics*, vol. 7, no. 2, p. 021009, 2015.

- [73] M. T. Tolley, S. M. Felton, S. Miyashita, D. Aukes, D. Rus, and R. J. Wood, "Self-folding origami: shape memory composites activated by uniform heating," *Smart Materials and Structures*, vol. 23, p. 094006, sep 2014.
- [74] J. K. Paik, E. Hawkes, and R. J. Wood, "A novel low-profile shape memory alloy torsional actuator," *Smart Materials and Structures*, vol. 19, no. 12, p. 125014, 2010.
- [75] J. K. Paik and R. J. Wood, "A bidirectional shape memory alloy folding actuator," *Smart Materials and Structures*, vol. 21, p. 065013, jun 2012.
- [76] Z. Zhakypov and J. Paik, "Design Methodology for Constructing Multimaterial Origami Robots and Machines," *IEEE Transactions on Robotics*, vol. 34, pp. 151–165, feb 2018.
- [77] A. Firouzeh, Yi Sun, Hyunchul Lee, and J. Paik, "Sensor and actuator integrated low-profile robotic origami," in *2013 IEEE/RSJ International Conference on Intelligent Robots and Systems*, pp. 4937–4944, IEEE, nov 2013.
- [78] A. Firouzeh and J. Paik, "The Design and Modeling of a Novel Resistive Stretch Sensor With Tunable Sensitivity," *IEEE Sensors Journal*, vol. 15, pp. 6390–6398, nov 2015.
- [79] R. Gurkewitz and B. Arnstein, *3-D Geometric Origami: Modular Polyhedra*. New York: Dover Publications, Inc., 1995.
- [80] D. Stewart, "A Platform with Six Degrees of Freedom," *Proceedings of the Institution of Mechanical Engineers*, vol. 180, pp. 371–386, jun 1965.
- [81] C. Yuan, R. Yin, W. Zhang, and G. Chen, "A new under-actuated resilient robot," in *2017 IEEE International Conference on Systems, Man, and Cybernetics (SMC)*, (Banff, AB, Canada), pp. 1202–1207, IEEE, oct 2017.
- [82] S. Hong, W. Lee, K. Kim, H. Lee, and S. Kang, "Connection Mechanism Capable of Genderless Coupling for Modular Manipulator System," in *2017 14th International Conference on Ubiquitous Robots and Ambient Intelligence (URAI)*, (Jeju, South Korea), pp. 185–189, IEEE, 2017.
- [83] C. Parrott, T. J. Dodd, and R. Groß, "HiGen: A high-speed genderless mechanical connection mechanism with single-sided disconnect for self-reconfigurable modular robots," *IEEE International Conference on Intelligent Robots and Systems*, no. Iros, pp. 3926–3932, 2014.
- [84] W. Saab and P. Ben-Tzvi, "A Genderless Coupling Mechanism with 6-DOF Misalignment Capability for Modular Self-Reconfigurable Robots," *Journal of Mechanisms and Robotics*, vol. 8, no. c, pp. 1–9, 2016.
- [85] A. I. Nawroj, J. P. Swensen, and A. M. Dollar, "Toward Modular Active-Cell Robots (MACROs): SMA Cell Design and Modeling of Compliant, Articulated Meshes," *IEEE Transactions on Robotics*, vol. 33, no. 4, pp. 796–806, 2017.
- [86] R. F. M. Garcia, J. D. Hiller, K. Støy, and H. Lipson, "A vacuum-based bonding mechanism for modular robotics," *IEEE Transactions on Robotics*, vol. 27, no. 5, pp. 876–890, 2011.
- [87] C. H. Belke and J. Paik, "Automatic Couplings With Mechanical Overload Protection for Modular Robots," *IEEE/ASME Transactions on Mechatronics*, vol. 24, pp. 1420–1426, jun 2019.
- [88] J. Davey, N. Kwok, and M. Yim, "Emulating self-reconfigurable robots - design of the SMORES system," in *2012 IEEE/RSJ International Conference on Intelligent Robots and Systems*, pp. 4464–4469, IEEE, oct 2012.

- [89] J. W. Romanishin, K. Gilpin, S. Claici, and D. Rus, "3D M-Blocks: Self-reconfiguring robots capable of locomotion via pivoting in three dimensions," *2015 IEEE International Conference on Robotics and Automation*, vol. 2015-June, no. June, pp. 1925–1932, 2015.
- [90] A. Brunete, A. Ranganath, S. Segovia, J. P. de Frutos, M. Hernando, and E. Gambao, "Current trends in reconfigurable modular robots design," *International Journal of Advanced Robotic Systems*, vol. 14, p. 172988141771045, may 2017.
- [91] T. Tosun, J. Davey, C. Liu, and M. Yim, "Design and characterization of the EP-Face connector," in *2016 IEEE/RSJ International Conference on Intelligent Robots and Systems*, vol. 19, pp. 45–51, IEEE, oct 2016.
- [92] M. Yim, Ying Zhang, and D. Duff, "Modular robots," *IEEE Spectrum*, vol. 39, no. 2, pp. 30–34, 2002.
- [93] N. Eckenstein and M. Yim, "Modular Robot Connector Area of Acceptance from Configuration Space Obstacles," in *2017 IEEE/RSJ International Conference on Intelligent Robots and Systems*, 2017.
- [94] A. Firouzeh and J. Paik, "Grasp Mode and Compliance Control of an Underactuated Origami Gripper Using Adjustable Stiffness Joints," *IEEE/ASME Transactions on Mechatronics*, vol. 22, no. 5, pp. 2165–2173, 2017.
- [95] T. Yoshikai, M. Hayashi, A. Kadowaki, T. Goto, and M. Inaba, "Design and development of a humanoid with Soft 3D-deformable sensor flesh and automatic recoverable mechanical overload protection mechanism," in *2009 IEEE/RSJ International Conference on Intelligent Robots and Systems*, pp. 4977–4983, IEEE, oct 2009.
- [96] X. Guo, W. Zhang, H. Liu, Z. Yu, W. Zhang, W. Conus, K. Hashimoto, and Q. Huang, "A torque limiter for safe joint applied to humanoid robots against falling damage," in *2015 IEEE International Conference on Robotics and Biomimetics (ROBIO)*, pp. 2454–2459, IEEE, dec 2015.
- [97] G. Yang and I.-M. Chen, "Task-based optimization of modular robot configurations: minimized degree-of-freedom approach," *Mechanism and Machine Theory*, vol. 35, pp. 517–540, apr 2000.
- [98] Z. M. Bi and W. J. Zhang, "Concurrent optimal design of modular robotic configuration," *Journal of Robotic Systems*, vol. 18, pp. 77–87, feb 2001.
- [99] Yangiong Fei, Xifang Zhao, and W. Xu, "Kinematics and dynamics of reconfigurable modular robots," in *SMC'98 Conference Proceedings. 1998 IEEE International Conference on Systems, Man, and Cybernetics (Cat. No.98CH36218)*, vol. 4, (San Diego, CA), pp. 3325–3334, IEEE, IEEE, 1998.
- [100] W. Wu, Y. Guan, Y. Yang, and B. Dong, "Multi-objective configuration optimization of assembly-level reconfigurable modular robots," in *2016 IEEE International Conference on Information and Automation (ICIA)*, pp. 528–533, IEEE, IEEE, aug 2016.
- [101] S. Ha, S. Coros, A. Alspach, J. Kim, and K. Yamane, "Joint Optimization of Robot Design and Motion Parameters using the Implicit Function Theorem," in *Robotics: Science and Systems XIII*, (Cambridge, Massachusetts), Robotics: Science and Systems Foundation, jul 2017.
- [102] A. Casal and M. H. Yim, "Self-reconfiguration planning for a class of modular robots," in *Photonics East'99* (G. T. McKee and P. S. Schenker, eds.), pp. 246–257, International Society for Optics and Photonics, aug 1999.

- [103] Feili Hou and Wei-Min Shen, "On the complexity of optimal reconfiguration planning for modular reconfigurable robots," in *2010 IEEE International Conference on Robotics and Automation*, pp. 2791–2796, IEEE, IEEE, may 2010.
- [104] F. Hou and W.-M. Shen, "Graph-based optimal reconfiguration planning for self-reconfigurable robots," *Robotics and Autonomous Systems*, vol. 62, pp. 1047–1059, jul 2014.
- [105] M. Yao, C. H. Belke, H. Cui, and J. Paik, "A reconfiguration strategy for modular robots using origami folding," *The International Journal of Robotics Research*, vol. 38, pp. 73–89, jan 2019.
- [106] H. Kurokawa, K. Tomita, A. Kamimura, S. Kokaji, T. Hasuo, and S. Murata, "Distributed Self-Reconfiguration of M-TRAN III Modular Robotic System," *The International Journal of Robotics Research*, vol. 27, pp. 373–386, mar 2008.
- [107] Hongxing Wei, Yingpeng Cai, Haiyuan Li, Dezhong Li, and Tianmiao Wang, "Sambot: A self-assembly modular robot for swarm robot," in *2010 IEEE International Conference on Robotics and Automation*, pp. 66–71, IEEE, IEEE, may 2010.
- [108] J. W. Romanishin, K. Gilpin, and D. Rus, "M-blocks: Momentum-driven, magnetic modular robots," in *2013 IEEE/RSJ International Conference on Intelligent Robots and Systems*, pp. 4288–4295, IEEE, IEEE, nov 2013.
- [109] L. Wang, M. M. Plecnik, and R. S. Fearing, "Robotic folding of 2D and 3D structures from a ribbon," in *2016 IEEE International Conference on Robotics and Automation (ICRA)*, pp. 3655–3660, IEEE, IEEE, may 2016.
- [110] J. K. Paik, A. Byoungkwon, D. Rus, and R. J. Wood, "Robotic Origamis: Self-Morphing Modular Robot," in *ICMC*, 2012.
- [111] R. J. Lang, "A Computational Algorithm for Origami Design," in *Proceedings of the twelfth annual symposium on Computational geometry*, pp. 98–105, ACM, 1996.
- [112] N. Watanabe and K.-i. Kawaguchi, "The Method for Judging Rigid Foldability," in *Origami 4*, vol. 4, pp. 165–174, A K Peters/CRC Press, aug 2009.
- [113] T. Tachi, "Simulation of Rigid Origami," in *Origami 4*, vol. 4, pp. 175–187, A K Peters/CRC Press, aug 2009.
- [114] E. T. Filipov, T. Tachi, and G. H. Paulino, "Origami tubes assembled into stiff, yet reconfigurable structures and metamaterials," *Proceedings of the National Academy of Sciences*, vol. 112, pp. 12321–12326, oct 2015.
- [115] Y. Chen, R. Peng, and Z. You, "Origami of thick panels," *Science*, vol. 349, pp. 396–400, jul 2015.
- [116] S. A. Zirbel, S. P. Magleby, L. L. Howell, R. J. Lang, M. W. Thomson, D. A. Sigel, P. E. Walkemeyer, and B. P. Trease, "Accommodating Thickness in Origami-Based Deployable Arrays," in *Volume 6B: 37th Mechanisms and Robotics Conference*, vol. 135, p. V06BT07A027, ASME, aug 2013.
- [117] D. J. Balkcom and M. T. Mason, "Robotic origami folding," *The International Journal of Robotics Research*, vol. 27, pp. 613–627, may 2008.
- [118] B. An and D. Rus, "Designing and programming self-folding sheets," *Robotics and Autonomous Systems*, vol. 62, pp. 976–1001, jul 2014.

-
- [119] J. M. Hollerbach, "A Recursive Lagrangian Formulation of Manipulator Dynamics and a Comparative Study of Dynamics Formulation Complexity," *IEEE Transactions on Systems, Man, and Cybernetics*, vol. 10, no. 11, pp. 730–736, 1980.
- [120] I.-M. Chen and G. Yang, "Automatic Model Generation for Modular Reconfigurable Robot Dynamics," *Journal of Dynamic Systems, Measurement, and Control*, vol. 120, no. 3, p. 346, 1998.
- [121] I.-M. Chen, S. H. Yeo, G. Chen, and G. Yang, "Kernel for Modular Robot Applications: Automatic Modeling Techniques," *The International Journal of Robotics Research*, vol. 18, pp. 225–242, feb 1999.
- [122] E. Meister, A. Gutenkunst, and P. Levi, "Dynamics and Control of Modular and Self-Reconfigurable Robotic Systems," *International Journal on Advances in Intelligent Systems*, vol. 6, no. 1, 2013.
- [123] J. Liu, Y. Wang, S. Ma, and Y. Li, "Enumeration of the Non-Isomorphic Configurations for a Reconfigurable Modular Robot with Square-Cubic-Cell Modules," *International Journal of Advanced Robotic Systems*, vol. 7, p. 31, dec 2010.
- [124] F. Park and J. Bobrow, "A recursive algorithm for robot dynamics using Lie groups," in *Proceedings of the 1994 IEEE International Conference on Robotics and Automation*, pp. 1535–1540, IEEE, IEEE Comput. Soc. Press, 1994.
- [125] R. Straub and H. Prautzsch, "Creating optimized cut-out sheets for paper models from meshes," tech. rep., Institut für Betriebs- und Dialogsysteme (IBDS), 2011.
- [126] Yishen Guan, K. Yokoi, O. Stasse, and A. Kheddar, "On robotic trajectory planning using polynomial interpolations," in *2005 IEEE International Conference on Robotics and Biomimetics - ROBIO*, pp. 111–116, IEEE, IEEE, 2005.
- [127] B. An, S. Miyashita, M. T. Tolley, D. M. Aukes, L. Meeker, E. D. Demaine, M. L. Demaine, R. J. Wood, and D. Rus, "An end-to-end approach to making self-folded 3D surface shapes by uniform heating," in *2014 IEEE International Conference on Robotics and Automation (ICRA)*, pp. 1466–1473, IEEE, IEEE, may 2014.
- [128] T. Haenselmann and W. Effelsberg, "Optimal strategies for creating paper models from 3D objects," *Multimedia Systems*, vol. 18, pp. 519–532, nov 2012.
- [129] D. M. Aukes and R. J. Wood, "PopupCAD: a tool for automated design, fabrication, and analysis of laminate devices," *Micro- and Nanotechnology Sensors, Systems, and Applications VII*, vol. 9467, no. May 2015, p. 94671B, 2015.
- [130] S. Felton, M. Tolley, E. Demaine, D. Rus, and R. Wood, "A method for building self-folding machines," *Science*, vol. 345, pp. 644–646, aug 2014.
- [131] A. Pagano, T. Yan, B. Chien, A. Wissa, and S. Tawfick, "A crawling robot driven by multi-stable origami," *Smart Materials and Structures*, vol. 26, p. 094007, sep 2017.
- [132] S. G. Faal, F. Chen, W. Tao, M. Agheli, S. Tasdighikalat, and C. D. Onal, "Hierarchical Kinematic Design of Foldable Hexapedal Locomotion Platforms," *Journal of Mechanisms and Robotics*, vol. 8, p. 011005, aug 2015.
- [133] Z. Zhakypov, K. Mori, K. Hosoda, and J. Paik, "Designing minimal and scalable insect-inspired multi-locomotion millirobots," *Nature*, vol. 571, pp. 381–386, jul 2019.

- [134] G. Jing, T. Tosun, M. Yim, and H. Kress-Gazit, "Accomplishing high-level tasks with modular robots," *Autonomous Robots*, vol. 42, pp. 1337–1354, oct 2018.
- [135] J. Seo, J. Paik, and M. Yim, "Modular Reconfigurable Robotics," *Annual Review of Control, Robotics, and Autonomous Systems*, vol. 2, pp. 63–88, may 2019.
- [136] S. S. R. Chennareddy, A. Agrawal, and A. Karuppiah, "Modular Self-Reconfigurable Robotic Systems: A Survey on Hardware Architectures," *Journal of Robotics*, vol. 2017, pp. 1–19, 2017.
- [137] M. Botsch, L. Kobbelt, M. Pauly, P. Alliez, and B. Levy, *Polygon Mesh Processing*. New York: A K Peters/CRC Press, oct 2010.
- [138] P. Alliez, M. Meyer, and M. Desbrun, "Interactive geometry remeshing," in *Proceedings of the 29th annual conference on Computer graphics and interactive techniques - SIGGRAPH '02*, (New York, New York, USA), p. 347, ACM Press, 2002.
- [139] P. Alliez, G. Ucelli, C. Gotsman, and M. Attene, "Recent Advances in Remeshing of Surfaces," in *Mathematics and Visualization*, no. 9783540332640, pp. 53–82, 2008.
- [140] M. Isenburg, S. Gumhold, and C. Gotsman, "Connectivity shapes," in *Proceedings Visualization, 2001. VIS '01.*, pp. 135–552, IEEE, 2001.
- [141] C. Jiang, C. Tang, M. Tomiči, J. Wallner, and H. Pottmann, "Interactive Modeling of Architectural Freeform Structures: Combining Geometry with Fabrication and Statics," in *Advances in Architectural Geometry 2014* (P. Block, J. Knippers, N. J. Mitra, and W. Wang, eds.), pp. 95–108, Cham: Springer International Publishing, 2015.
- [142] A. Lyder, R. Garcia, and K. Stoy, "Mechanical Design of Odin, an Extendable Heterogeneous Deformable Modular Robot," in *2008 IEEE/RSJ International Conference on Intelligent Robots and Systems*, pp. 883–888, IEEE, sep 2008.
- [143] J. Bruce, K. Caluwaerts, A. Iscen, A. P. Sabelhaus, and V. Sunspirial, "Design and evolution of a modular tensegrity robot platform," *Proceedings - IEEE International Conference on Robotics and Automation*, pp. 3483–3489, 2014.
- [144] E. H. Østergaard, K. Kassow, R. Beck, and H. H. Lund, "Design of the ATRON lattice-based self-reconfigurable robot," *Autonomous Robots*, vol. 21, no. 2, pp. 165–183, 2006.
- [145] S. G. M. Hossain, C. A. Nelson, K. D. Chu, and P. Dasgupta, "Kinematics and Interfacing of ModRED: A Self-Healing Capable, 4DOF Modular Self-Reconfigurable Robot," *Journal of Mechanisms and Robotics*, vol. 6, p. 041017, aug 2014.
- [146] Y. Zhu, J. Zhao, X. Cui, X. Wang, S. Tang, X. Zhang, and J. Yin, "Design and implementation of UBot: A modular Self-Reconfigurable Robot," *2013 IEEE International Conference on Mechatronics and Automation, IEEE ICMA 2013*, pp. 1217–1222, 2013.

Christoph H. Belke

Avenue de Montchoisi 49, 1006 Lausanne, Switzerland; +41 788 377 466
chbelke.com; christophbelke@icloud.com; [linkedin.com/in/christophbelke](https://www.linkedin.com/in/christophbelke)

Research Interests

Reconfigurable and modular robotic systems – design and control of robots with variable shape and function
Adaptable and intelligent structures – embedded functionalities in smart mechanical and mechatronic structures
Assistive and interactive devices – interfacing smart systems with humans and their environment

Education

- Aug 2015 - **PhD Candidate in the Doctoral School for Robotics, Control, and Intelligent Systems**
Present – **École polytechnique fédérale de Lausanne (EPFL)**
- Thesis title: From Modular Origami Robots to Polygon-based Modular Systems: a New Paradigm in Reconfigurable Robotics
- Supervisor: Prof. Jamie Paik, Reconfigurable Robotics Lab
- Oct 2010 - **Master of Engineering (Mechanical Engineering)**
Jul 2014 – **Imperial College London**
- Grade: First Class Honours (top 20% for overall degree)
- Award: Engineering Dean's List for academic excellence 2013/2014 (top 10%)
- Courses included: Advanced Control; Design; Mechatronics; Embedded C for Microcontrollers; Machine System Dynamics; Mathematics; Human Centred Design of Assistive & Rehabilitation Devices; Vehicle Propulsion Technology; Manufacturing Technology & Management
- Jul 2010 **International Baccalaureate Diploma (IB)**
– **Haileybury & Imperial Service College**
- 41 out of 45 points – Higher Levels: Maths, Physics, German; Standard Levels: Economics, English, French

Publications

- [J1] C. H. Belke and J. Paik, "Couplings with Mechanical Overload Protection for Modular Robots," *IEEE/ASME Transactions on Mechatronics*, vol. 24, no. 3, pp. 1420-1426, Oct. 2019.
- [J2] M. Yao, C. H. Belke, H. Cui and J. Paik, "A Reconfiguration Strategy for Modular Robots using Origami Folding," *International Journal of Robotics Research*, vol. 38, no. 1, pp. 73-89, Jan 2019.
- [J3] M. Yao, H. Cui, C. H. Belke, X. Xiao and J. Paik, "Optimal Distribution of Active Modules in Modular Robots," *Journal of Mechanisms and Robotics*, vol. 11, no. 1, pp. 011017, Dec 2018.
- [J4] C. H. Belke and J. Paik, "Mori: A Modular Origami Robot," *IEEE/ASME Transactions on Mechatronics*, vol. 22, no. 5, pp. 2153-2164, Oct. 2017.
- [C1] M. Yao, H. Cui, X. Xiao, C. H. Belke, and J. Paik, "Towards Peak Torque Minimization for Modular Self-folding Robots," *2018 IEEE/RSJ International Conference on Intelligent Robots and Systems (IROS)*, Madrid, Spain, 2018, pp. 7975-7982.
- [C2] Z. Zhakypov, C. H. Belke and J. Paik, "Tribot: A deployable, self-righting and multi-locomotive origami robot," *2017 IEEE/RSJ International Conference on Intelligent Robots and Systems (IROS)*, Vancouver, BC, 2017, pp. 5580-5586.

Experience

- Aug 2015 - **Doctoral Assistant at the Reconfigurable Robotics Lab**
Present – **École polytechnique fédérale de Lausanne (EPFL), Prof. Jamie Paik**
A modular origami robot is a new type of robot that addresses the needs and challenges of an entirely modular, reconfigurable, mobile, autonomous, and interactive surface. It yields a new type of robot that overcomes some of the limitations of existing origami robots and introduces an innovative concept for a new type of reconfigurable modular robot. Taking inspiration from the concepts behind both modular and origami robots, the proposed robotic system consists of quasi-2D robotic modules that, when combined with one another, can fold up on each other to create any desirable 3D configuration.

- Jul 2013 - **Research Internship at the Robotics and Human Engineering Laboratory**
 Sep 2013 - **University of California, Berkeley, Prof. Homayoon Kazerooni**
 Worked on a medical device that aims to reduce fatigue at the knee during various ambulation activities by re-using stored energy and providing additional strength and support. I developed and manufactured the entire electronic control module of the device (using EAGLE), as well as the firmware (in C) which incorporates the control mechanisms by analysing gait dynamics. In combination with this I wrote a smartphone application (in Java) to wirelessly communicate with the device allowing for the modification of various control parameters.
- Jul 2012 - **Intern in Risk & Portfolio Management, Trade Finance & Cash Management**
 Sep 2012 - **Deutsche Bank AG, Frankfurt**
 Analysing risk parameters for various trade finance products and their effect on risk-weighted assets (RWA). Analysis of the effects of precisely calculating RWAs with load terms of less than one year. Development of an application that simplifies the automatic export of product definitions using Visual Basic. Preparation and presentation of key performance indicators for senior management. Created a new cost management scheme for external vendors.
- Jul 2011 - **Intern, Whole Vehicle Engineering**
 Sep 2011 - **Bentley Motors Ltd, Crewe**
 Development of a test matrix for endurance tests (EWP) using Visual Basic. Reviewed all existing test procedures with the management responsible and created new procedures to enhance the out-dated methods. Development of a database and automatic report generation for the oil consumption on test vehicles using Microsoft Access and Visual Basic. Practical experience in the workshop and on a proving ground while setting up and carrying out various endurance tests.
- Jan 2008 **Intern, Watch Repair**
 - **Sinn Spezialuhren GmbH, Frankfurt**
 Technical introduction into watch manufacture and repair, including workshop training and independent clock repair.

University Projects

- Oct 2013 - **Control of Assistive Exoskeletons using Mechanomyography**
 Jul 2014 Master thesis [top 10%] - I worked on an existing assistive hand exoskeleton which serves as a hand rehabilitation device for stroke patients. I devised a new way for the exoskeleton to detect the intended movement of the subject's hand by using Mechanomyography (muscle sound sensors) to sense the muscle activity in the arm. By processing the muscle sound signals, I derived a decision-based control algorithm (using Matlab) that predicts what stage the hand is at during a sequence of movements with a robustness of over 80% for all five test subjects. This allows for the control of the hand-exoskeleton solely from the sound produced by muscles. My thesis was chosen as one of the Top 10 projects of the year.
- Jan 2014 - **Human Centred Design of Assistive & Rehabilitation Devices**
 Mar 2014 [Awarded: Best project] - GRAM (GRip Assessment Module); I led a team of five to rethink the current method used to assess the fine manipulation skills of stroke patients with impaired motor control. We built a novel medical assessment device incorporating different feedback strategies for the patient as well as force sensing ability and wireless communication. Our method allowed us to regard the patient as the control system to assess various aspects of their manipulation skills. I was responsible for the entire electronics and firmware development (in EAGLE and C) and I was involved in the mechanical design of the product itself. We were awarded the prize for the Best Project.
- Oct 2012 - **Rapid Prototyping for Body Armour**
 Jul 2013 Bachelor thesis [top 10%] - I worked in a group of four building a novel 3D printer which is able to print thermoplastic elastomer (TPE, a soft plastic) to be able to quickly prototype soft protection pads. During the course of this project we designed and built a 3D-printer from scratch in order to account for the different material properties of TPE compared to the usual ABS or PLA. At the end of the project, we successfully printed a novel grade of thermoplastic elastomer, something that had not been done before at the time. I was in charge of mechanical design (emphasis on precise movement of degrees of motion) and manufacture.
- Jan 2013 - **Explosive Ordnance Disposal Challenge**
 Mar 2013 [Awarded: Best robot] - Developed and programmed a robot using Embedded C that could automatically locate an explosive device, retrieve a disarm code and return to the initial position. I designed and optimized the electronics and firmware using different control strategies in order to create a control system that allowed the robot to seamlessly complete its task. For this I was awarded the prize for the Best Robot.

Skills

Engineering	Robotics, Control, Human Engineering, Mechatronics, Electronics, Embedded Systems, Micro-Controllers, Design, Manufacturing, Rapid Prototyping
Computer	Programming (C, Matlab, Java, Visual Basic, html/CSS), CAD modelling (SolidWorks, EAGLE)
Leadership & Teamwork	Captain of the 1st Men's Hockey Team at Imperial College London; Team leader for several university projects including Explosive Ordnance Disposal Challenge (first page); Coaching of several youth Hockey teams at Haileybury; Representative of three year groups at high school.
Languages	German (native), English (bilingual), French (intermediate)

*References and recommendations are available upon request.
Thank you very much for your consideration!*



Lausanne, December 21st, 2019